Design of robust terminal procedures

By optimization of arrival and departure trajectories

L. H. Geijselaers

TU Delft

Design of robust terminal procedures

By optimization of arrival and departure trajectories

by

L. H. Geijselaers

to obtain the degree of Master of Science
at the Delft University of Technology,
to be defended publicly on Monday January 30, 2017 at 14:00 PM.

Student number: 4081978

Thesis committee:	Dr. Ir. S. Hartjes,	TU Delft, supervisor
	Dr. Ir. H.G. Visser,	TU Delft
	Dr. Ir. J.A. Melkert,	TU Delft

TU Delft

Abstract

With the growth of the air traffic movements and the population of people living around airports, the number of awakenings due to aircraft noise has increased. ICAO has defined four research fields to reduce noise and one of them is implementation of noise abatement operational procedures. This includes different trajectory optimization methods, one of which is rerouting of trajectories around noise sensitive areas.
Research has proven that rerouting has a positive effect on reducing the number of people getting disturbed while keeping the fuel consumption as low as possible. Until now these trajectory optimization problems focused on either a departure or an arrival trajectory. When implementing these optimized routes, it may result in a conflict with other existing routes and this is the problem that is the main focus of this research. Within this research trajectories will be combined and optimized for number of awakenings and fuel consumption while assessing the effect of terminal operations.

The model that combines trajectories is based on existing models, including a point-mass model and a noise model. These are combined in a multi-objective evolutionary algorithm where the objectives are the number of awakenings and the fuel consumption. The results of the optimization problems are presented as Pareto-optimal solutions.
To contribute to the field of noise abatement terminal operations, two trajectories are combined in an optimization problem. To assure enough distance between the two trajectories the minimum separation constraint is used. When a loss of separation happens, the flight path angle of one of the trajectories is adjusted.

The designed model is used to optimize four trajectory optimization problems. The first being a departure trajectory, this is the current Spijkerboor standard instrumental departure that departs from runway 24 at Amsterdam Airport Schiphol. The second problem is the current night standard terminal arrival route starting at sea and landing on runway 18R at Schiphol. For the third optimization problem the two trajectories of the previous optimization problems are combined with keeping the minimum separation constraint in mind. The final case study was used to focus more on the effect of the minimum separation constraint.

From the departure optimization problem can be concluded that there is a big diversity in the vertical and horizontal trajectory between the minimum fuel and minimum awakening solution.
For the arrival optimization problem the difference between these two solutions is not significant. The vertical trajectory is for both solutions almost the same, the main difference is caused by the ground trajectory.
When combining the trajectories the results of the objective functions for the combined problem are the sum of the arrival and departure objective functions. This results in a bias to the departure trajectory because these numbers are atleast twice the value compared to the arrival trajectory. This also results in the arrival trajectory always being created around the departure trajectory.
From the final case study can be concluded that when designing the trajectories the influence of the minimum separation constraint is mostly on the vertical profile of the departure trajectory. Also can be observed that small rerouting of the trajectories sometimes is needed to give both trajectories enough space to cross each other.

Preface

When starting this research I had heard about standard departure and arrival trajectories that are used at the moment around Schiphol to reduce the noise and I was eager to work on improvements in this field. After I got familiar with the subject of trajectory optimization and all the rules and guidelines that are connected with it, I got more enthusiastic and was looking forward to trying to start combining trajectories and finding out what problems would occur doing this and how to solve them.

During the design of my model many problems had to be solved and without the help of my daily supervisor, Sander Hartjes, this would have taken much more time. He is also the first person I would like to thank for fast responses on my questions and the many times it was possible to have a meeting with him within a day.

I would also like to thank Dries Visser for his attendance during my literature review, midterm presentation and my green light presentation. Always during these meetings I got feedback from him that brought me to new ideas.

Finally I would like to thank my family, roommates and friends for supporting me and listen to my stories about my thesis. Probably they not always understood what I was talking about but it helped me a lot to come to the final results and conclusions.

Liset Geijselaers
Delft, January 2017

Contents

List of Figures

List of Tables

Nomenclature

Symbols	Description	Units
%awakening	percentage of awakening	%
D	drag	N
E	total energy	J
ff	fuel flow	kg/s
g_0	gravitational acceleration	m/s^2
h	altitude	m
L	straight leg	m
m_{fuel}	Fuel consumed	kg
$max(L_A)$	maximum A-weight sound level	dBA
$n_{awakening}$	number of awakenings	
n_{eng}	number of engines	
P	current population	N
P	ambient air pressure	N/m^2
P_0	air pressure at sea level	N/m^2
Q	new population created by crossover and mutation	N
R	population	2N
R	Radius	m
r	heading vector	
s	length of the turn	m
s	distance flown	m
SEL	Sound Exposure Level	dBA
T	thrust	N
t	time	sec
V_{EAS}	Equivalent velocity	m/s
V_{TAS}	True velocity	m/s
V_{ZF}	clean velocity	m/s
W	weight	N
x	location vector	

Greek symbols	Description	Units
α	flight path restriction angle	°
β	flight path angle range	°
Γ	thrust setting	
γ	flight path angle	°
ΔE	difference between energy states	J
Δs	remaining distance to be flown	m
$\Delta\chi$	heading difference	degree
$\frac{\delta\rho}{\delta h}$	vertical pressure variation	kg/m^2
μ	bank angle	rad
ρ	ambient air density	kg/m^3
ρ_0	air density at sea level	kg/m^3
χ	heading	degree

Superscript	Description
·	derivative

Abbreviations	Description
ATC	Air Traffic Control
ATM	Air Traffic Management
CBS	Centraal Bureau voor de Statistiek
CDA	Continious Descent Approach
DER	Departure End of the Runway
EA	Evolutionary algorithm
FAA	Federal Aviation Administration
FAF	Final Approach Fix
FATO	Final Approach and Take Off area
FICAN	Federal Interagency Committee and Aviation Noise
FMS	Flight Management System
IAF	Initial Approach Fix
ICAO	International Civil Aviation Organisation
IF	Initial Fix
ILS	Instrumental Landing System
INM	Integrated Noise Model
MAPt	Missed Approach Point
MLW	Maximum Landing Weight
MOC	Minimum Obstacle Clearance
MOEA	Multi-Objective Evolutionary algorithm
NADP	Noise Abatement Departure Procedure
NM	Nautical Mile
NSGA	Non-dominant Sorting Genetic Algorithm
NSGA-2	Non-dominant Sorting Genetic Algorithm II
NTD	Noise-Thrust-Distance
OIS	Obstacle Identification Surface
PDG	Procedure Design Gradient
RF	Radius to a Fix
RNAV	Area navigation
SID	Standard Instrumental Departure
STAR	Standard Terminal Arrival Route
TF	Track to a Fix
ISA	Standard atmosphere
u	control variables
x	state variables

Subscript	Description
0	initial state
i	current segment
indoor	value inside a house
i+1	next segment
max	maximum value
min	minimum value
n	normalized value
net	net value
outdoor	value outside a house
seg	segment
t	current state
tot	total
t+1	next state

1

Introduction

The air traffic industry has been growing the last few decades, resulting in more air traffic movements around airports. In combination with the population growth around airports this has resulted in more people getting disturbed by aircraft noise[13].

The International Civil Aviation Organization (ICAO) has established four areas, which can be focused on to reduce the noise around an airport. The first area is reducing the noise at the source, the aircraft; this means that with the use of technological improvements the noise that is created by an aircraft is reduced. The aircraft noise is a combination of the engines and the noise created by the airframe. NASA has been doing research on engine noise for years and as can be seen in Figure 1.1 the noise by engines has been reduced with around 20dB over the last 50 years. One of the reasons of engine noise reduction is because the exhaust velocity of the engines is decreased. The only problem of technological improvements is that it takes a long time before they are implemented[1].

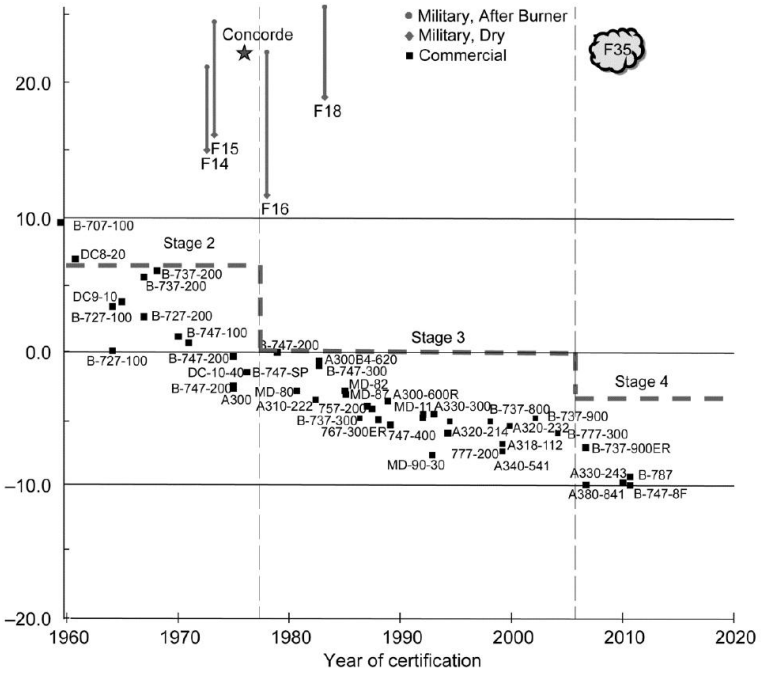

Figure 1.1: Noise reduction trend of aircraft engines [1]

The second area that can be focused on is land-use planning and management. The land around an airport should be planned and managed such that the least amount of people is affected by aircraft noise. With existing airfields this planning and land-use changes can be limited but the focus can be on preventing creation of residential areas in noise sensitive locations[14].

The third area is giving noise related restrictions to specific aircraft types. For instance an aircraft that is very noisy can be limited or prohibited from the airport. Other operational restrictions are to establish noise quota or night-time restrictions[14].

The fourth and final area is the use of noise abatement operational procedures. There are a few ways of implementing noise abatement procedures. An example for arrival is the continuous descent approach (CDA). With this procedure the aircraft will continuously descent and decelerate without returning to level flight. This includes the aircraft flying idle which results in not only reduction of noise but also of fuel consumption[15]. The problem of flying CDA is that the capacity of the runway decreases because the prediction of the arrival time becomes more difficult. This means that the space between two arriving aircraft must be increased[16].
Another noise abatement procedure is rerouting the arrival and departure routes such that noise sensitive areas are avoided. This is done by optimizing the routes with respect to not only fuel consumption but also noise reduction. On this subject research has been done using different types of algorithms. One study uses an evolutionary algorithm to optimize a departure route over a noise sensitive area at Schiphol[9]. By using a genetic algorithm in this research multi-objective functions could be evaluated. The resulting route is compared to the departure that is used at the moment and it is concluded that it has a positive effect on the noise impact as well as fuel consumption.
Noise abatement procedures have also been optimized using a dynamic trajectory optimization algorithm[17, 18]. In this research a tool was created which combines a geographic information system, a noise model and a non-linear programming algorithm. This tool is called NOISHHH and generates a measure for the noise impact on the population around an airport. One of the conclusions of using this tool was that current departure procedures could potentially be improved in order to reduce the noise impact.
Over the years the focus has been on routes that can be programmed into the Flight Management System(FMS). To create more lateral freedom while improving the navigational accuracy, area navigation (RNAV) has been introduced [9, 19, 20]. The main advantage of RNAV is that it results in reduced flight track dispersion and more realistic optimized routes. Another result of including RNAV is that the routes have a slight decrease in environmental performance, compared to their non-RNAV routes, due to the straightening of the lateral flight path. This reduction can be minimized by increasing the number of way points in the trajectory. The major disadvantage of increasing the number of way points is that the complexity of the RNAV route will increase.

From the studies described above it can be concluded that noise abatement procedures do have a beneficial effect on reducing the number of people affected by noise. Usually individual existing routes are modified to noise abatement routes. However there is still a possibility that implementation of a newly generated route is not feasible, because it interferes with other existing routes. In this research the problem is approached by combining trajectories, like arrival and departure trajectories, while keeping other terminal operations in mind.
When combining routes a minimum distance between the trajectories needs to be ensured. This protective zone around the aircraft in which no other aircraft is allowed to fly has been discussed in the field of air traffic management and is called minimum separation constraint. When an other aircraft is flying through this protective zone a loss of separation occurs[21]. For this research this minimum separation constraint is used as guidance to assure that no loss of separation will occur.

To discover what the influence is when optimizing trajectories while taking other terminal operations into account the research objective of this thesis is "To assess the effect of existing terminal operations on the environmental and economic impact of procedures optimized using a multi-objective genetic algorithm whilst taking into account separation and procedure design regulations". The research question of this thesis is stated as "What will be the effect of terminal operations on the environmental and economical impact of optimized routes compared to separate arrival and departure routes?"

This report starts with the explanation of the literature study behind the design of RNAV trajectories. In Chapter 3 the aircraft model is described which also includes a description of how and why the parameters are normalized and how the minimum separation constraint is implemented. The aircraft model is verified and validated in Chapter 4 and in Chapter 5 four case studies are described which use the designed aircraft model. The conclusion and recommendation on this research are stated in Chapter 6.

2

Literature review

Before the aircraft model is discussed and results of the case studies are shown first the theory is explained on which the model is based. The trajectory has to be designed while keeping some rules in mind. Next the method that is used to optimize the optimization problem is described and finally the theory behind the noise measurement for this thesis is explained.

2.1. Trajectory design

When an aircraft is flying from one airport to another airport the main part of the flight is en-route i.e., the part between the departure and arrival procedure. At this part of the flight the aircraft uses its Flight management system (FMS) using waypoints to navigate. When an aircraft is descending and arriving at the terminal area of the arrival airport the pilot contacts the Air Traffic Control (ATC) and the controller often vectors the aircraft all the way to the runway. This results in a lot of communication over the radio between the pilot and ATC and there is a diversity between the trajectories. To reduce the problems above, area navigation (RNAV) is introduced. RNAV routes are trajectories or legs between pre-determined waypoints in the terminal area. Every aircraft departing or arriving at an airport and flying an RNAV route will fly the same trajectory. The design of an RNAV trajectory should comply with the guidelines and rules established by ICAO [3] and Eurocontrol [22].

2.1.1. Leg types

The design of RNAV routes is done by using legs with specified characteristics. Out of the many leg types that exist, RNAV route design in terminal area only uses three types, namely the Initial Fix (IF), Track to a Fix (TF), and the Radius to a Fix (RF) [2].
The IF leg is defined as a point in space, a waypoint. It is not a track itself but is used to define the beginning of a route or procedure. The TF leg is used to connect two waypoints, which is why it is also called a point-to-point leg, as shown in Figure 2.1. This type is preferred for straight legs of a route.

Figure 2.1: Track to a Fix or TF leg segment [2]

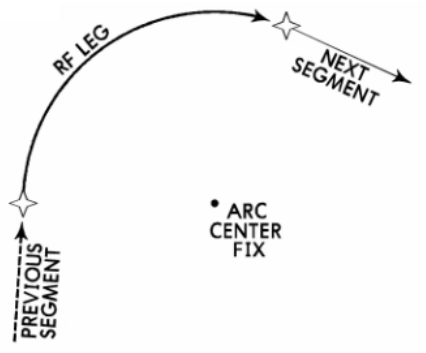

Figure 2.2: Radius to a Fix or RF leg segment [2]

The Radius to a Fix (RF) leg is used for making a turn in a route. It defines a constant radius turn between two waypoints. The flight path is tangent to the arc and the turn has a centre fix. RF guarantees that all aircraft will fly the same turn.

2.1.2. Departure

For every departure route obstacle clearance should be ensured. The guidelines to ensure this safety measure can be divided into a horizontal and vertical profile.

Vertical plane

The departure procedure starts at the Departure End of the Runway (DER) which represents the end of the area declared for take-off. The DER is not always the end of the runway, it can also be the point where the clearway is provided. From the DER, the Obstacle Identification Surface (OIS) is defined. This surface starts 16ft above the DER and has a gradient of 2.5%. The DER and OIS slopes are shown in Figure 2.3.

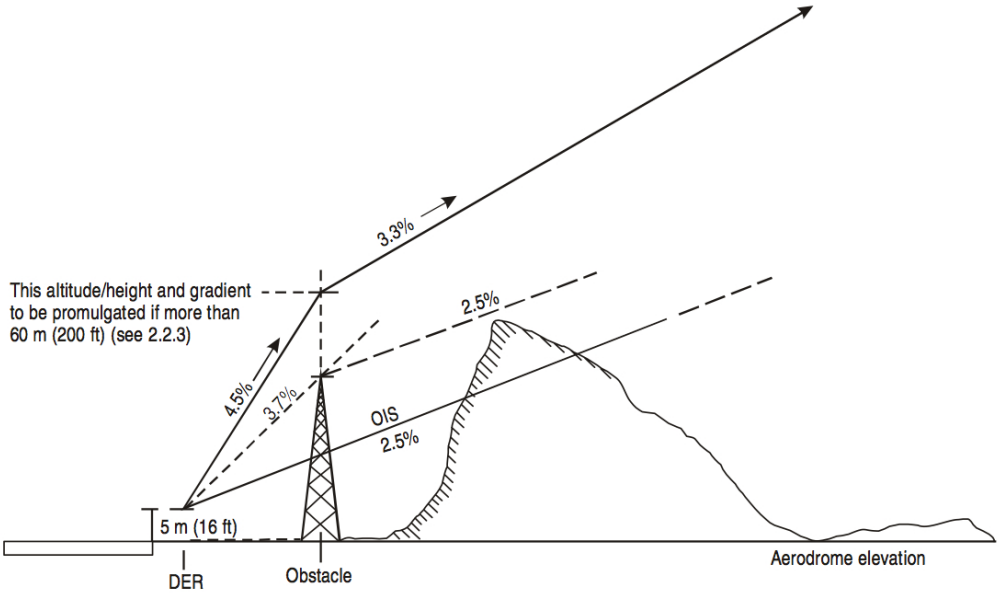

Figure 2.3: Procedure design gradient [3]

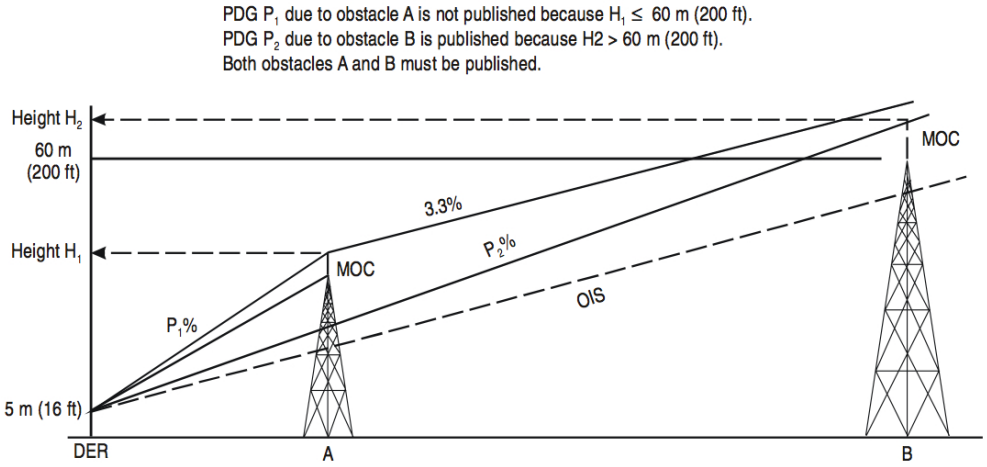

Figure 2.4: Close-in obstacles [3]

When there is no obstacle penetrating the OIS, the Procedure Design Gradient (PDG) is measured from the OIS origin and is calculated as the OIS gradient plus 0.8% Minimum Obstacle Clearance (MOC), which results

in a standard PDG of 3.3%. When the OIS is penetrated the PDG should be adjusted to avoid the obstacle. In the example Figure 2.3, the obstacle (a power pole) is penetrating the OIS and it has a gradient of 3.7% from the DER. With an extra 0.8% MOC this results in a PDG of 4.5%. When the aircraft has passed the obstacle the PDG may be reduced to the standard PDG of 3.3%. For obstacles lower than 200ft the required higher PDG does not have to be published but the obstacle itself should. When the obstacle is higher than 200ft the obstacle and required PDG should be published (see Figure 2.4).

Not only the PDG is a rule established by ICAO [3]. In this thesis the focus is on reducing noise, which means that for the departure route a noise abatement procedure is used. There are two different procedures, noise abatement departure procedure 1 (NADP 1) (see Figure 2.5) and noise abatement departure procedure 2 (NADP 2) (see Figure 2.6). If the first procedure type, NADP 1, is used, the focus is on reducing the noise for noise-sensitive areas close to the runway. With NADP 2 the focus is more on the noise reduction for areas further away from the runway.

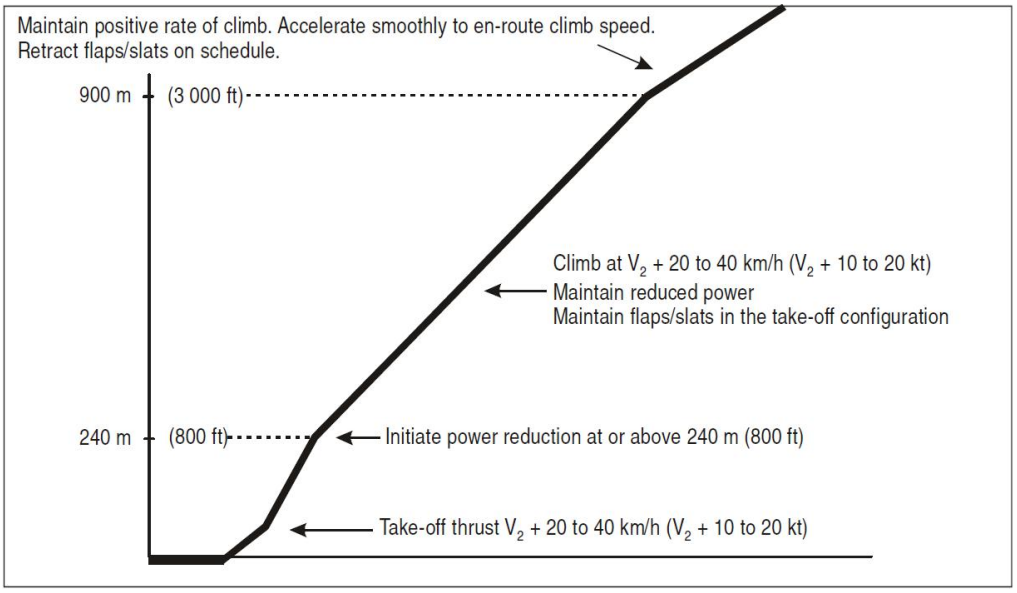

Figure 2.5: Noise Abatement Departure Procedure 1[3]

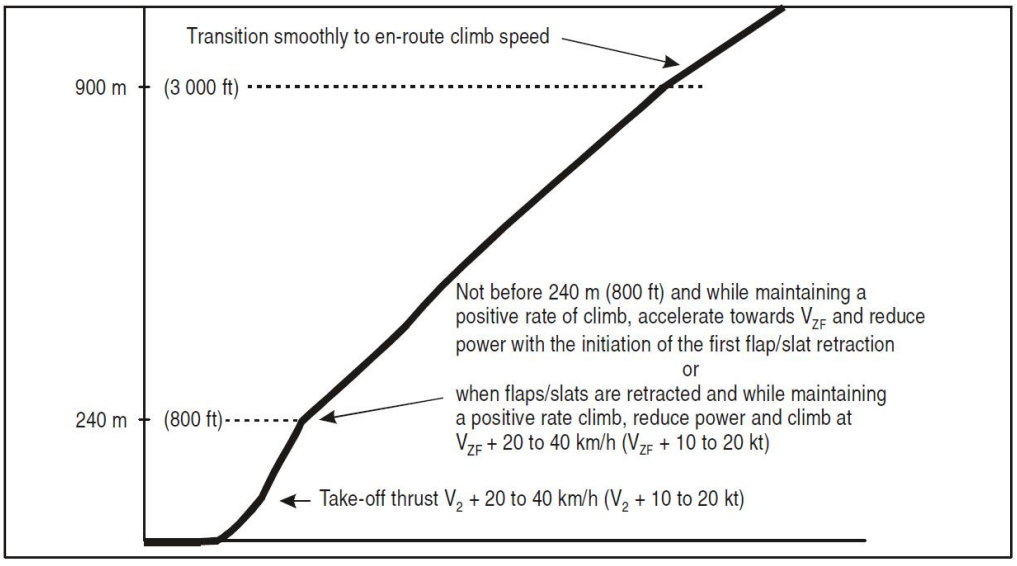

Figure 2.6: Noise Abatement Departure Procedure 2[3]

When flying the NADP 1 the aircraft starts with take-off thrust and a constant initial velocity of $V_2 + 10$kts until

it reaches a height of at least 800ft. At 800ft the thrust is reduced to climb thrust and with a constant velocity of $V_2 + 10$kts the aircraft climbs to a height of 3000ft. From this height the aircraft will continue with a positive flight path angle and the velocity is smoothly increased to en route climb speed.
The NADP 2 has the same start as the NADP 1, taking off with take-off thrust and a constant velocity of $V_2 +$ 10kts until at least 800ft. At 800ft again the thrust is reduced to climb thrust but at this moment the aircraft is allowed to accelerate, which means that the aircraft is no longer flying at its maximum flight path angle. Depending on the flight path angle the aircraft is climbing and accelerating. The aircraft transits to a smooth en-route climb speed and flight path angle when either a height of 3000ft is reached or the clean velocity of $V_{ZF} + 10$kts is reached.

Horizontal plane

In the horizontal plane, two types of departure can be distinguished; a straight departure, when the turning angle is less than 15°, and a turning departure. This turning angle is determined between the centreline of the runway and the first waypoint.
For the conventional turning departure the heading change can vary between 5° and 120°. When flying RNAV, the maximum heading change can be increased to 300° when using a constant RF.
When looking at the horizontal profile, the first restriction is that the aircraft should maintain the runway direction up to an altitude of 394ft above the Final Approach and Take Off area (FATO). This results in an absolute altitude of 410ft when the FATO is coinciding with the DER. When using a PDG of 3.3%, the first turning point should not be closer than 1.9 nautical mile (NM) to the DER. When the PDG is increased, the first turning point can be closer to the DER.

The second restriction has to do with the maximum allowed bank angle. The bank angle is limited as a function of the altitude, as follows:

- 15° below 1000ft
- 20° from 1000ft to 3000ft
- 25° from 3000ft and onwards

When an obstacle is present, the maximum bank angle is limited. In this case the bank angle should not be larger than 15°, unless an obstacle clearance of 295ft is achieved.

2.1.3. Arrival

The approach procedure should be executed within 9 waypoints starting from the initial approach point until the waypoint that concludes the missed approach leg. As can be seen in Figure 2.7 the approach procedure consists of the following 5 legs:

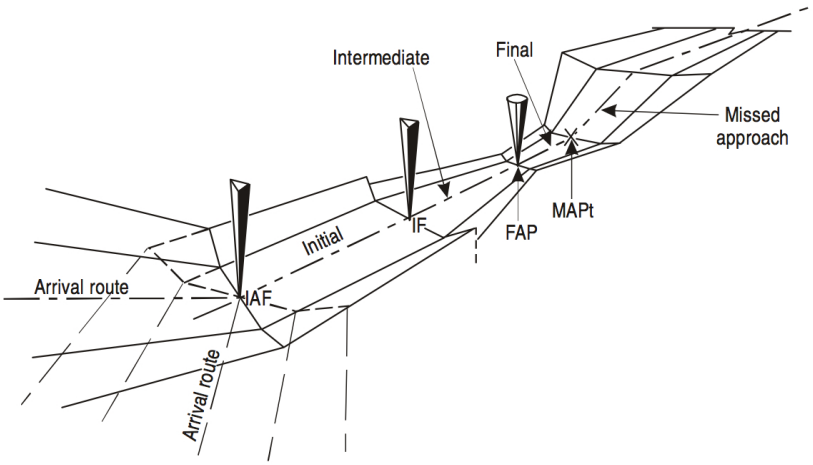

Figure 2.7: Legs of an instrument approach route [3]

- The approach starts with the **arrival leg**. This leg starts at the en-route structure and ends at the Initial Approach Fix (IAF).
- The **initial approach leg** starts at the IAF and ends at the Intermediate Fix (IF).
- The **intermediate approach leg** starts at the IF and ends at the Final Approach Fix (FAF). At the end of this leg the aircraft is lined up with the centreline of the runway.
- The **final approach leg** starts at the FAF and ends at the Missed Approach Point (MAPt).
- The **missed approach leg** starts at the MAPt and ends at the point at which a new approach, holding or return to en-route flight can be initiated.

Leg length

For each leg described above, the following guidelines concerning the length are given [22]:

- For the initial approach leg the optimal length is 5 NM. The maximum length is not specified and the minimum length depends on the required descent gradient.
- For the intermediate approach leg the minimum length should be 2 NM, so the aircraft can stabilize before the FAF waypoint is reached. A turn at the IF is allowed, which will result in increasing the leg length due to the stabilization distance needed after the turn. The optimal length is 5 NM. It is recommended not to use an intermediate leg that is longer than 8 NM.
- The final approach leg has an optimal length of 5 NM and it should not exceed 10 NM. The minimum distance allows the aircraft to meet the required descent rate and to regain course alignment when a turn is required over the FAF.

Vertical profile

In the vertical direction the following constraints are encountered for selected segments [22]:

- For the initial approach segment the optimal descent gradient is 4%. This can be increased if needed, to ensure obstacle avoidance. The maximum descent gradient is 8%. The Minimum Obstacle Clearance (MOC) should be at least 984 ft.
- The intermediate approach segment should have a descent gradient of 0%. If the aircraft should descent, a maximum gradient of 5% is allowed. The final part of the intermediate approach segment should have a horizontal path of 1.5 NM for aircraft category C and D and 1.0 NM for aircraft category A and B, to allow the pilot to prepare its speed and configurations for entering into the final approach segment. The MOC in this segment should be at least 492 ft.
- For the final approach segment the optimal descent gradient depends on the glide slope angle and is equal to 3.0°. The minimum descent gradient is 2.5°. The maximum descent gradient depends on the aircraft category. For category C and D it is 3.5° and for category A and B it is 3.77°. For ILS-CAT II and ILS-CAT III precision approach the maximum descent gradient is equal to 3.0°. The MOC for straight-in approach where the tracking angle is $\leq 5°$ is equal to 246 ft.

2.2. Optimization Method

Many types of numerical methods exist for solving trajectory optimization problems. The two methods discussed from the example papers in the introduction chapter, evolutionary algorithm and optimal control-based method, will be compared in this section. The main difference between these methods is that optimal control-based algorithms use gradient information to converge to a local minimum quickly, whereas evolutionary algorithms in a smart way search the entire feasible region, without gradient information.
Using an evolutionary algorithm (EA's) will result in a higher probability to find the global optimum compared to optimal control-based methods because of the stochastic behaviour of EA's. When an optimization problem consists of multiple objective functions, a multi-objective function problem, with EAs the functions do not have to be combined into a smooth function. Also, when a multi-objective function problem is optimized it results in a set of optimal solutions. The biggest disadvantage of EA's is the high run time before the

algorithm converges to an optimal solution [23].

The main advantage of optimal control-base methods is, that they converge to an optimal solution much faster than EA's. A disadvantage of optimal control-base methods is that in a multi-objective function problem, the objective functions must be combined to one smooth function. Also due to using gradient information the search space is fast decreased. This means that the probability of finding a local minimum is increased. Finally implementing constraints is much more work when using a optimal control-based method compared to EA's [24].

For this research it is chosen to use an evolutionary algorithm to optimize the trajectory problem. In the sections below the basic theory on evolutionary algorithms is described as well as the EA that is used in this research.

2.2.1. Evolutionary Algorithm

The optimization method used in this research is based on mimicking the evolution of species and the survival of the fittest and is called an evolutionary algorithm [25]. An evolutionary algorithm is used to search for the best solution in a search space; the minimum solution. EAs are stochastic algorithms, which means they use randomness to produce solutions that are evolving toward the optimal solution.
A simple EA starts with generating a number of random designs representing each design from the search space as a chromosome. For each chromosome the fitness function is determined. The fitness shows how good the solution is, and the designs with the highest fitness are used for reproduction. Also the reproduction operators have to be determined. These operators are directly applied on the chromosomes and are used to perform mutation or recombination of a possible solution [25].
To optimize a problem the EA uses iterations to evolve the population. The steps followed at each iteration are expressed below:

- Selection: the first step is to determine which chromosomes will be used for reproduction. This is done randomly, with a probability that depends on the relative fitness of the individuals. This means that the best chromosomes are most likely to be used for reproduction.
- Reproduction: The second step is generating offspring from the selected individuals. For the generation of new chromosomes EA can use recombination and mutation.
- Evaluation: In the third step the fitness of the new chromosomes is evaluated.
- Replacement: The final step of the iteration is removing individuals - usually the least fit - from the old population and replacing them with new ones.

The iteration is finished when the solution is converging toward an optimal solution. The initial population of chromosomes should be as diverse as possible to obtain a wide initial search space. Good representations and reproduction operators are the basics for the good behaviour of a EA.

Evolutionary algorithms can also be used for multi-objective functions. The advantage of multi-objective evolutionary algorithms (MOEA's) compared to optimal control methods is that they are more robust. Also MOEAs are able to generate multiple trade-off solutions in a single run [23].
A multi-objective optimization problem is expressed in number of objectives and potentially includes a number of equality and inequality constraints. The solution of a multi-objective optimization problem is expressed in terms of non-dominated or superior points. A solution is called a non-dominated solution when no improvement is possible in any objective without sacrificing at least one of the other objectives. The optimal solutions of a multi-objective optimization problem are the non-dominated solutions or Pareto-optimal solutions as can be seen in Figure 2.8[23].
In the world of MOEA's there are two different classes, the non-Pareto-base and Pareto-based MOEA's. Again, the Pareto-based methods the algorithms can be divided into non-elitist and elitist MOEA's. Non-elitist MOEA's do not keep the non-dominated solutions that are generated, which can result in losing them after applying the evolutionary operators. A popular non-elitist MOEA is the Non-dominant Sorting Genetic Algorithm (NSGA)[23].

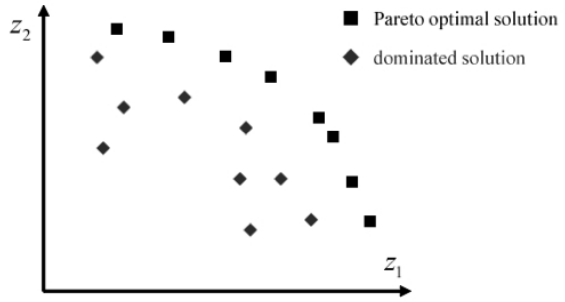

Figure 2.8: Pareto optimal solutions (maximization case)[4]

2.2.2. NSGA-2

The Non-dominant Sorting Genetic Algorithm II (NSGA-2) is one of the most popular elitist MOEA. The NSGA-2 is an improvement of the NSGA because compared to the NSGA the NSGA-2 does keep the non-dominated solutions. With this method not only the fitness functions of the individuals are compared with each other on dominance, but also the density of the solutions around a particular solution is estimated by determining the average distance between two points on either side of the solution along each of the problem objectives. This is called the crowding distance. When two solutions have the same non-dominance ranking, the one that resides in the least crowded region is preferred for the next generation [5].

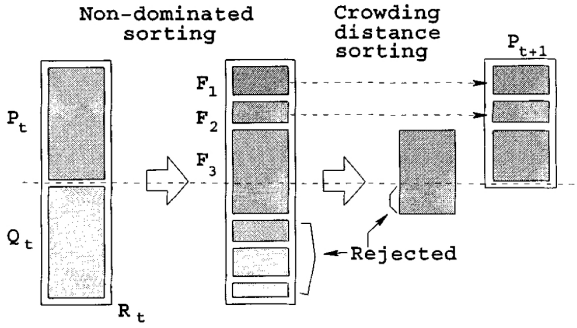

Figure 2.9: NSGA-II procedure [5]

The procedure of the NSGA-II algorithm is simple and straightforward as shown in Figure 2.9. It starts with a population of the size 2N, R_t, which exists of the current population P_t, and the new population Q_t, which is created by selection, crossover and mutation of P_t. This population, R_t, is then sorted according to non-domination. The new population, P_{t+1}, is then filled with the obtained groups of non-dominated solutions, starting with the best non-dominated set. When a set is bigger than the remaining space in the new population the remaining members are chosen by using the crowded comparison operator and the new population is filled with the last members until it is full. The new population P_{t+1} is then used for selection, crossover and mutation to create a new population, Q_{t+1}, of size N [5].

2.3. Noise

Noise impact reduction is one of the objectives of this research. The optimization of the model will be a balance between minimizing the fuel used during the flight and the number of people that wake up during a single fly over. This section will start by introducing how noise is measured and processed. Secondly the noise model that will be used in this thesis will be discussed. Finally, the method to determine the expected number of awakenings (people disturbed) will be specified.

2.3.1. Noise measurement

Noise is an unwanted sound, representing a vibration generated by a source (an aircraft in this case) which travels via the atmosphere and is observed by an observer [26].

To better quantify aviation noise and specifically to quantify the noise taking into account the specific characteristics of the human ear, weighting filters are applied. These weighting filters are based on the findings of a large number of listeners indicating the perceived loudness of a sound level in a specific frequency. Based on these loudness levels (see Figure 2.10) weighting filters have been developed to correct the raw noise measurement for the sensitivity of the human ear. Specifically for aviation noise the A-weighting filter is applied, which can be seen in Figure 2.11 [7].

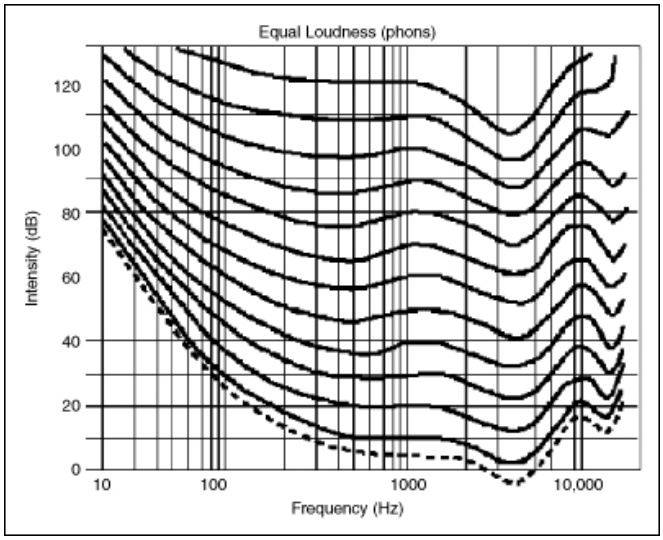

Figure 2.10: Equal loudness contours [6]

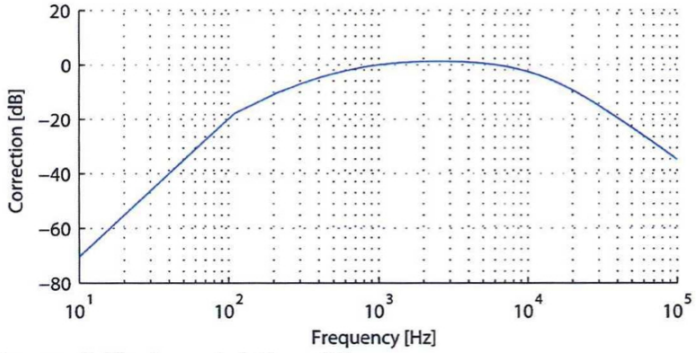

Figure 2.11: A-weight filter [7]

The A-weighting filter is based on the inverted 40 phon contour. This filter is used to reduce the impact of frequencies that are considered less effective on the human ear. For a given frequency band, the maximum A-weight sound level $max(L_A)$ is:

$$max(L_A) \approx 10\log_{10}\sum 10^{\frac{L_A(t)}{10}}, \tag{2.1}$$

where $L_A(t)$ is the instantaneous A-weighted sound level in dBA.

In terms of the impact on the human environment, apart from noise levels to which humans are exposed, the duration of exposure also has a significant impact on the perception of noise. To account for this, the A-weighted sound level can be integrated over time to obtain the Sound Exposure Level (SEL) measured in dBA, see Equation 2.2.

$$SEL = 10\log_{10}\left[\frac{1}{t_1}\int_0^{t_f} 10^{\frac{L_A(t)}{10}}\,dt\right], \tag{2.2}$$

where, t_f is the total exposure time at the specified location in seconds and t_1 is the reference time (one second).

2.3.2. Noise model

To estimate the SEL at a specific observer location around the airport, a computer based noise prediction model is used. There are a few models available and the one used in this case has been designed by the Federal Aviation Administration (FAA) and is called Integrated Noise Model (INM). The reason for the use of INM is that it has become a standard tool for noise impact assessment [26].
INM uses a flight path represented as a sequence of straight-line segments of finite length to model the movement of an aircraft in 3D. INM determines the distance between the aircraft and an observation point. From the Noise-Thrust-Distance (NTD) table, the corresponding sound level is determined at the specified observer location. The NTD is a database, which contains the noise exposure level for specific reference conditions for each aircraft type [26].
The reference conditions on which the NTD tables are based assume an infinitely long segment directly overflying the observer at a constant airspeed of 160 knots. To determine the noise levels in non-reference conditions, three corrections need to be applied to the NTD tables [7]:

- To accommodate for finite length segments the noise-fraction adjustment is applied.
- To account for non-reference speeds the duration adjustment is applied.
- To account for observer situated astride the flight path, the lateral attenuation adjustment is applied.

2.3.3. Relation between aircraft noise and awakening

Although the noise model described above can be used to determine the sound levels in a number of observer locations, an additional step is required to determine the impact on near-airport communities and as such to define a single optimization criterion to be included in this study. One possible approach is to determine the total number of expected awakenings due to a single night time fly over.

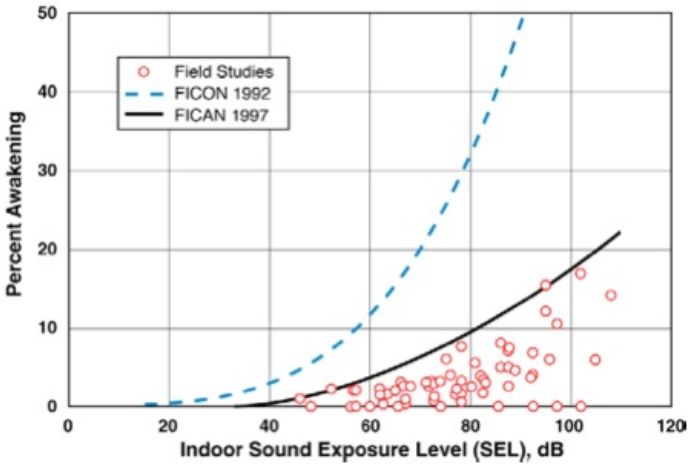

Figure 2.12: FICON SEL-awakening relationship [8]

The relation between aircraft noise and the percentage of people awakening from a flyover was initially proposed by the Federal Interagency Committee on Aviation Noise (FICAN) in 1992 and later updated in 1997 [8] (see Figure 2.12). The first curve (FICON 1992) was obtained by laboratory studies. The update consisted of including field data, which was gathered from different studies around several airports. The maximum percentage of the exposed population expected to be behaviourally awakened, as represented by the FICAN 1997 curve is given by:

$$\%awakening = 0.0087 \cdot (SEL_{indoor} - 30)^{1,79} \tag{2.3}$$

In Equation 2.3 the awakenings represent the percentage of people that will wake up due to noise of an aircraft and SEL_{indoor} represent the SEL inside a house in decibels (dB). The SEL_{indoor} is determined by reducing

the outdoor SEL that is determined by the INM noise model by 20.5 dB. Finally when the distribution of the density of the population around the airport is known, the absolute number of people that is awakened can be determined [17].

2.4. Conclusion

As can be concluded from this chapter the aircraft model that will be designed needs to implement the RNAV rules and guidelines designed by ICAO. The RNAV route will consist of straight legs and turns with a fixed radius. The departure trajectory starts with the noise abatement departure procedure. There are two types procedures available, viz. NADP-1 and NADP-2. Depending on the focus, reducing the noise for noise-sensitive areas close to or further away from the runway, one of the two procedures is used. For the vertical profile of the departure trajectory the turn radius is limited by the altitude and velocity of the aircraft at the beginning of the turn.
For the arrival route the most important ICAO rule used is the 1.5NM level flight with constant speed before the trajectory intercepts the ILS. This level flight is introduced to give the pilots enough time to do the final checks before the final descent is started.

For the optimization method there are two types of methods that can be used, evolutionary algorithms and optimal control-based methods. For this thesis an evolutionary algorithm (EA) is used that can evaluate multiple objective functions. The reason for this is twofold, firstly the when using EAs the resulting Pareto front includes multiple optimal solutions and secondly, it is more robust when it comes to using multiple objective functions.

Finally, one of the objective functions was discussed, the noise impact of the flyover on the population living around the designed trajectory. A standard tool used to calculated the noise impact is called Integrated Noise model (INM) and from this tool the Sound Exposure Level (SEL) is measured created by the aircraft. Knowing the population density around the trajectory and using an dose-response relationship designed by the FICAN the absolute number of people getting disturbed by the flyover can be determined.

In the next chapter the design of the aircraft model will be discussed using the literature reviewed in this chapter.

3

Aircraft model

The theory explained in Chapter 2 is used as a basis to define the aircraft model. This chapter starts with the equations of motions. This is a set of differential equations to simulate the aircraft. Secondly, the design of the vertical and horizontal trajectory is discussed. Next the solver of the equations of motion and the method used to combine multiple routes while keeping the minimum distance constraint in mind will be discussed. Finally, the noise model and optimization algorithm are explained and in the conclusion some limitations to this model are discussed.

3.1. Equations of motion

The aircraft performance model is defined as a point-mass model. The assumptions included in this model are 1) there is no wind vector present, 2) the earth is flat and non-rotating and 3) the flight is coordinated. Also the flight path angle is considered sufficiently small ($\gamma < 15°$)[9].
The equations of motion consist of the following differential equations [9]:

$$\dot{V}_{EAS} = g_0 \cdot \frac{T - D - W \cdot sin(\gamma)}{W} + \frac{1}{2 \cdot \rho} \cdot \frac{\delta \rho}{\delta h} \cdot V_{TAS}^2 \cdot sin(\gamma), \tag{3.1}$$

$$\dot{h} = V_{TAS} \cdot sin(\gamma), \tag{3.2}$$

$$\dot{s} = V_{TAS} \cdot cos(\gamma), \tag{3.3}$$

$$\dot{W} = -ff \cdot g_0. \tag{3.4}$$

The equations of motion include the derivatives of the equivalent velocity, $\dot{V}_{EAS}$, altitude, $\dot{h}$, distance flown, $\dot{s}$ and weight, $\dot{W}$. Due to the low altitude the equivalent velocity, V_{EAS}, is serving as an approximation of the indicated velocity. The derivatives of the velocity, altitude and distance flown are calculated with the true velocity, V_{TAS}, as can be seen in Equation (3.1), (3.2), and (3.3). The true velocity can easily be calculated from the equivalent velocity by using Equation (3.5). In this equation ρ_0 is the air density at sea level and ρ is the ambient air density.

$$V_{TAS} = V_{EAS} \cdot \sqrt{\frac{\rho_0}{\rho}} \tag{3.5}$$

The thrust, T, fuel flow, ff, and drag, D, of the equations of motion are determined by an aircraft specific model. The $\frac{\delta \rho}{\delta h}$ is determined from the standard atmosphere, ISA.

The aircraft performance model has two control variables: the flight path angle and thrust setting, u=[γ Γ], and four state variables x=[V_{EAS} h s W].

3.2. Vertical trajectory

The trajectory can be divided into a vertical and horizontal part and both parts are evaluated independently. This section starts with how the input parameters are normalized to increase the probability of feasibility of the trajectory. Secondly the energy deficit is explained, this is used to stimulate the trajectory to achieve its final conditions.

3.2.1. Normalized parameters

The vertical trajectory is divided into a number of segments, N. For each segment the flight path angle, γ_i, and thrust, T_i, is constant. From the ICAO rules it can be concluded that when an aircraft is departing it is only allowed to climb or fly horizontally, so $\dot{h} \geq 0$, and maintain velocity or accelerate, $\dot{V}_{EAS} \geq 0$. This sets boundaries to the flight path angle, γ, and the thrust, T, required. The boundary conditions of the flight path angle and thrust depend on numerous factors, such as local airspeed and altitude, which means that the boundary conditions can not be kept constant during the flight, as this could result in a flight situation which does not agree with the ICAO rules stated above. For instance when the aircraft is flying at its maximum flight path angle but the thrust is idle the aircraft probably will not be able to maintain its velocity and altitude.
To keep the results feasible and to reduce the number of input parameters the thrust and the flight path angle are normalized, $\Gamma_{n,i}$ and $\gamma_{n,i}$ and the boundaries are determined every time the equations of motion are solved. The method described in this section is based on the normalization of parameters as described in Hartjes[9].
As already stated the constraints for the departure route are $\dot{V}_{EAS} \geq 0$ and $\dot{h} \geq 0$. With these constraints it follows that the minimum climb angle, γ_{min}, is equal to 0°. From the aircraft specific model the maximum thrust, T_{max}, is derived. By assuming that at maximum thrust $\dot{V}_{EAS} = 0$, and rewriting Equation (3.1) the maximum climb angle, γ_{max}, can be derived:

$$\gamma_{max} = \sin^{-1}\left(\frac{-2 \cdot \rho \cdot g_0 \cdot (T_{max} - D)}{W\left(\frac{\delta\rho}{\delta h} \cdot V_{TAS}^2 - 2 \cdot \rho \cdot g_0\right)}\right). \tag{3.6}$$

With a value for γ_{min} and γ_{max} and a given $\gamma_{n,i}$, the flight path angle for this segment, γ_i, can be derived:

$$\gamma_i = (\gamma_{max} - \gamma_{min}) \cdot \gamma_{n,i} + \gamma_{min}. \tag{3.7}$$

For the thrust the only unknown left is the T_{min}. The T_{min} depends on the flight path angle γ_i, because the aircraft should at least maintain its airspeed. This means that again the assumption $\dot{V}_{EAS} = 0$ is used and Equation (3.1) is rewritten as shown below:

$$T_{min} = D - \left(\frac{W}{2 \cdot \rho \cdot g_0} \cdot \frac{\delta\rho}{\delta h} \cdot V_{TAS}^2 \cdot \sin(\gamma_i)\right) + W \cdot \sin(\gamma_i). \tag{3.8}$$

Now the upper and lower bound of the thrust have been obtained the actual thrust setting is determined using the normalized thrust setting $\Gamma_{n,i}$:

$$T_i = (T_{max} - T_{min}) \cdot \Gamma_{n,i} + T_{min}. \tag{3.9}$$

When the aircraft arrives at its final altitude, h_{max}, or velocity, $V_{EAS,max}$, the normalized input parameters are overruled. This means that when the final altitude is reached $\gamma_{n,i}$ becomes zero, which means the aircraft will start maintain constant altitude. When the final velocity is reached the normalized thrust setting, $\Gamma_{n,i}$ will be reduced to zero. This means that the thrust generated by the aircraft will be equal to the minimum required thrust, T_{min}, and as such sufficient to maintain airspeed.

For the arrival the assumptions for $\dot{V}_{EAS}$ and $\dot{h}$ are swapped, so $\dot{V}_{EAS} \leq 0$ and $\dot{h} \leq 0$, which means that the aircraft is only allowed to descend and decelerate or keep its altitude or velocity. This changes the minimum and maximum value for the thrust and the flight path angle. From the aircraft specific model T_{min} is derived which is equal to the net idle thrust. From the constraints it can be derived that $\gamma_{max} = 0°$. Because the aircraft is not allowed to increase velocity when γ_{min} is flown at T_{min}, Equation (3.6) is used again but now γ_{max} becomes γ_{min} and T_{max} becomes T_{min}.
Now again γ_{max} and γ_{min} are known; with a given $\gamma_{n,i}$ and Equation (3.7), γ_i is derived. The only unknown left is T_{max}, again for the derived γ_i also the maximum thrust can be determined such that the aircraft maintain its velocity. This is done by using Equation (3.8) where T_{min} becomes T_{max}. With again the bounds of the thrust are known the actual thrust setting is determined using Equation (3.9).
Similarly in Section 3.3 normalisation is applied to the turning radius and in Section 3.5.3 the flight path angle will be normalized to assure minimum separation between inbound and outbound routes.

3.2.2. Energy deficit

When the optimization algorithm generates a chromosome, the input parameters may result in a solution where the final boundary conditions are not met. This for instance happens when at every segment a low flight path angle and thrust setting is chosen. To improve the probability that the aircraft is arriving at its final conditions a check on the energy deficit is introduced.
With the energy deficit it can be checked whether the total energy difference between the current state of the aircraft and its intended state is still smaller than the maximum energy the aircraft can produce, $T_{max} - D$, times the distance still to be flown, Δs:

$$\Delta E \leq (T_{max} - D) \cdot \Delta s \tag{3.10}$$

The total energy is a combination of the potential and kinetic energy. The total energy of the aircraft with its local conditions, h_i and V_i is defined as:

$$E_i = W_i \cdot h_i + \frac{W_i}{2 \cdot g_0} \cdot V_i^2 \tag{3.11}$$

$$E_{max} = W_i \cdot h_{max} + \frac{W_i}{2 \cdot g_0} \cdot V_{max}^2 \tag{3.12}$$

In Equation (3.11) W_i is the weight of the aircraft, h_i is the altitude of the aircraft and V_i is the velocity of the aircraft. After the total energy has been determined for the aircraft at local conditions, the total energy is also determined for the final conditions, with Equation (3.12). The difference between these two total energies gives the value for ΔE.
If the total energy difference becomes larger than the maximum energy the aircraft can gain times the remaining distance to be flown, the aircraft will be forced to start flying with maximum flight path angle and maximum thrust. With this method there is assumed that maximum thrust and drag are the same at local and final conditions. This is not true because the maximum thrust and drag decrease with altitude and this decreases the accuracy of this method.

For the arrival trajectory the aircraft should lose its energy surplus before arriving at its final boundary conditions. Again for the arrival trajectory the potential and kinetic energy are used for the local and final conditions and there is checked if this energy difference is smaller than the maximum energy the aircraft can lose, $D - T_{min}$. When the total energy difference becomes larger than the minimum thrust times the remaining distance to be flown the aircraft is forced to fly at minimum flight path angle and minimum thrust.
The accuracy of the energy surplus is less compared to the energy deficit. This is the result of the drag changes a lot when an aircraft is flying at low velocity. Even though the accuracy is reduced it is still not significant and this is why this method is used.

3.3. Horizontal trajectory

For the horizontal trajectory the rules and guidelines explained in Section 2.1.1 are used. This theory states that a RNAV route consists of a sequence of straight legs and turns with a fixed radius. To explain how the routes are derived in this research an example route is used that consists of two straight legs with a turn between them (see Figure 3.1). With the initial, $\mathbf{x}_0$, and final, $\mathbf{x}_f$, coordinates known there are only four unknowns left: two distances, L_1, L_2, the heading change, $\Delta\chi$, and the turn radius, R.
When two out of the four unknowns are given as input parameters the other two can be determine using vector calculus. The distance that will be flown when flying the turn, s_1, is calculated with:

$$s_1 = R \cdot \Delta\chi \tag{3.13}$$

In the next sections the derivation of the remaining unknowns is shown separately for the departure and arrival route.

3.3.1. Departure

For the departure distance L_1 and radius R are chosen as input parameters for the optimization algorithm, which leaves L_2 and $\Delta\chi$ to be determine analytically. As stated in Section 2.1.2 the first turn after take off is allowed when the aircraft is flying 394ft above Final Approach and Take Off area (FATO). This gives the value the minimum distance L_1 should have.

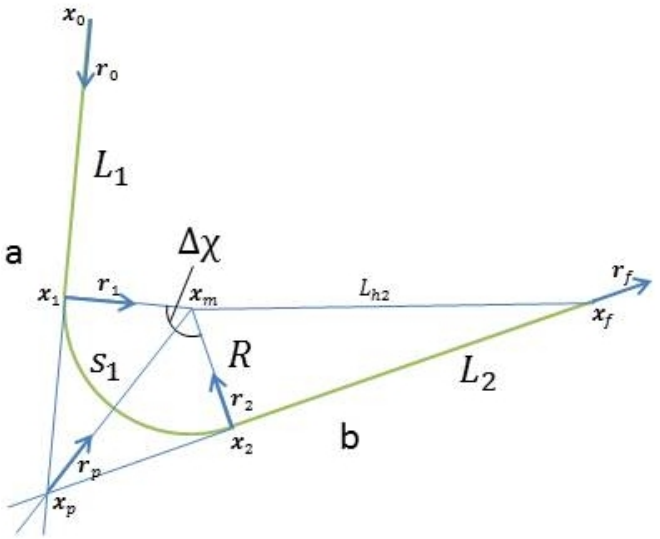

Figure 3.1: Trajectory in vector coordinates

For the turn radius ICAO has also given some rules as described in Section 2.1.2. These rules stated that the bank angle has a maximum value depending on the altitude the aircraft is flying at.

$$R = \frac{V^2}{g_0 \cdot \tan(\mu)} \tag{3.14}$$

As can be seen in Equation (3.14), the turn radius, R, depends on the velocity, V, and the bank angle, μ[9]. In Section 2.1.2 the maximum bank angle depends on the altitude at which the aircraft is flying. As such, the turn radius can only be determined once the aircraft has flown the first straight leg, L_1. At this point the velocity and altitude of the aircraft is known.
In order to ensure a range of feasible solutions, the turn radius needs to be normalized, R_n. This is done in a similar approach as for the vertical trajectory, as fixed boundary conditions may result in turn radii that do not comply with the ICAO regulations. With regards to the minimum boundary condition, the minimum turn radius, R_{min}, depends on the maximum bank angle corresponding to the given altitude and velocity at the beginning of the turn. The maximum boundary condition is the maximum achievable turn radius, R_{max}, which is depending on the velocity at which it is flying as can be seen in Equation (3.14). For the calculation of the maximum turn radius, a fixed bank angle of 5° is used.
Once the minimum and maximum allowed turn radii are computed, depending on the value of the normalized turn radius, the actual turn radius, R, can be computed as shown below:

$$R = (R_{max} - R_{min}) \cdot R_n + R_{min}. \tag{3.15}$$

Now the two input parameters, L_1 and R are known the two still unknown variables, L_2 and $\Delta\chi$, can be determined given that the initial, $\mathbf{x}_0$, and final coordinate, $\mathbf{x}_f$, and initial headings vector, $\mathbf{r}_0$, are also known. The final heading vector, $\mathbf{r}_f$, depends on the heading change.

$$\mathbf{x}_1 = \mathbf{x}_0 + L_1 \cdot \mathbf{r}_0 \tag{3.16}$$

$$\mathbf{r}_1 = \begin{bmatrix} -\mathbf{r}_0(2) \\ \mathbf{r}_0(1) \end{bmatrix} \tag{3.17}$$

$$\mathbf{x}_m = \mathbf{x}_1 + R \cdot \mathbf{r}_1 \tag{3.18}$$

$$L_{h2} = ||\mathbf{x}_f - \mathbf{x}_m|| \tag{3.19}$$

$$L_2 = \sqrt{L_{h2}^2 - R^2} \tag{3.20}$$

Now only $\Delta\chi$ should be determined. This is done by determine $\mathbf{r}_m$ which is the inverse of $\mathbf{r}_2$ in Figure 3.1.

$$\begin{bmatrix} R & -L_2 \\ L_2 & R \end{bmatrix} \cdot \mathbf{r}_m = (\mathbf{x}_f - \mathbf{x}_m) \tag{3.21}$$

$$\Delta\chi = \cos^{-1}(-\mathbf{r}'_m \cdot \mathbf{r}_1) \tag{3.22}$$

3.3.2. Arrival

For the arrival trajectory L_2 and R are used as optimization parameters. For L_2 instead of L_1 is chosen because because the ILS should be included in L_2. The L_2 consist of two parts, the distance that is needed to fly the ILS and added to that an extra 1.5NM because this is stated by ICAO, see Section 2.1.3. This extra distance will be flown with constant velocity and altitude so the pilot will have enough time to do the final checks before the ILS is intercepted. The ILS distance depends on the height the ILS will be intercepted, h_{ILS}. For this arrival it is assumed that the h_{ILS} is between 2000ft and 4000ft. The determination of L_2 is shown:

$$L_2 = \frac{h_{ILS}}{tan(3°)} + 1.5NM \tag{3.23}$$

For the arrival trajectory there is no maximum bank angle stated by the ICAO. But for this research there is assumed that a bank angle higher than 25° is not preferred.
The remaining unknowns, L_1 and $\Delta\chi$ can be determine with equations that are used to determine the departure trajectory.

3.4. 4^{th} order Runge-Kutta Integration Method

The equations of motion consist of four first order differential equations which are integrated over time. The fourth order Runge-Kutta integration method is used to integrate the equations of motion.
The fourth order Runge-Kutta integration method is based on the Euler method and has a fourth order error term. It is a method that has been used for many purposes and that is very robust [27].
For almost every trajectory the distance flown is specified, rather than the time, before the vertical trajectory is determined. To make the results more accurate it is chosen to exchange time for distance as the independent variable of the integration, as can be seen in Equation (3.24). This change resulted in more accuracy when it comes to the moment the aircraft starts making the turn and arriving at its final coordinates. The state variables change to x=[V_{EAS} h t W] and the equations of motion is solved for a iteration step ds.

$$\frac{d\bullet}{ds} = \frac{d\bullet}{dt} \cdot \frac{dt}{ds} = \frac{1}{V} \cdot \frac{d\bullet}{dt} \tag{3.24}$$

3.5. Combining routes

In the previous sections it was explained how the vertical and horizontal trajectory of the arrival and departure route are set up. In this section it will be explained how they are combined so they can be optimized simultaneously. The main problem in combining arrival and departure routes is that a minimum distance between the trajectories needs to be ensured, this is discussed in the first section. Next it is explained if two trajectories cross each other, intersection point, how this is determined. Finally the method used to ensure the minimum distance constraint is met during the optimization of the trajectories is discussed.

3.5.1. Constraint

In the Air traffic management (ATM) field a minimum separation constraint is used to assure a minimum distance between two aircraft. This minimum separation constraint is stated as a cylinder with the aircraft in the middle. This cylinder has a total vertical distance of 2000ft, so a 1000ft above and below the aircraft, and a horizontal diameter of 5NM [21].
For this thesis this ATM minimum separation constraint is used as guidance to assure that the combined trajectories will always keep its minimum distance. How this minimum distance constraint is implemented will be discussed in Section 3.5.3.

3.5.2. X- and Y-coordinates

As can be concluded from the equations of motion the location of the aircraft in x- and y-coordinates is not determined at every integration step as only the distance flown is known. This is because this information is not necessary for the vertical trajectory. By leaving the x- and y-coordinate calculations out of the equations of motion also the computation time decreases. To allow combining of the routes the x- and y-coordinates are important because knowing the horizontal trajectory, if present, the intersection point between two routes can be determined.

Keeping again the example trajectory in mind shown in Figure 3.1. For the first straight leg, L_1 the x- and y-coordinates are determined with the equations below:

$$x_i = \mathbf{x}_0(1) + s_i \cdot \sin\chi_0 \tag{3.25}$$

$$y_i = \mathbf{x}_0(2) + s_i \cdot \cos\chi_0 \tag{3.26}$$

The s_i is the total distance flown until that point, χ_0 is the initial heading angle of the aircraft, $\mathbf{x}_0$ is the initial coordinate at which the aircraft starts is route. Finally x_i and y_i are the x- and y-coordinate at the given distance s_i.

At the end of L_1 the aircraft starts its turn. At each position the heading angle change first has to be determined with Equation (3.27). Next the x- and y-coordinate can be determined as is shown below.

$$\chi_i = \chi_0 - \frac{s_i - L_1}{R} \tag{3.27}$$

$$x_i = \mathbf{x}_m(1) + R \cdot \sin(\chi_i + 90°) \tag{3.28}$$

$$y_i = \mathbf{x}_m(2) + R \cdot \cos(\chi_i + 90°) \tag{3.29}$$

In the equations above R is the turn radius, and $\mathbf{x}_m$ is the turn center, as can be seen in Figure 3.1. The equations for the final straight leg, L_2, looks almost the same as for the first straight leg, L_1 as can be seen in the equation below.

$$x_i = \mathbf{x}_2(1) + (s_i - L_1 - s_1) \cdot \sin(\chi_f) \tag{3.30}$$

$$y_i = \mathbf{x}_2(2) + (s_i - L_1 - s_1) \cdot \cos(\chi_f) \tag{3.31}$$

In the above equations $\mathbf{x}_2$ is the coordinate where the turn ends and the final straight leg starts (see Figure 3.1). The final heading angle, χ_f is the initial heading angle minus the heading change, $\Delta\chi$, and s_1 is the distance flown in the turn.

3.5.3. Flight path angle determination

To show the method that is used to ensure that the minimum distance constraint is met an example is given. Assume a situation where a departure and an arrival route are combined. From both routes the horizontal trajectories, in x- and y-coordinates (see Figure 3.2) are known. In this figure the departure route is in blue and takes off from the blue cross, at the left side of the figure, and flies to the red cross on the right side of the figure. The arrival route is in green and similarly to the departure flies from the blue cross to the red cross. From the ground trajectory it can be seen that both trajectories cross each other, which highlighted with the pink circle. For both trajectories the vertical altitude profile is also determined (see Figure 3.3 and 3.4).
Figure 3.3 shows the vertical trajectory of the departure route where the red cross indicates the interception location. When looking at the arrival route (see Figure 3.4) the red cross shows again the interception point. The red cross is at an altitude of 6000ft because that is the altitude the departure route is flying while crossing. Around this red cross a restricted area is created which meets the minimum distance constraint. As can be seen the arrival route is flying through the restricted area, which means a loss of separation occurs.

To make sure that the arrival route is flying around the restricted area the flight path angle should be adjusted. When the aircraft arrives around 20km before the restricted area the model starts to look if the minimum, γ_{min}, and maximum, γ_{max}, flight path angles should be adjusted such that the restricted area is avoided. In Figure 3.5 and 3.6 this adjustment of the flight path angle boundaries is shown. In both figures the red square represents the restricted area and the blue circle the remaining flight path angle range. When the situation in Figure 3.5 occurs γ_{min} becomes $-\alpha_1$ and when the situation in Figure 3.6 occurs γ_{max} becomes $-\alpha_2$. From the remaining flight path angle range the flight path angle of that segment, γ_i, is chosen with its normalized input parameter, $\gamma_{n,i}$.
When the restricted area is between the minimum and maximum flight path angle the situation is a little different. As in the previous figures in Figure 3.7 again the red square is the restricted area and the blue arc the remaining flight path angle range. As can be seen this new flight path angle range is divided over two regions of the original range. When the situation in Figure 3.7 occurs a new variable β is used to sum up the new flight path angle range as shown in the equation below.

$$\beta = -\gamma_{min} + \alpha_2 - \alpha_1 \tag{3.32}$$

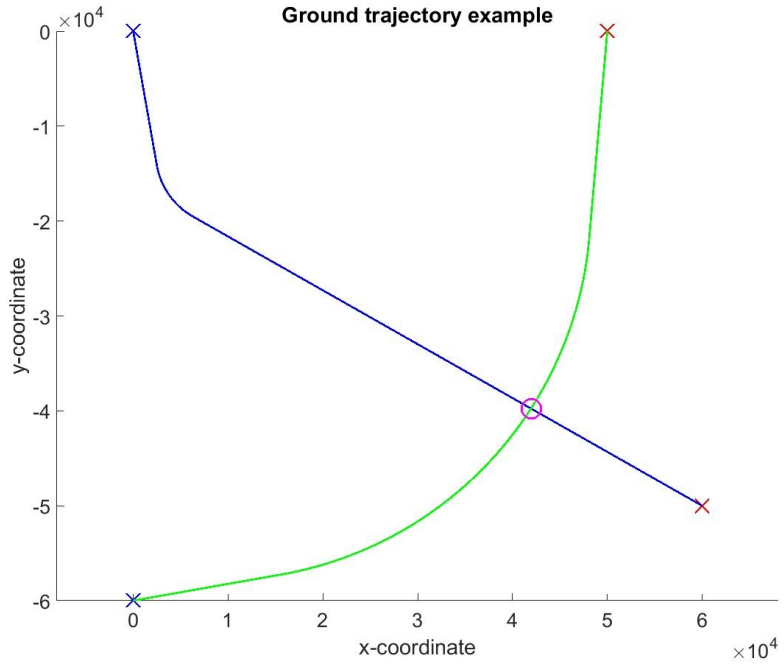

Figure 3.2: Ground trajectory of example arrival (green) and departure (blue) route

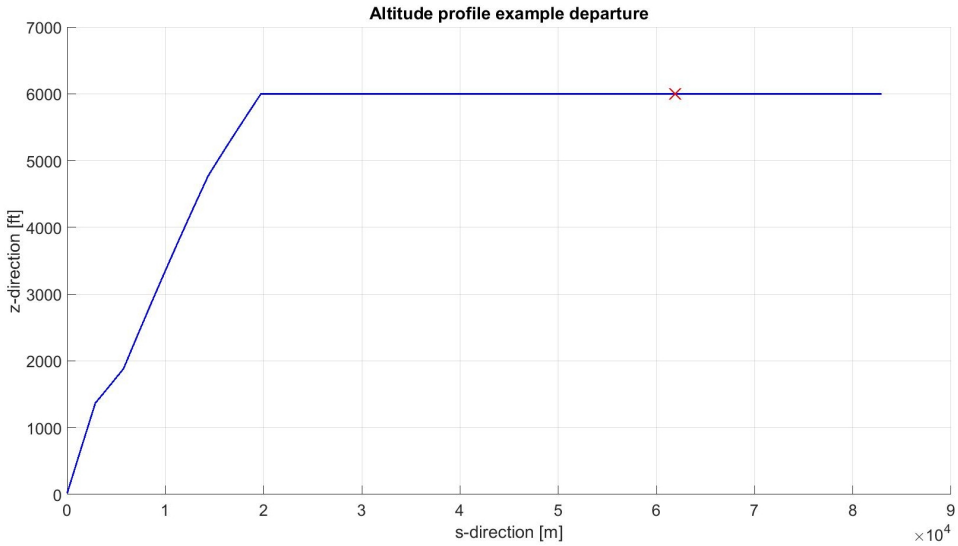

Figure 3.3: Altitude profile of the example departure route including interception point (red cross)

The next step is to determine the flight path angle the aircraft will fly over that segment, β_i as is show in the equation below.

$$\beta_i = \beta \cdot \gamma_{n,1} \tag{3.33}$$

Finally it should be checked whether this angle is located in the range of $-\alpha_1$ or on the other side of the restricted area. This is checked with a constraint:

$$\gamma_i = \begin{cases} \beta_i & \text{if } \beta_i \geq -\alpha_1 \\ \beta_i - \alpha_1 + \alpha_i & \text{if } \beta_i \leq -\alpha_1 \end{cases} \tag{3.34}$$

When using the method described above the arrival trajectory shown in Figure 3.4 is again determined. The resulting arrival route is shown in Figure 3.8. From this figure it can be seen that with this improved altitude profile the aircraft is flying around the restricted area.

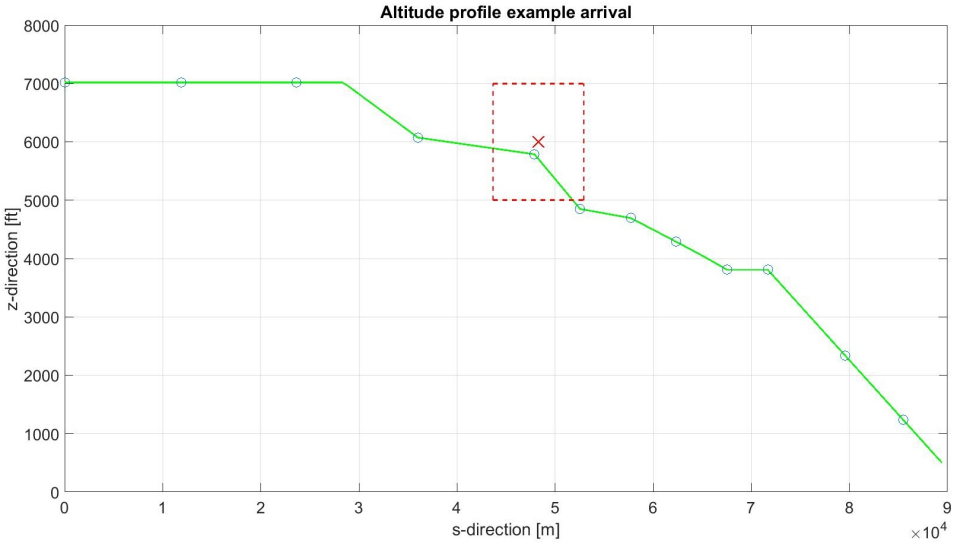

Figure 3.4: Altitude profile of the example arrival route including interception point (red cross) and restricted area

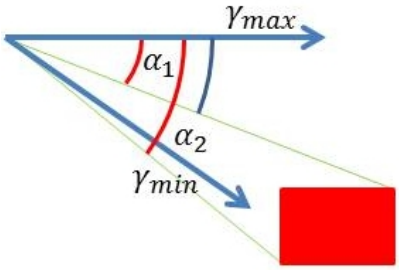

Figure 3.5: Adjustment of γ_{min}

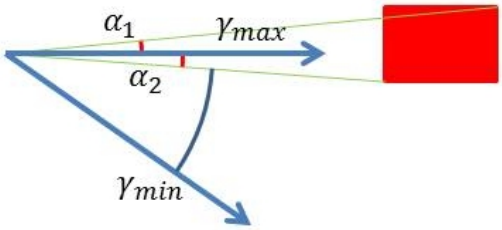

Figure 3.6: Adjustment of γ_{max}

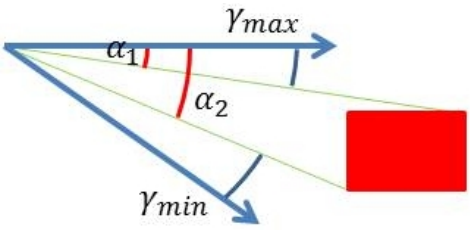

Figure 3.7: Restricted area between γ_{min} and γ_{max}

3.5.4. Final implementation

For the case study a departure and arrival trajectory will be combined. When generating the results of one chromosome the model starts with generating the horizontal and vertical plane of the departure trajectory. Next the ground trajectory of the arrival route is determined. Knowing the ground trajectory of both trajectories the intersection point is localized. If the intersection occurs, at this location in the vertical trajectory a restricted area is created. The middle of this restricted area is the altitude the departure trajectory has when cross the arrival route and the dimensions are 2000ft vertical and 5NM horizontally. Finally the arrival trajectory is determined keeping the restricted area in mind and if needed the flight path angle is adjusted to fly around it.

This order is chosen because the horizontal trajectory of the departure route is determined while generating the vertical trajectory. This is because the boundaries of the turn radius depends on the altitude and velocity when starting the turn and these are not known at front. The ground trajectory of the arrival route is determined independently of the vertical trajectory. This is possible because ICAO did not state a maximum bank angle for an aircraft in landing however, for this research a bank angle higher then 25° is not preferred. The bounds for the arrival turn radius are calculated op front by solving Equation (3.14) using the initial ve-

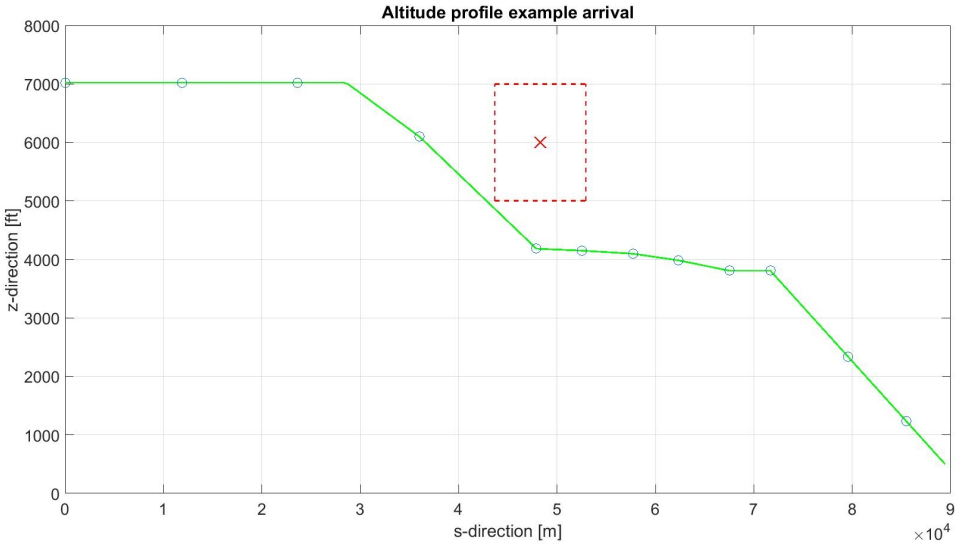

Figure 3.8: Altitude profile of the improved example arrival route including interception point (red cross) and restricted area

locity. This will result in a less accurate turn radius parameter bounds compared to the departure trajectory but this is neglected because the turns flown are all feasible and determine the arrival vertical and horizontal trajectory separately is needed to determine the intersection point.

3.6. Noise model

As already discussed in Section 2.3 noise is one of the objective functions for which the optimization needs to be solved. For this thesis a replication of the INM is used which is discussed in Section 2.3.2. This replication is named INMTM and calculates the noise exposure on a user-defined grid [28].
The input variables of this model consist of a number of location points, x- and y-coordinates, at which the altitude, velocity and the net corrected thrust per engine of the aircraft is determined by the equations of motion. The net corrected thrust is determined from the thrust setting, T_i and is the thrust one engine would generate at sea level for a given throttle setting, Γ_i. The equation below shows how the net corrected thrust is determined:

$$T_{net} = \frac{T_i}{n_{eng}} \cdot \frac{P_0}{P} \tag{3.35}$$

As can be seen from Equation (3.35) the thrust setting is divided by the number of engines, n_{eng}, and then multiplied by the ratio of the air pressure at sea level, P_0, and the ambient air pressure, P.
With the given trajectory information and a specified grid the INMTM program calculates the noise generated by the aircraft, $SEL_{outdoor}$, at each grid-point (see Figure 3.9). By using the Equations (2.3) from Section 2.3.3 the percentage of people getting disturbed by the noise the trajectory of Figure 3.9 is making can be determined (see Figure 3.10). From this figure it can be seen that the influence of the noise is reduced to only a strip around the trajectory. This is carried by the fact that awakenings only occur above 50.5 dB, as can be seen in Equation (2.3).
For this example the population data around Schiphol is used, issued by the CBS (see Figure 3.11) [29]. By knowing the population density around the trajectory and the percentage of people that will be awaken by the flyover the exact number of people that will be awakened can be determined (see Figure 3.12).

3.7. Optimization algorithm

For the optimization of this model a multi-objective evolutionary algorithm called NSGA-2 algorithm was used, as described in Section 2.2.2. With the use of this algorithm the model is optimized for three objective functions as is shown below.

$$J = \begin{cases} m_{fuel} \\ t \\ n_{awakening} \end{cases} \tag{3.36}$$

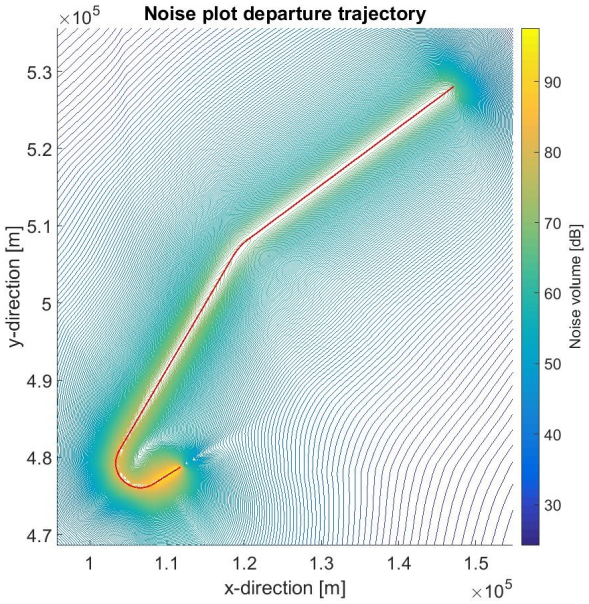

Figure 3.9: Noise contour of example departure trajectory

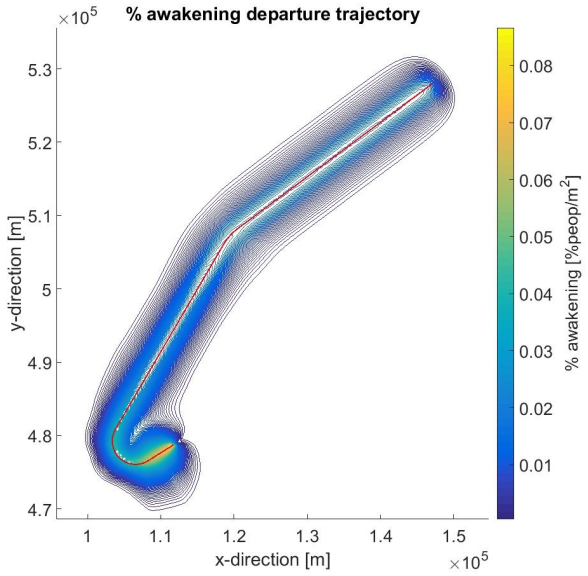

Figure 3.10: Percentage awakening of example departure trajectory

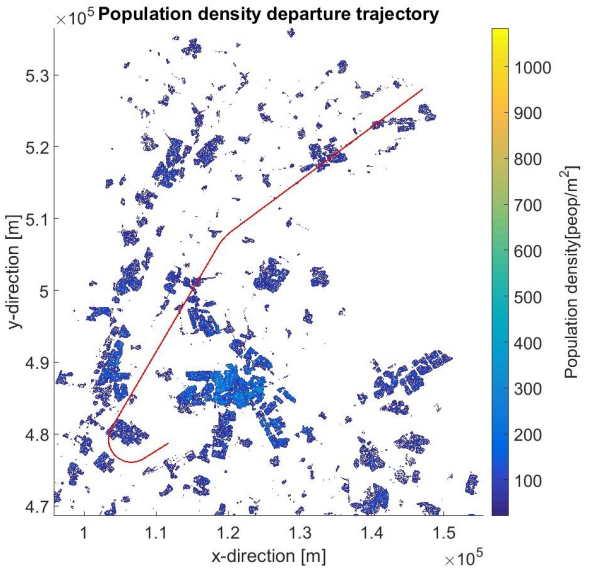

Figure 3.11: Population density

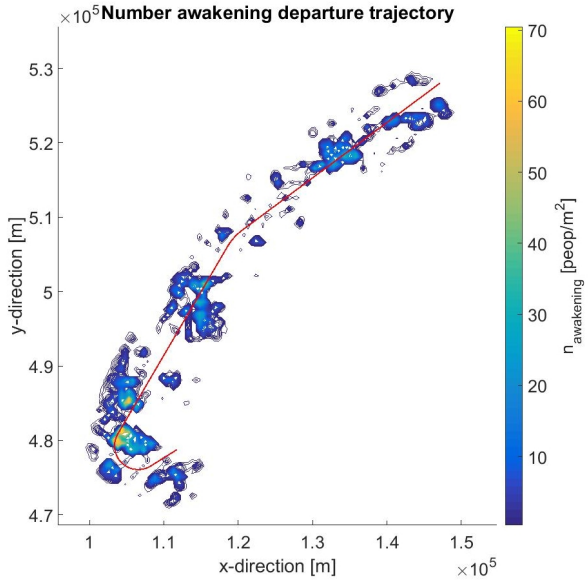

Figure 3.12: Number of awakening

The fuel consumption, m_{fuel}, is derived by the difference between the weight of the aircraft at the beginning of the trajectory and the weight at the end of the trajectory. The weight reduction is estimated by the equations of motion, see Equation (3.4). The time, t, is defined as the time the aircraft needs to get from its initial location to the final location. The third objective is the number of people getting disturbed by the flyover, $n_{awakening}$.
When the aircraft does not manage to get at its final conditions a penalty should be given to this trajectory. The penalty is also given when the aircraft somehow does not manage to fly around the restricted area.

3.8. Conclusion

In this chapter the aircraft model was discussed. A few methods implemented in this aircraft model are from a research by Hartjes [9]. For this thesis a multi-objective evolutionary algorithm, NSGA-2, will be used to optimize the model using normalized input parameters and a point-mass model. The objective functions include the fuel consumption, the number of awakenings and travel time. As noise model a replication of the

INM will be used, called INMTM.

For this research also a few new methods were introduced. Since each segment has a fixed distance rather than a fixed time, to improve accuracy the time has been replaced by distance as the independent variable in the integration of the equations of motion.

Also, by combining two trajectories the minimum distance constraint was introduced. First the vertical and horizontal plane of the departure route will be generated and the horizontal plane of the arrival trajectory. Next the intersection location is determined and at this location in the arrival vertical plane a restricted area is created to comply with the minimum distance constraint. To ensure that the distance between the trajectories is kept at intersection point the flight path angle of the arrival is adjust if necessary to avoid the restricted area.

There are also some limitations to this thesis. The first limitation is that the arrival trajectory does not include a missed approach trajectory. This implementation could be done by creating a specific trajectory that would be fixed in space. When combining the trajectories in this thesis first the departure route is created and from the take-off it can be checked if the trajectory is crossing this fixed missed approach trajectory and if so the flight path angle or route can be adjusted to avoid this. After creating the departure trajectory the arrival trajectory can be determine as discussed in Section 3.5.
Also, for this optimization problem only the number of people getting disturbed by a single fly-over for only a single type of aircraft has been considered. To make it more representable to the actual number of people getting disturbed by aircraft activity around an airport the model should be expand by allowing it to optimize for multiple types of aircraft [30].

Now that the aircraft model is discussed a current standard instrumental departure is used to verify and validate the model with another research paper in Chapter 4. Next the aircraft model will be used to optimize a few case studies, see Chapter 5. Finally the thesis will be concluded in Chapter 6.

4

Verification and Validation

To verify and validate the aircraft model the current Spijkerboor Standard Instrumental Departure (SID) will be optimized and the results will be compared to results from Hartjes [9]. This comparison is done to check the aircraft model and optimization method is working properly. This chapter will start with an introduction on the current Spijkerboor SID. Next the input parameters are discussed and finally the result of this research is compared with the results from [9].

4.1. Introduction

The current Spijkerboor SID is shown in Appendix A and in Figure 4.1. As can be observed it starts with a turn around Hoofddorp and then flies a straight line between the populated areas of the cities of Haarlem and Amsterdam. After Amsterdam a final turn is made to the waypoint ANDIK.

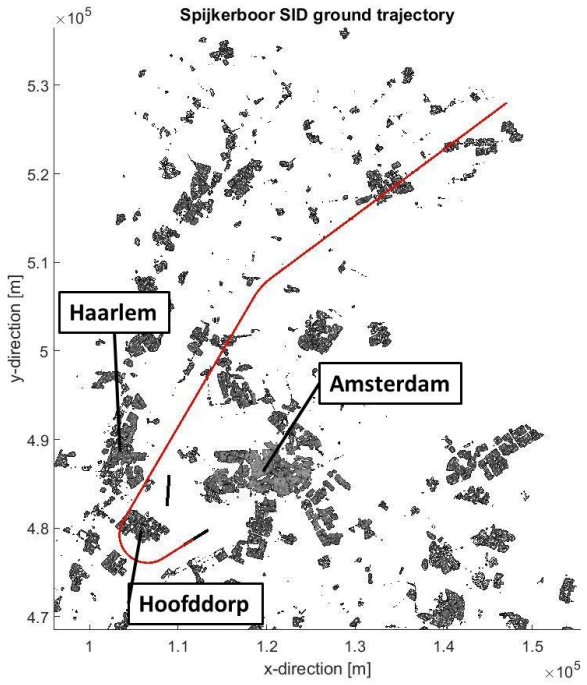

Figure 4.1: Current Spijkerboor SID

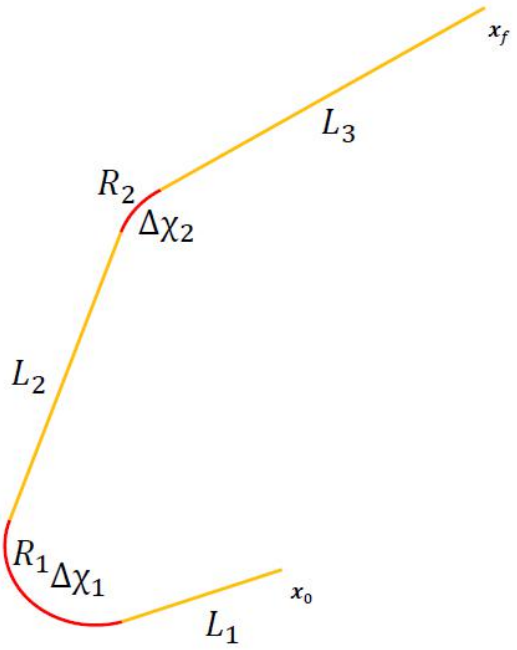

Figure 4.2: Optimization parameters Spijkerboor SID

For this research a Boeing 737-300 model is used. The initial velocity, V_{min} is equal to $V_2 + 10$kts and V_2 is set at 150kts and the initial altitude, h_{min} is set at 16ft. The second part of the NADP is finished when an altitude of 3000ft is obtained or a clean velocity, $V_{ZF} + 10$kts. This clean velocity, V_{ZF}, is set at 180kts. The

final conditions include a velocity, V_{max} of 250kts and a altitude, h_{max} of 6000ft [9]. The take-off weight is equal to 53482.5 kg, this weight is the sum of the operational empty weight, 75% of the payload weight and 50% of the fuel weight.
Also, the vertical trajectory is divided into 10 segments. The length of one segment is determined by dividing the total flying distance by the number of segments. To include the NADP four extra optimization parameters are included, Two flight path angle parameters, $\gamma_{n,0}$ and $\gamma_{n,0.1}$, and two thrust setting parameters, $\Gamma_{n,0}$ and $\Gamma_{n,0.1}$. The NADP lies on top of the segments. This means that the optimization parameters of the first and sometimes also the second segment are overruled by the NADP parameters. This occurs when the length of a segment is smaller than the distance needed for the NADP to be accomplish. The population dataset is from 2012 and a grid size of $500m \cdot 500m$ is used [29].

The results from [9] were obtained using a Boeing 737-800 model. The vertical trajectory was divided into 11 segments. The take-off weight is not given in the paper and also it is not known from what year the population dataset is used and what the grid size is.

4.2. Input parameters

As already discussed in Chapter 3 the horizontal and vertical trajectory are determined independently from each other. The horizontal plane of the Spijkerboor departure route consist of three straight legs and two turns, as can be observed in Figure 4.2. The seven parameters for the horizontal trajectory of this research are the same as [9] and are shown in Table 4.1.

Table 4.1: Parameters for current SID horizontal trajectory [9]

Parameter	SID
L_1	4,100m
R_1	3,183m
$\Delta\chi_1$	152.4°
L_2	29,150m
R_2	7,500m
L_3	33,127m
$\Delta\chi_2$	23.0°

Similar to [9] two vertical trajectories are compared: an ICAO-A departure and an optimal awakening departure. The ICAO-A departure take-off the NADP-1 and after 3000ft for the remaining trajectory it is minimized for fuel consumption. Flying the NADP-1 gives a maximum bound to the second part of the NADP, $\gamma_{n,0.1}$, also the value of the altitude where NADP switch from the first part to the second, h_1, is fixed at 1500ft (see Table 4.2).
The optimal awakening departure focuses on minimizing the number of awakenings. For this problem $\gamma_{n,0.1}$ and h_1 will be optimization parameters as can be observed from Table 4.2.
From the table it can also be noticed that the flight path angle and thrust setting for the first part of the NADP, $\gamma_{n,0}$ and $\Gamma_{n.0}$, and the thrust setting for the second part of the NADP, $\Gamma_{n,0.1}$, are fixed at the maximum bound. The reason for this is discussed in Section 2.1.2.

Table 4.2: Parameters bounds for current SID vertical trajectory [9]

Parameter	ICAO-A	Minimum awakening
h_1	1500ft	[800ft, 1500ft]
$\gamma_{n,0}$	1	1
$\gamma_{n,0.1}$	1	[0, 1]
$\gamma_{n,1-10}$	[0,1]	[0, 1]
$\Gamma_{n,0}$	1	1
$\Gamma_{n,0.1}$	1	1
$\Gamma_{n,1-10}$	[0,1]	[0, 1]

To conclude the ICAO-A SID problem will include a total of 20 optimization parameters; only the flight path

angle and thrust setting of the 10 segments will be optimized and the NADP-1 procedure is used. For the minimum awakening optimization problem the total number of input parameters is equal to 22. This optimization problem also includes the $\gamma_{n,0.1}$ and h_1 as optimization parameters.

4.3. Verification and validation

Both problems from this research were optimized for 200 generations with a population of 50 individuals. Table 4.3 shows the results of both optimization problems for not only this research but also [9]. The resulting vertical profile of the ICAO-A optimization problem of this thesis and [9] are shown in Figure 4.3 and the results for the minimum awakening problem are shown in Figure 4.4.

Table 4.3: Results objective function of ICAO-A and minimum awakening current SID

Type trajectory	Fuel [kg]	Awakening	Time [sec]
ICAO-A	556.1	7358	634.2
ICAO-A [9]	572.5	5531	609.9
Minimum awakening	547.1	5385	626.5
Minimum awakening [9]	562.9	4903	618.3

When comparing the results of the objective functions of this thesis with each other it can be noticed that when giving full freedom for the optimization method to optimize the vertical the results of all objective functions are lower than for the ICAO-A trajectory. This is the result of the low altitude at the beginning of the trajectory (see Figure 4.4) where the aircraft uses all its energy to accelerate. By accelerating the exposure time of the noise on the population is decreased and by keeping a low altitude the lateral sound attenuation is increased. With lateral sound attenuation is meant that by flying low over a populated area the people directly under the trajectory are fully exposed by the noise but the noise is reduced quickly when living further away from the trajectory.

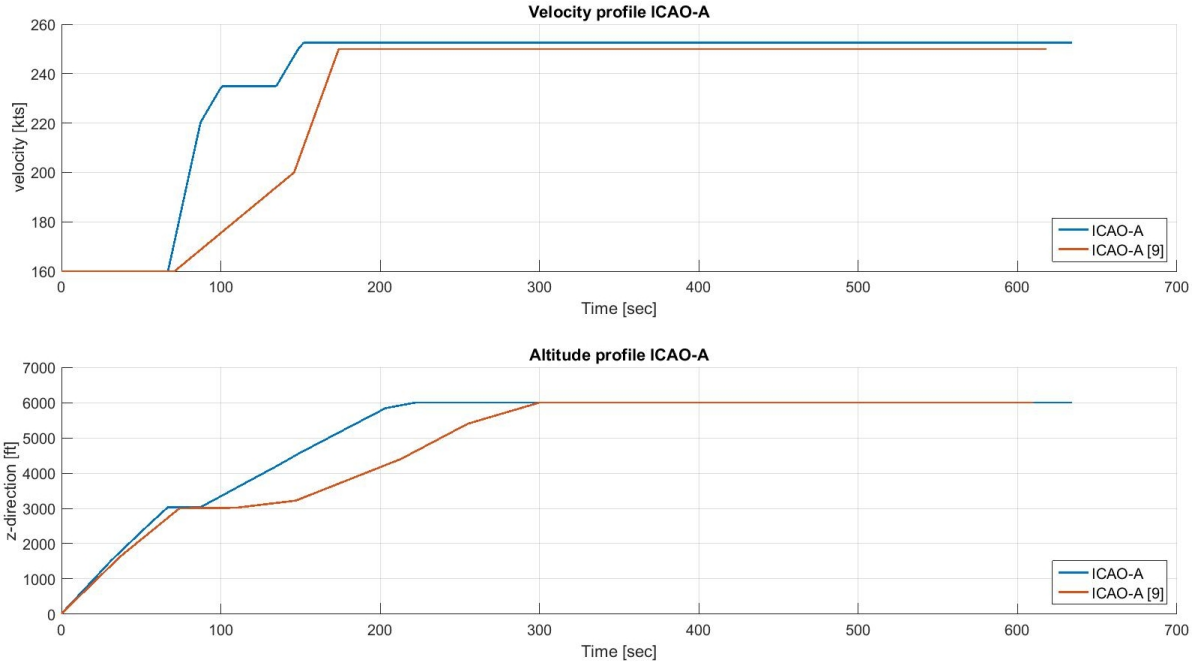

Figure 4.3: Vertical profile ICAO-A results this research and [9]

When comparing the shape of the altitude profile ICAO-A trajectory of the paper with the results of this research they are almost the same. The ICAO-A trajectory of [9] only has a little longer level flight just after arriving at 3000ft. When comparing the velocity profile the shape is a little different but also can be seen that

both trajectories start with a constant velocity until around 80 seconds. After 80 seconds both trajectories start accelerating until final velocity. The fuel consumption and travel time are in the same region when comparing the results of the objective function. The number of awakenings of this research is significantly higher compared to the result of [9]. From the shape comparison can be concluded that the aircraft model of this research is behaving the same as the aircraft model of [9].

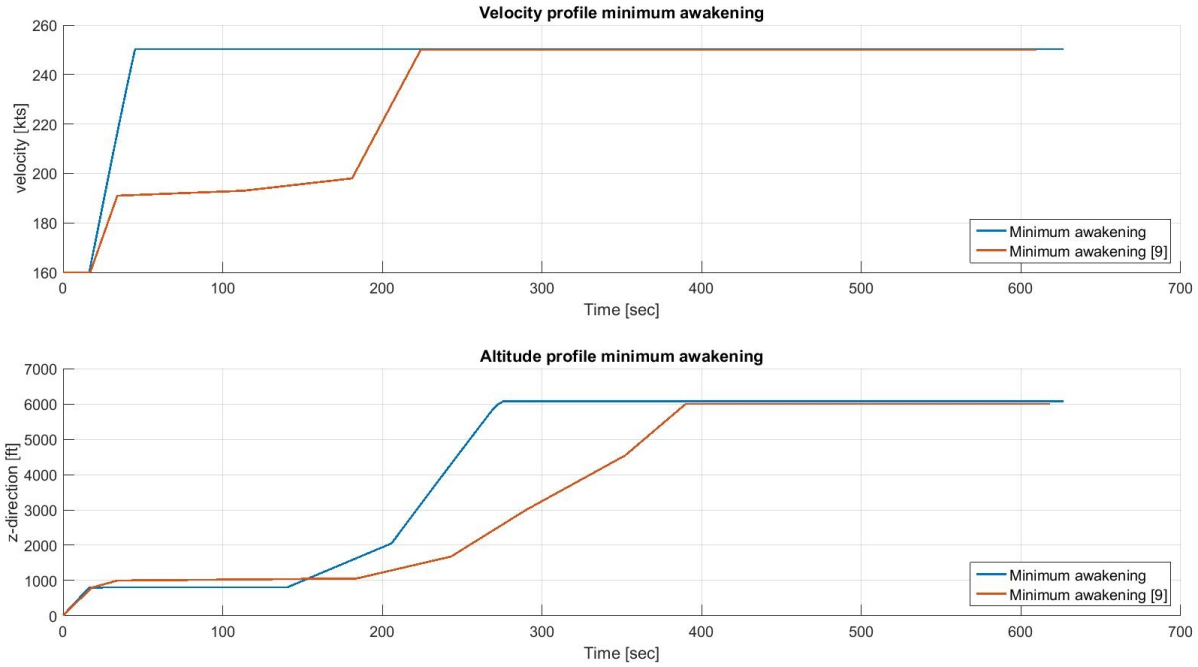

Figure 4.4: Vertical profile minimum awakening results this research and [9]

To check if the optimization model is working correctly the minimum awakening results of this thesis are compared with the results of [9] (see Figure 4.4). When comparing the altitude profiles of both cases it can be seen that the shape is almost the same, starting with a level flight after the first phase of the NADP and after 150 seconds they start climbing to its final altitude. The moment of increasing the flight path angle is different between both cases. There is a difference in velocity profile, where the minimum awakening case of this research has a steady acceleration to its final velocity, [9] keeps an almost constant velocity after 40 seconds. When comparing the results of the objective functions it can be observed that all results are within 10% range of the results of [9]. Even though there are some difference in velocity profile, from these observations can be concluded that the optimization model is working properly.

A final remark should be made on the difference in the shape of the velocity profiles and results of the objective functions. This can be attributed to the fact that for this research a different aircraft specific model is used. Also the number of segments used in this research is less and there was no data on aircraft weight and population dataset in [9].

5

Case Study

Now the aircraft model has been verified and validated and assumed to be working properly it is used to observe what the influence will be when combining two trajectories with each other. For this case study Schiphol airport has been used because this airport consists of many runways, routes that intersect each other and is located in a populated area.

This case study includes the following scenario: assume that the wind is coming from the southwest. Aircraft are taking off from runway 24, the Kaagbaan (see Figure 5.1) in southwest direction, and the arriving aircraft are landing on runway 18R, the Polderbaan, in south direction. The departure from runway 24 is based on the Spijkerboor Standard Instrumental Departure (SID) and is shown in Figure 5.2 with a red line. The arrival trajectory will start at the North sea and is based on the RNAV night arrival, Standard Terminal Arrival Route (STAR). This trajectory is shown in Figure 5.2 with the green line. As can be observed already the trajectories cross when the current route is flown. The Spijkerboor departure used for the case studies is the trajectory that has been used to verify and validate the model.

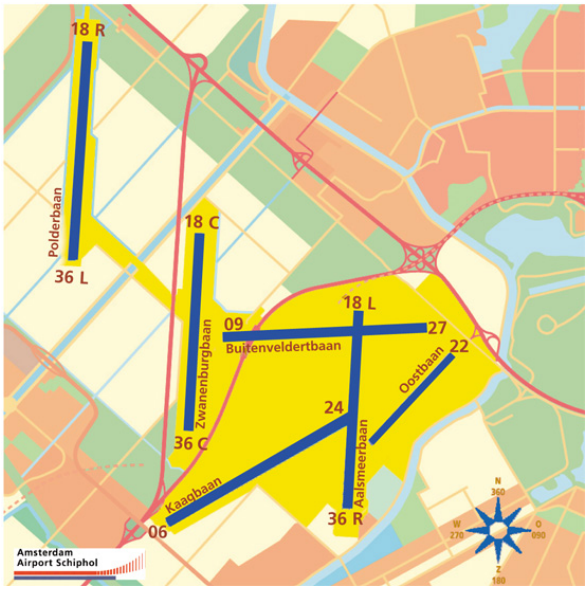

Figure 5.1: Runway overview Schiphol [10]

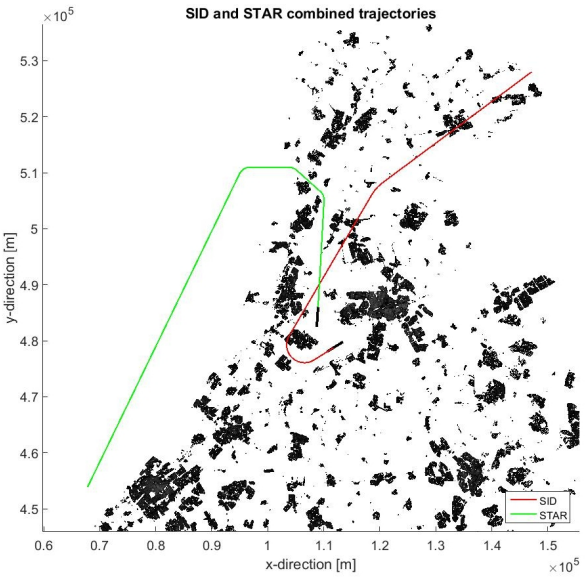

Figure 5.2: Current SID and STAR

For this case study around Schiphol, a population dataset was used from the Centraal Bureau Voor de Statistiek (CBS). The x- and y-coordinates defined in this dataset are based on a Rijksdriehoekscoördinate (RD-coördinate) system. The origin of this system lies around 120km Southeast of Paris. With the origin at this location and the x-coordinates defined positive in East direction and the y-coordinates defined positive in North direction, all

coordinates located in the Netherlands are positive. By using the RD-coordinate system the initial and final coordinates for this case study have to be converted from longitude and latitude to RD-coordinates.
The population in the dataset is defined on a $100 \cdot 100 m^2$ grid and the grid size of the noise model is $500 \cdot 500 m^2$. To be able to calculate the total number of awakenings the grid size of the population dataset is changed from $100 \cdot 100 m^2$ to $500 \cdot 500 m^2$. This results in the population dataset being less refined. Changing the population grid size is chosen over making the grid size of the noise model smaller because the computation time will increase with a smaller noise model grid size.

The optimization method used for these optimization problems is a NSGA-2 model based on a paper of Deb et al. [5]. This model includes a number of settings that can be adjusted to let the optimization converge better. The settings include the distribution index for crossover, the distribution index for mutation and the mutation probability. In Table 5.1 the settings used for the optimization problems are shown. These values are obtained by running the optimization model for a specific case multiple times and adjusting only one while keeping the other values constant.

Table 5.1: Settings NSGA-2 optimization model

Setting	Value
Distribution index crossover	15
Distribution index mutation	15
Mutation probability	0.5

This chapter starts with the optimization problem of both the arrival and departure route separately. For these problems first the input parameters are explained en next the results are shown. Secondly, the combined optimization problem is discussed. Also a different combined trajectory is optimized where the horizontal trajectory of the departure route is fixed. Finally the results of the case studies are discussed.

5.1. Spijkerboor departure from runway 24

The main part of the input parameters used for Spijkerboor departure have already been discussed in the chapter validation and verification, Chapter 4. The difference between the optimization problem of this section and the two discussed in the previous chapter is that the horizontal trajectory now also added optimization parameters. The parameter bounds used in this optimization problem are shown in Table 5.2. For reference the parameter values used for the current SID are also shown in this table. The remaining two unknowns L_3 and $\Delta\chi_2$ are determined using vector calculation as described in Section 3.3.1. From the table can also be observed that the radii of the turns are not yet defined. This is because the turn radius depends on the velocity and altitude of the aircraft at the start of the turn, as also discussed in Section 3.3.1.

Table 5.2: Parameters bounds for horizontal trajectory departure problem

Parameter	Current SID	Lower bound	Upper bound
L_1	4,100m	614m	10,000m
R_1	3,183m	0	1
$\Delta\chi_1$	152.4°	32°	163°
L_2	29,150m	1,000m	45,000m
R_2	7,500m	0	1

The vertical trajectory has the same structure as the current SID minimum noise problem and for completeness the parameter bounds for the input parameters are shown in Table 5.3. The boundary conditions for this optimization problem are also the same as for the cases in Chapter 4.

For this optimization problem the number of input parameters is 27: 5 for the vertical plane and 22 for the horizontal plane.

Table 5.3: Parameters bounds for vertical trajectory departure problem

Parameter	Lower bound	Upper bound
h_1	800ft	1500ft
$\gamma_{n,0}$	1	1
$\gamma_{n,0.1}$	0	1
$\gamma_{n,1-10}$	0	1
$\Gamma_{n,0}$	1	1
$\Gamma_{n,0.5}$	1	1
$\Gamma_{n,1-10}$	0	1

5.1.1. Results departure route

The departure problem was optimized over 600 generations using a population set of 50 individuals. The resulting Pareto front is shown in Figure 5.3. The results of the current SID discussed in Section 4.3 are also included in the front. From this figure it can be observed that the results of the current SID are not part of the optimal solution.

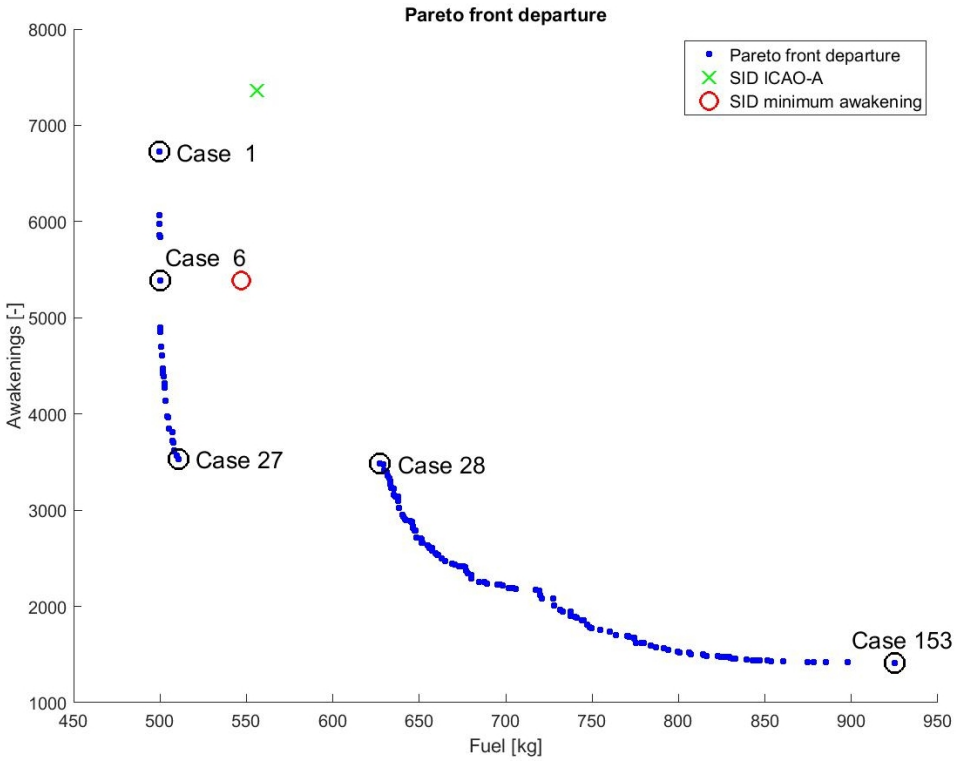

Figure 5.3: Pareto front of results departure optimization problem

The first two cases that are discussed are the minimum fuel case, case 1, and minimum awakening case, case 153 (see Figure 5.3). The ground trajectories of these cases are shown in Figure 5.4, the vertical profile is shown in Figure 5.5 and the results of the objective function shown in Table 5.4.
From the ground trajectory clearly can be observed that for flying the fuel optimal case the trajectory is short. When looking at the vertical profile it can be noticed that the optimization model chooses to let the aircraft fly a steep turn which forces the aircraft to fly with a low velocity, indicated with the green dot. During the turn the aircraft uses its energy to gain some extra height. After the turn the flight path angle is reduced to accelerate to its final velocity first and then the flight path angle is increased again to climb to its final altitude. The minimum awakening case starts with flying at low altitude while using all energy to accelerate, as can be observed in the vertical profile. When the aircraft arrives near Lisse the thrust is reduced to minimize the number of people getting disturbed, indicated with the dark green dot. By flying low but fast over populated areas the lateral sound attenuation is increased, as has been discussed in Section 4.3. The aircraft starts to

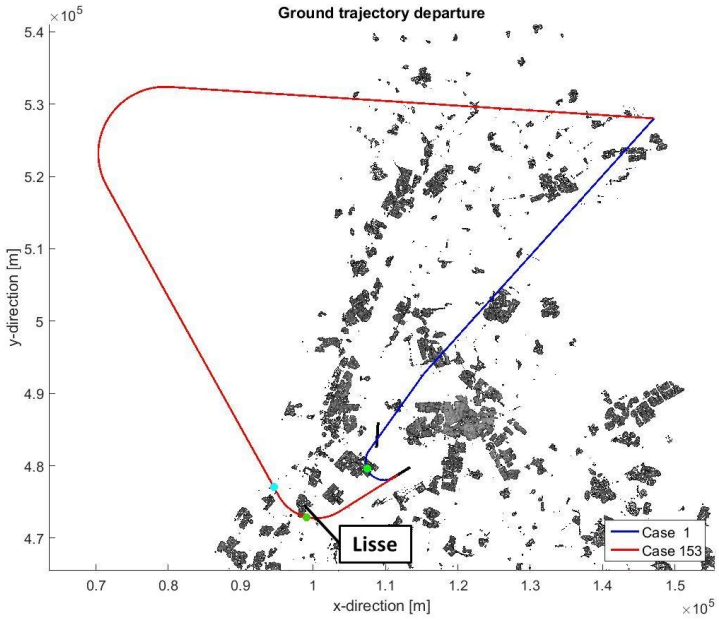

Figure 5.4: Ground trajectory of the minimum fuel and awakening case departure

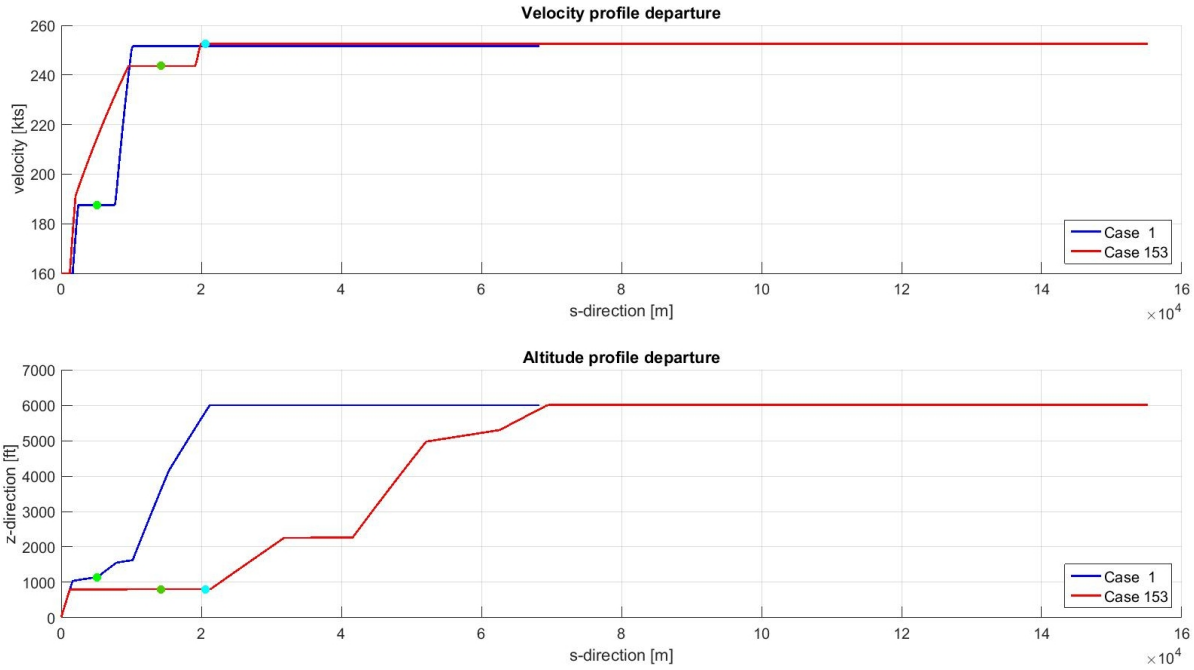

Figure 5.5: Vertical profile of minimum fuel and awakening case departure

climb to its final altitude when it has passed the populated area around Schiphol, indicated with the light blue dot. From the ground trajectory can be observed that the trajectory makes a large detour over sea before making the final turn back to the final way point. This is done so the final straight leg is flown over the least densely populated area North of Schiphol.

From the Pareto front it can be noticed that a gap occurs between case 27 and 28. Between these cases the number of awakenings is almost the same but the fuel consumption increased. To take a closer look on why this happens the ground trajectories of these cases are shown in Figure 5.6, the vertical profiles are shown in Figure 5.7 and the results of the objective functions are shown in Table 5.4.
From the ground trajectory it can be concluded that the main reason why the gap in the Pareto front occurs

Table 5.4: Results objective functions of case 1, 6, 27, 28, 153 and SID minimum awakening departure

Trajectory	Fuel [kg]	Awakening	Time [sec]
Case 1	499.7	6727	560.2
Case 6	500.0	5384	562.0
Case 27	510.6	3535	576.2
Case 28	627.4	3485	771.2
Case 153	925.0	1411	1231.2
SID Minimum awakening	547.1	5385	626.5

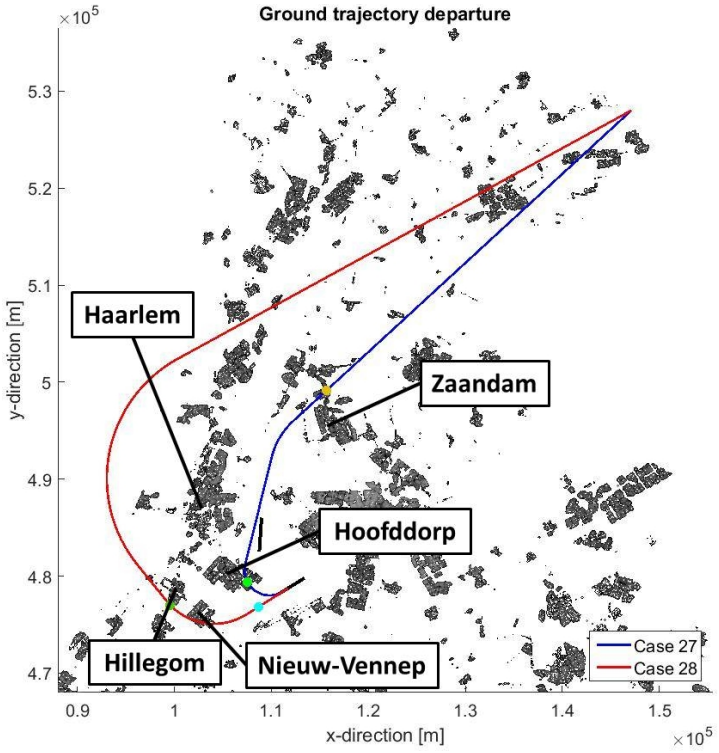

Figure 5.6: Ground trajectory of case 27 and 28 departure

is because the trajectory switch from turning before Haarlem over Hoofddorp to a trajectory turning around Haarlem.
When looking at the vertical trajectory a few things can be observed. When looking at case 27 the aircraft is reducing its thrust during the turn above Hoofddorp, indicated with a green dot. After Hoofddorp the aircraft starts climbing until Zaandam is coming close. At that moment the aircraft starts flying at almost level flight. By doing this the thrust of the engines is reduced and the number of awakening in Zaandam is minimized.
Case 28 starts after the first part of the NADP with a level flight to use all energy to accelerate. After the final velocity is reached the aircraft starts climbing until the populated cities of Nieuw-Vennep and Hillegom are reached, indicated with a green dot. The same as for case 27 the aircraft is flying an almost level flight to reduce the engine noise. After Hillegom passed the aircraft starts to climb to its final altitude.

Finally when looking at the current SID's minimum awakening solution it can be observed that case 6 would be an optimal solution where the number of awakenings would stay the same but the fuel consumption is reduced 10%. The ground trajectory of the SID minimum awakening solution is combined with case 6 in Figure 5.8. From this figure it can be noticed that case 6 makes a turn before Hoofddorp and the current SID around it.
When looking at the results of the objective function (see Table 5.4) it can be observed that the number of awakenings only differ 1 person. The fuel consumption is reduced with 10% and also the flight time is reduced.

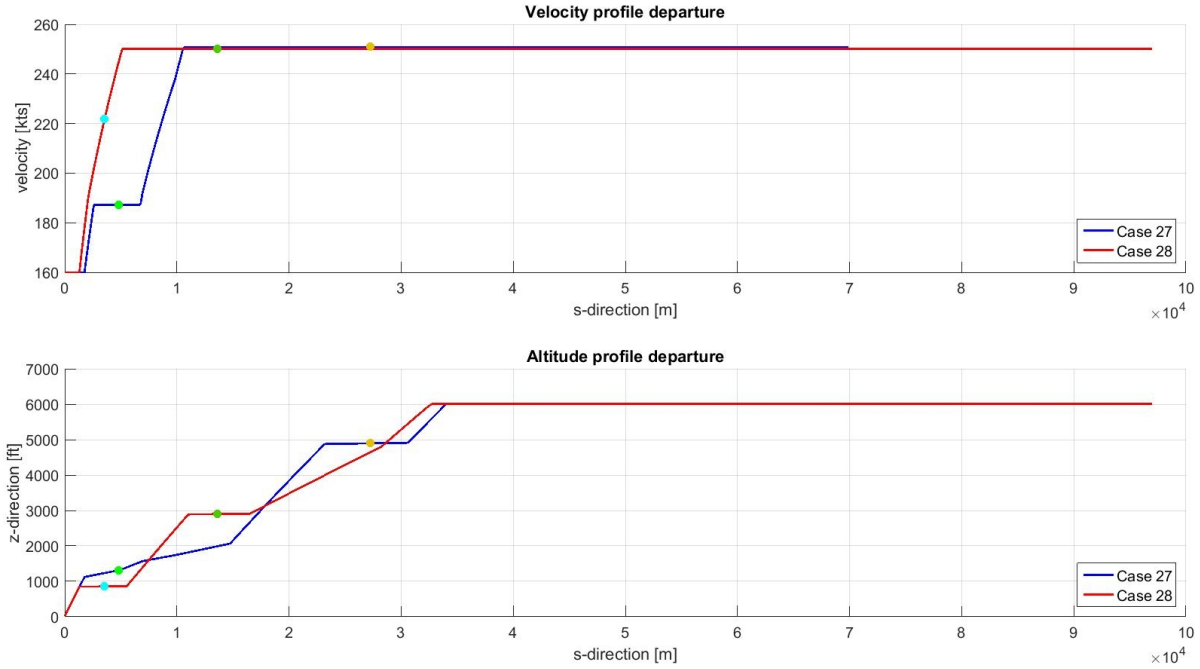

Figure 5.7: Vertical profile of case 27 and 28 departure

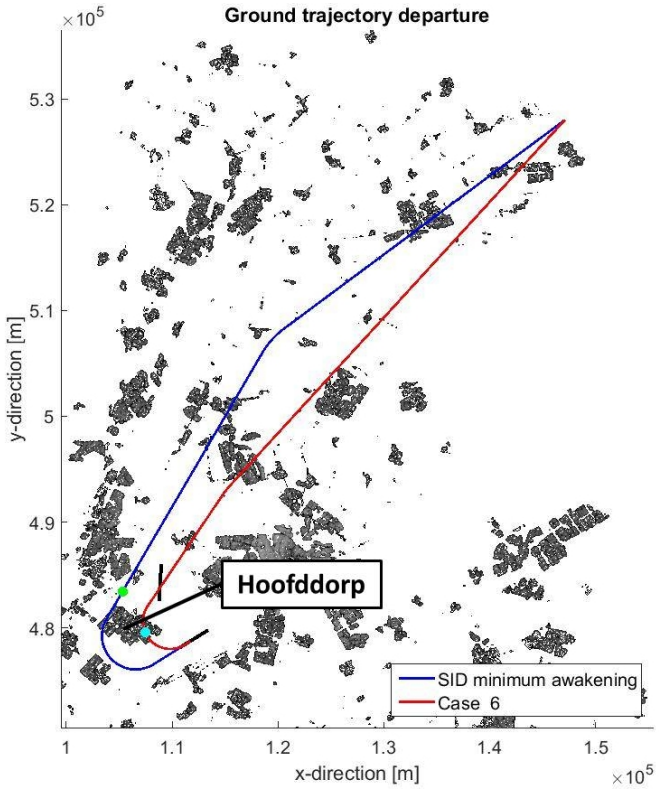

Figure 5.8: Ground trajectory of SID minimum awakening case and case 6 departure

When looking at the vertical profile of both cases (see Figure 5.9) it can be noticed that there is a big difference between the two trajectories. Where the current SID keeps a low altitude until Hoofddorp is passed but is accelerating, indicated with the green dot, case 6 also keeps a constant speed above Hoofddorp to reduce the engine noise even more. After Hoofddorp both trajectories start climbing to the final altitude.

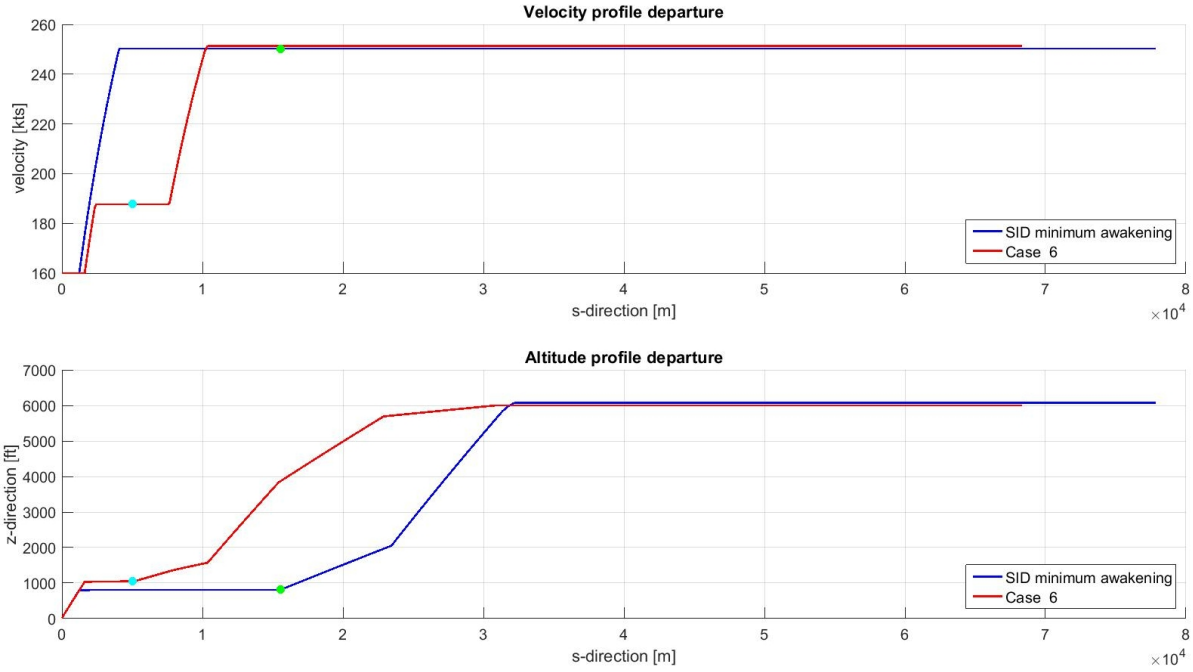

Figure 5.9: Vertical profile of SID minimum awakening case and case 6 departure

5.2. Over sea arrival for runway 18R

As already discussed the arrival trajectory starts at the sea and flies parallel to the shore for a long time until it makes in total three turns to arrive in line with the runway, see Appendix A. In this section first, the input parameters for the arrival optimization problem are discussed and secondly the results of the current STAR and optimization problem are shown.

5.2.1. Input parameters

As for the departure route, the horizontal trajectory of the arrival route also consists of a number of straight legs and turns with fixed radius (see Figure 5.10). For the arrival four straight legs are used and three turns. Due to the fact that the final heading is known and the straight leg, L_4, depends on the height of the ILS interception, the unknown variables will be the first straight leg, L_1, and the heading change of the first turn, $\Delta\chi_1$. The parameter bounds for the other input parameters are shown in the table below.

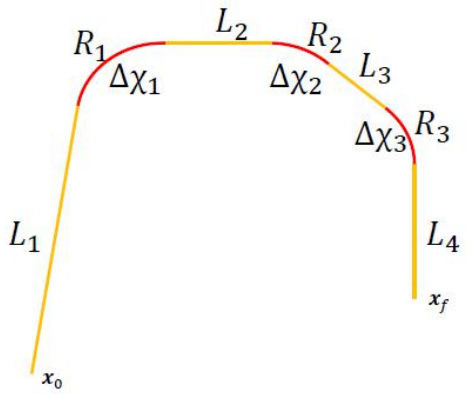

Figure 5.10: Horizontal trajectory over sea arrival 18R

As already stated above and as can also be seen in Table 5.5 the lower bound of L_4 depends on the horizontal length of the ILS, L_{ILS}. The horizontal length of the ILS again depends on the altitude at which the aircraft intercepts the ILS, h_{ILS}. This interception altitude is stated as an input parameter for the vertical trajectory,

Table 5.5: Parameters bounds for horizontal trajectory arrival

Parameter	Current STAR	Lower bound	Upper bound
L_4	19,043.4m	L_{ILS}	L_{ILS}+15,000m
L_3	5,682.0m	1,000m	10,000m
L_2	7,057.3m	1,000m	10,000m
R_{1-3}	3,000m	3,000m	10,000m
$\Delta\chi_{2-3}$	42°, 51.20°	5°	75°

see Table 5.6. By knowing the interception altitude, L_{ILS} is determined with the equation below.

$$L_{ILS} = \frac{h_{ILS}}{\tan(3°)} + 1.5NM \tag{5.1}$$

From the equation it can be observed that an extra 1.5NM is included in the L_{ILS}. This 1.5NM is needed to give the pilots time to do the final checks before the ILS is flown, as stated by ICAO, see Section 2.1.3.

For the vertical trajectory the arrival procedure described in a paper by Visser [31] is used. In this paper arrival trajectories are optimized for noise abatement. The arrival route in this paper is divided into five phases of which the final two are used for the ILS. With each phase the velocity decreases and the flap settings are changed. With the change of the flap setting also a different drag polar is used.
For the Boeing 737-300 model used in this research the different drag polars are combined to a single one. This envelope of drag polars of different flap settings.

The vertical trajectory is divided into 10 segments. The distance used to determine the segment length is only the trajectory between the beginning of the arrival trajectory, $\mathbf{x}_0$, and the moment the aircraft starts to fly its 1.5NM level flight. This is done because the ILS is a standard part of the trajectory and there is not much to be optimized at that part of the trajectory. The length of one segment is calculated with:

$$L_{seg} = \frac{L_{tot} - L_{ILS}}{n_{seg}} \tag{5.2}$$

For each segment the flight path angle, γ_i, and thrust setting, Γ_i, is given. In these segments the aircraft is reducing altitude from its initial conditions, V_0 = 220kts and h_0 = 7000ft, to ILS interception height and velocity, V_{ILS}=170kts.
The moment the ILS is intercepted, as defined in Visser [31], phase four starts and the aircraft will descend with a constant flight path angle of 3°. At the same time, the velocity is reduced from 170kts to its final velocity, V_{min}, of 140kts. This velocity reduction should be reached before an altitude of 1200ft. When the aircraft reaches 140kts the fifth phase is started. At this phase the aircraft will descent until its final altitude, h_{min}, of 500ft, with a constant velocity of 140kts. The aircraft will land with its Maximum Landing Weight (MLW) of 51700kg.
The bounds of the vertical input parameters are shown in table 5.6. The input parameters for the 10 segments are $\gamma_{n,1-10}$ and $\Gamma_{n,1-10}$. To the level flight before the ILS and the ILS itself also input parameters are assigned even though it is a standard part of the arrival route. The input parameters for the level flight with constant velocity are indicated with $\gamma_{n,0.3}$ and $\Gamma_{n,0.3}$ and given the maximum parameter bound. The first part of the ILS the velocity is reduced from 170kts to 140kts, this gives the input parameter $\Gamma_{n,0.2}$, the flight path angle is set to −3°. For the final part of the ILS the velocity is again constant, giving the maximum bound to the input parameter $\Gamma_{n,0.1}$ and still the aircraft is descending with a constant flight path angle of −3°.

The same as for the departure, for the arrival optimization problem also the current route is optimized. As can be observed from the AIP chart, see Appendix A, the horizontal trajectory only exists of straight legs connected to each other via waypoints. These waypoints are called fly-by waypoints, which means that the aircraft start making the turn in front of the waypoint instead of flying over the waypoint and then making the turn. To determine when the aircraft should start with the turn, and also the distances the straight legs will get, the calculations described in the PANS-OPS are used [3]. Figure 5.11 shows the values needed to determine the distance between the waypoint and the location, indicated with L, this distance is determined using:

$$L = R \cdot \tan(\frac{\Delta\chi}{2}) \tag{5.3}$$

Table 5.6: Parameters bound for vertical trajectory arrival

Parameter	Lower bound	Upper bound
h_{ILS}	2000ft	4000ft
$\gamma_{n,0.3}$	1	1
$\gamma_{n,1-10}$	0	1
$\Gamma_{n,0.1}$	1	1
$\Gamma_{n,0.2}$	0	1
$\Gamma_{n,0.3}$	1	1
$\Gamma_{n,1-10}$	0	1

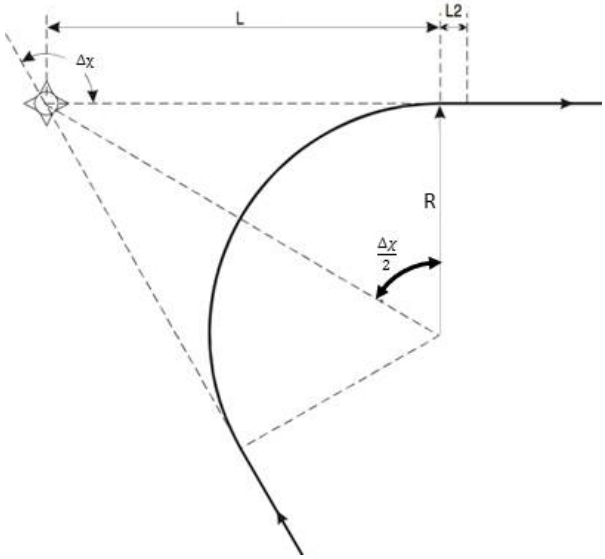

Figure 5.11: Determine the turn location [3]

With the ability to determine the location where the turn will start the remaining lengths of the straight legs can be determined and are shown in Table 5.5.
The vertical trajectory is determined freely by the optimization algorithm. In the instrument approach chart the aircraft is flying with a constant flight path angle from an initial waypoint using the continuous descent approach until the ILS is intercepted. For this research a level flight just before the ILS is intercepted is added. This is added to the comparison with the other arrival results. The ILS interception altitude is set at 2500ft.

To conclude the arrival optimization problem consists of in total 30 parameters: 9 parameters are needed to define the ground trajectory, including the input parameter for the h_{ILS}, and 21 are needed for the vertical profile. For the current STAR the ground trajectory is already defined including the ILS interception altitude. This means that only the remaining 21 parameters are needed to determine the vertical trajectory.

A final remark should be made on the weight used for the arrival trajectories. For this thesis the MLW is used as the weight the aircraft will have when landing. The MLW is the maximum weight the aircraft is allowed to have when landing. Usually the landing weight is lower than the MLW and equal to the Operational Empty Weight plus the payload and enough fuel to fly for at least 30 more minutes if a missed approach occurs.
Reducing the weight of the aircraft when landing will have effect on the objective functions. When flying with a lighter aircraft the fuel consumption will be reduced and also the number of awakenings will be less.

5.2.2. Results current STAR

The STAR was optimized over 200 generations and with a population of 50 individuals. The ground trajectory has already been discussed in Figure 5.2. Figure 5.12 shows the minimum fuel consumption and the awakening of the STAR trajectory optimization. Looking at the shape of both trajectories it can be concluded that there is not much difference between both trajectories. When looking at the results of the objective functions,

shown in Table 5.7, the fuel consumption is almost the same, only the number of awakenings reduces with 100 people when flying the awakening optimal case.

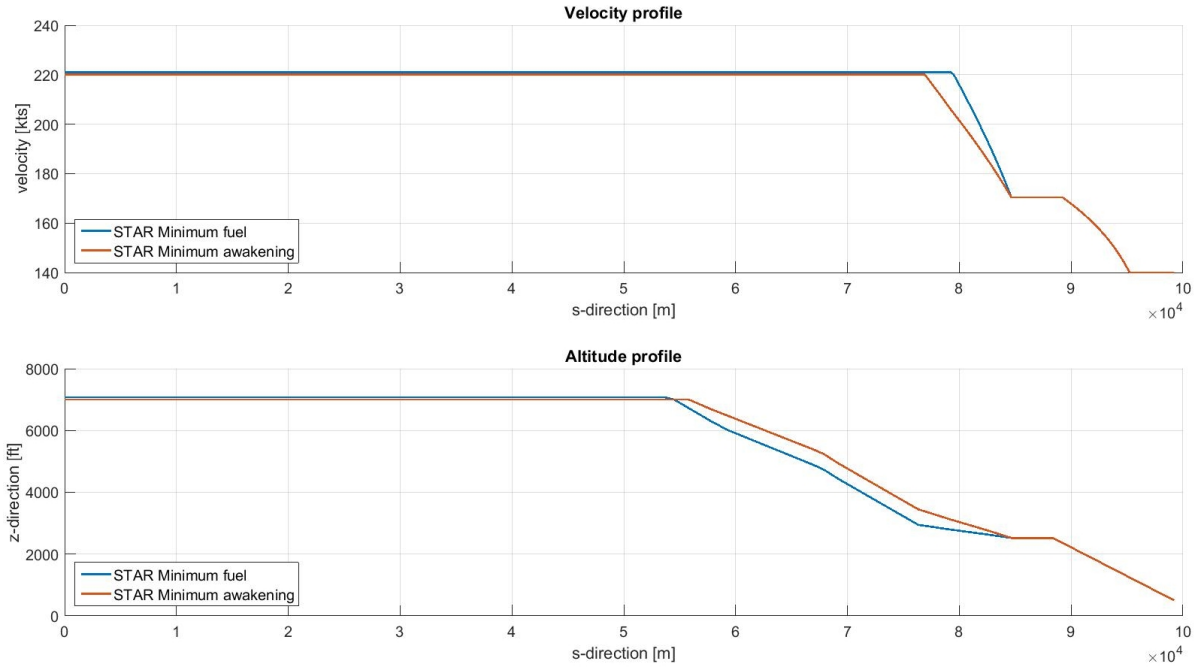

Figure 5.12: Vertical profile of current STAR

Table 5.7: Results objective function of minimum fuel and awakening case STAR

Type trajectory	Fuel [kg]	Awakening	Time [sec]
Minimum fuel	414.3	949	934.8
Minimum awakening	416.9	849	939.9

A final observation can be made the reduction in flight path angle in the final segment before the level flight. In this segment the velocity is reduced from its initial velocity to the ILS interception velocity. By decreasing the flight path angle more drag is created to make it easier for the aircraft to decelerate.

5.2.3. Results arrival route

The same as for the departure route, the arrival route is also optimized over 600 generations with a population of 50 individuals. The resulting Pareto front is shown in Figure 5.13. This figure also includes the current STAR minimum fuel and awakening case discussed in the section above. From this figure it can be noticed that the results of the current STAR are located in the minimum awakening region but not on the Pareto front.
From this figure the minimum awakenings, case 1, and minium fuel, case 108, are discussed. The ground trajectory of these cases are shown in Figure 5.14 and their vertical profiles are shown in Figure 5.15. From the results of the objective function (see Table 5.8) can be observed that there is a significant difference between these cases.

Table 5.8: Results objective function of case 1, 34, 77,78 and 108 arrival

Trajectory	Fuel [kg]	Awakening	Time [sec]
Case 1	318.8	1483	773.4
Case 34	330.3	1121	793.6
Case 77	358.9	857	841.1
Case 78	383.4	855	884.3
Case 108	403.9	808	918.8

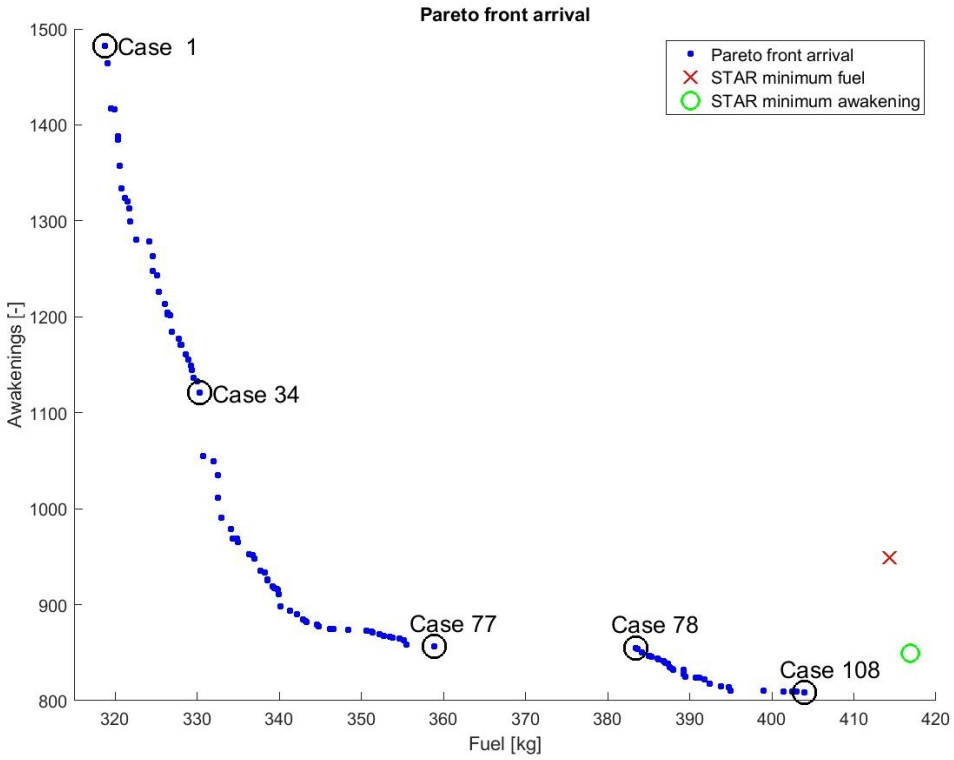

Figure 5.13: Pareto front of results arrival optimization problem

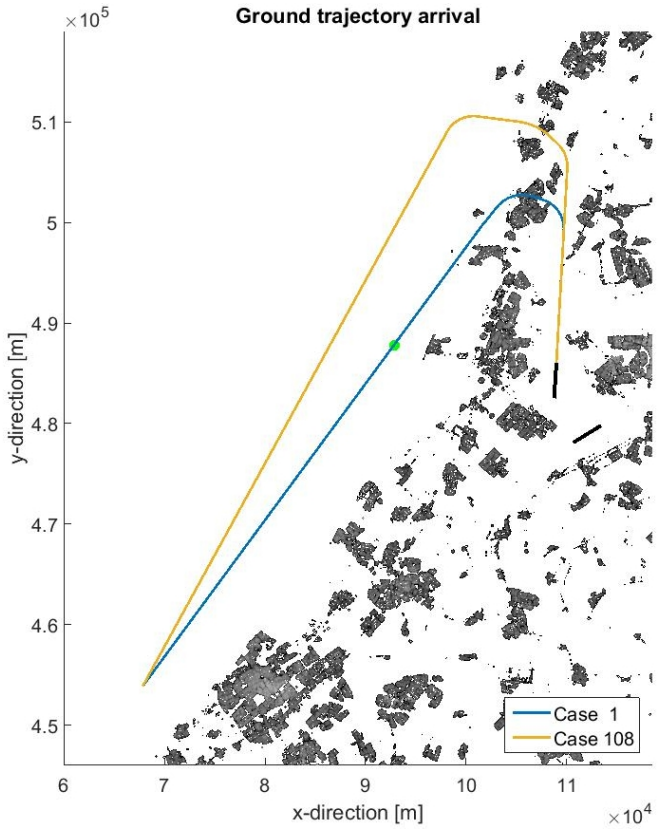

Figure 5.14: Ground trajectory of minimum fuel and awakening case arrival

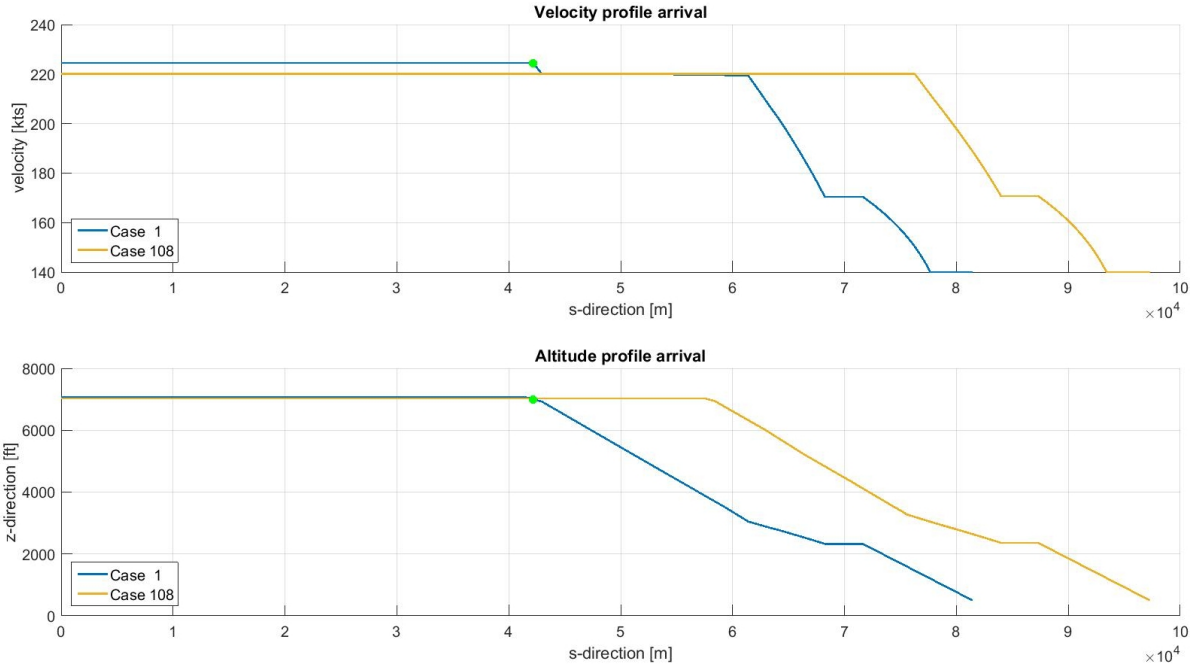

Figure 5.15: Vertical profile of minimum fuel and awakening case arrival

When comparing the vertical profiles of the minimum cases it can be observed that there is not much difference between them, which was also concluded from the optimal solutions of the current STAR. Also in these cases the flight path angle is reduced in the final segment before the level flight to give the aircraft the possibility to decelerate to the ILS interception velocity.
The small velocity bump in the velocity profile indicated with the green dot happens because the arrival route is generated inverted. Before each iteration of the equations of motion it is checked if the velocity is already at its initial velocity and when this occurs the normalized thrust setting is overruled by its maximum bound, which results in a constant velocity from that moment on. The velocity bump occurs because, even though for the eye it looks like the aircraft is flying at constant initial velocity to the right side of the bump, this is not yet the case; the aircraft is flying with an almost constant velocity only a few knots below the initial velocity. With a new segment a new normalized thrust setting is given and this results in the last acceleration to a value a little above the initial velocity.

From the vertical profiles of the minimum cases it is observed that there is no difference in the shape. From this can be concluded that the change in results of the objective functions is the effect of the ground trajectory. Figure 5.16 show the ground trajectory of the five cases highlighted in the Pareto front and the ground trajectory of the current STAR. The results of the objective functions for the remaining cases are shown in Table 5.8.
The significant decrease in awakening between case 1 and 34 is the result of avoiding the populated area of Beverwijk and Wijk aan Zee. Between case 77 and 78 a gap occurs in the Pareto front and when looking at the ground trajectories of these cases it can be noticed that case 77 makes its turn before Castricum and 78 after Castricum. The main reason why the number of awakenings of case 78 is almost the same as case 77 is because case 78 is passing close by Castricum, which results in still a lot of people getting disturbed. This is also why for case 108 the number of awakenings is even less than case 78. Touching Limmen results in less people getting disturbed than flying closer to Castricum.
Finally as already discussed the STAR minimum cases are located in the awakening optimal region but not part of the optimal Pareto front. In Figure 5.16 also the ground trajectory of the STAR is shown. When comparing case 78 with the STAR minimum awakening in the Pareto front it can be noticed that the number of awakenings is almost the same but the fuel consumption can be reduced with 10%. When comparing the ground trajectories of these cases it can be observed that they both try to fly around Castricum and Uitgeest but case 78 stays closer to the shore compared to the STAR, this results in the fuel difference.

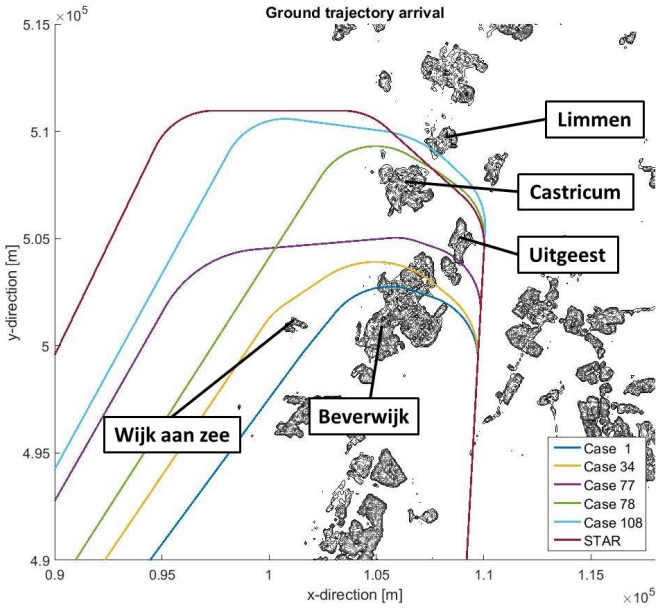

Figure 5.16: Close up ground trajectory of case 1, 34, 77, 78,108 and current STAR arrival

5.3. Combined

To analyse what the influence is of other terminal operations on the optimization of routes, the arrival and departure route discussed above are combined. To make sure both trajectories would be feasible the minimum distance constraint was included as discussed in Section 3.5.

The results of the objective functions for the combined problem are the sum of the arrival and departure objective functions. For the fuel consumption this means that the results of the arrival and departure route are weighted equally. So reducing the total fuel consumption can be done by reducing the fuel consumption of the arrival route and/or the departure route.
For the number of awakening the effect of summing the number of awakening will result in sometimes people getting disturbed twice by both the arrival and departure route. This can be expected as when implementing the trajectories this would also happen.
From the separate trajectory it can be noticed that the results of the objective functions for the departure are much higher than for the arrival. When optimizing the combined problem the summing of the results of the separate objective functions may have a bias for the departure trajectory.

As already described in Section 3.5.4 first the horizontal and vertical departure trajectory are generated. Secondly, the horizontal trajectory of the arrival route is generated and, if occurring, the intersection point is localized. Finally, the vertical trajectory is created keeping, if needed, the restricted area in mind to keep the minimum distance constraint valid.
The number of input parameters for the combined optimization problem is the sum of the departure and arrival route. This means that in total 57 input parameters were defined: 30 for the arrival trajectory and 27 for the departure trajectory.

The original SID and STAR were also combined and optimized for fuel and awakenings. For the ground trajectory the same input parameters are used as shown in Table 4.3 and 5.7. As for the independent SID and STAR the vertical trajectory is defined freely by the optimization model to get the best results. In total this results in 43 input parameters: 22 for the SID and 21 for the STAR. The SID has one more because the altitude at which the first part of the NADP will be finished is given as an input parameter.

5.3.1. Results current STAR and SID combined

Starting with combining the current SID and STAR, the optimization problem was optimized over 600 generations with a population of 50 individuals. The ground trajectory was already shown in Figure 5.2. The

vertical trajectory of the minimum fuel and minimum awakening are shown in Figure 5.17 and the results of the objective functions for these cases are shown in Figure 5.9.
The red square in the altitude arrival profile indicates the location of the restricted area and the red cross in this restricted area is the altitude at which the departure trajectory is crossing the arrival trajectory. This crossing point is also indicated in the altitude arrival profile with a green star. The intersection location is the same for these minimum cases because there is no change in the horizontal trajectory. The altitude of the departure trajectory is also the same because the departure trajectory is at its final altitude when it crosses the arrival trajectory. The two cases are indicated with two different line types. This is done to show which arrival trajectory is connected to its departure trajectory.

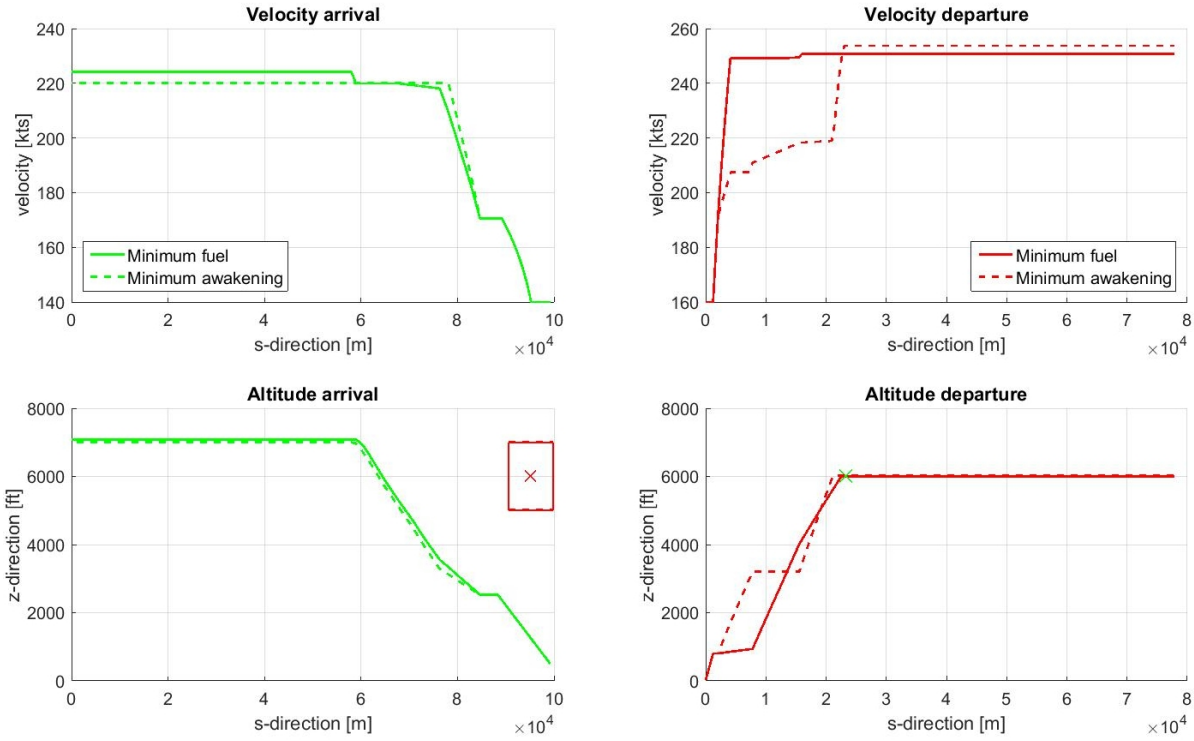

Figure 5.17: Vertical profile of current SID and STAR combined

Table 5.9: Results objective function of minimum fuel and awakening case current SID and STAR combined

	Minimum fuel	Minimum awakening
Total fuel [kg]	944.3	967.2
Total awakening	7608	6717
Departure fuel [kg]	535.9	551.6
Departure awakening	6753	5871
Departure time [sec]	619.3	638.4
Arrival fuel [kg]	408.5	415.5
Arrival awakening	855	846
Arrival time [sec]	930.9	938.4

When comparing the results of this table with the results of the minimum cases of the separate current SID and STAR a few thing can be observed. First when comparing the results of the arrival trajectory with Table 5.7 it can be noticed that the minimum cases are in the same optimal region, even the vertical profiles look alike, see Figure 5.12.
When comparing the results of the departure minimum awakening case of Table 5.9 and the altitude profiles in Figure 5.17, with the results of the current SID shown in Section 4.3, it can be observed that the departure

from the combined problem is not at its best. This is the result of the minimum distance constraint. Where the minimum awakening case in Section 4.3 is able to fly at low altitude for along time, this is not possible any more when combining this trajectory with the STAR. This results in the departure aircraft starting to climb at an earlier stage. To reduce the number of awakening above Hoofddorp the trajectory is flying a level flight with constant speed when flying around the city.

5.3.2. Results combined routes

As discussed in the introduction of this section the combined problem includes the arrival and departure trajectory with the full freedom in the vertical and horizontal plane while keeping the minimum distance constraint valid. The combined optimization problem was optimized over 1200 generations with a population of 50 individuals. The number of generations is doubled compared to the separate optimization problems because the number of input parameters was doubled. The Pareto front of this optimization problem is shown in Figure 5.18. In this figure clearly a gap can be noticed between case 28 and 29. Also the results of the current STAR discussed in the previous section are included in the figure. From this it can be noticed that the results of the STAR are located in the fuel optimal region but not part of the optimal Pareto front.

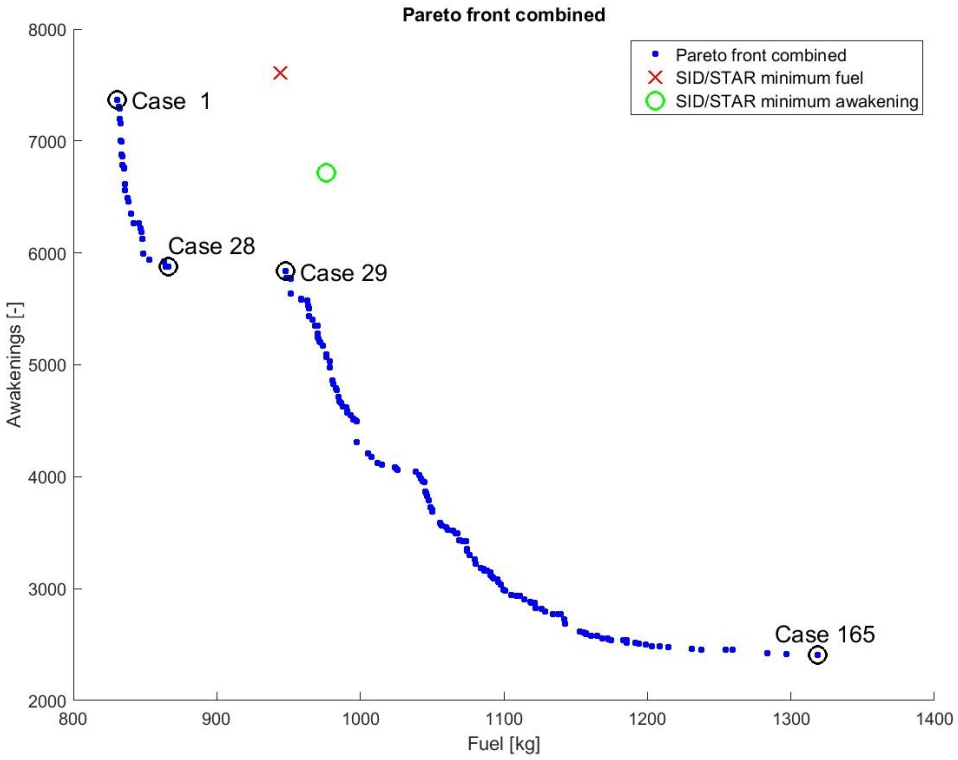

Figure 5.18: Pareto front of results combined optimization problem

The first two cases considered are case 1 and 165, the minimum fuel and minimum awakening case. The ground trajectory of these cases are shown in Figure 5.19 and their vertical profiles are shown in Figure 5.20. From the results of the objective functions (see Table 5.10) it can be noticed that there is a significant difference between the total fuel and awakening between the two extreme cases.
The trajectories of the different cases are indicated with different line types to make the comparison easier. As for the combined SID and STAR the restricted area is also indicated in the arrival altitude profile. The line type of the restricted area corresponds with the line type of the discussed case.
Starting with the ground trajectory, it can be noticed that for the minimum fuel case, as is concluded for the separate optimization problems, both trajectories are flying their shortest route. For the minimum awakening case also the noise optimal trajectories of the separate optimization problems are flown.
Compared to the arrival optimization problem the altitude profiles of the arrival trajectories are behaving a little different. This is not only the result of the arrival trajectory being overpowered by the departure trajectory but also of the stochastic behaviour of the optimization method. Case 1 has more of a step descent shape

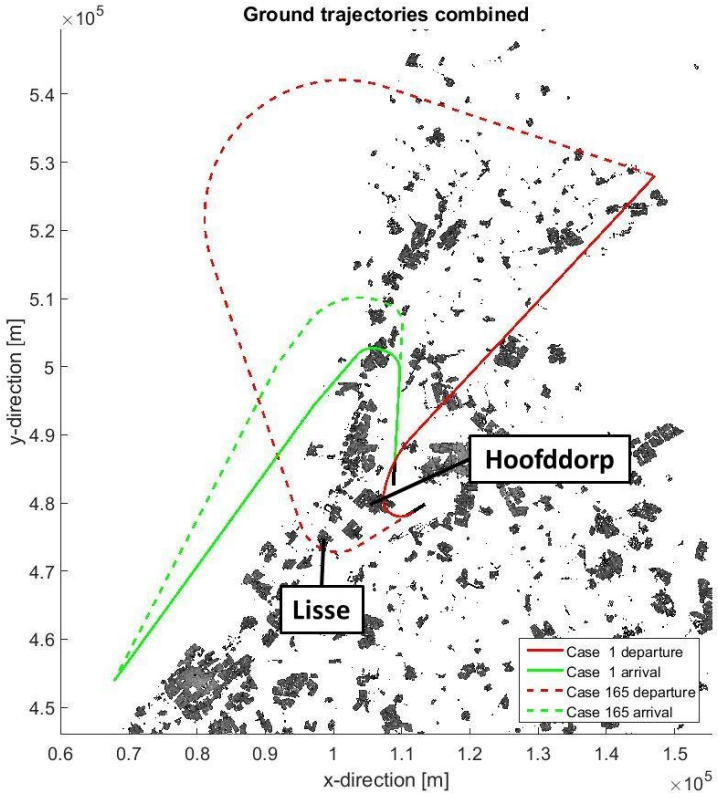

Figure 5.19: Ground trajectory of minimum fuel and awakening case combined

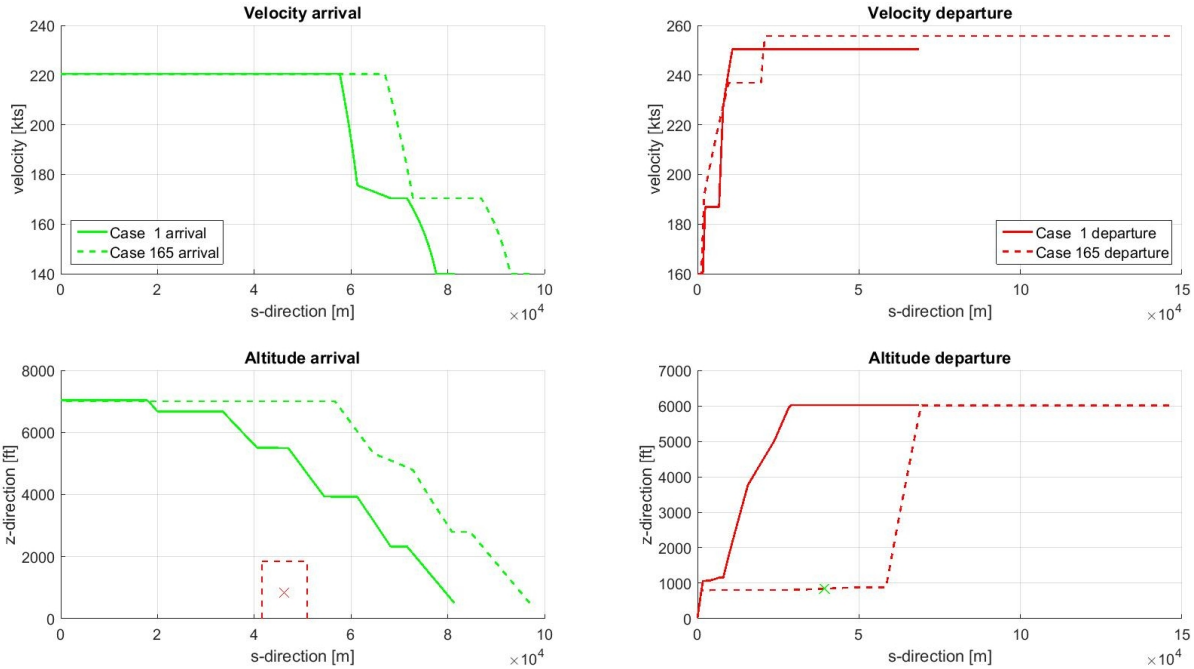

Figure 5.20: Vertical profile of minimum fuel and awakening case combined

instead of a continuous descent shape. The final steps flown before the ILS do have influence on the number of awakenings because at those steps the aircraft is flying above populated areas. The first few steps do not have any effect on the results of the objective functions an are not easily filtered out because of the reduced effect.

The altitude profile cases of the departure route do differ a lot. The minimum fuel case has the same pattern as

Table 5.10: Results objective functions of case 1, 28, 29 and 165 combined

Trajectory	Case 1	Case 28	Case 29	Case 165
Total fuel [kg]	830.6	866.0	946.3	1318.9
Total awakening	7370	5868	5837	2400.3
Departure fuel [kg]	500.5	508.8	615.1	907.5
Departure awakening	5724	4740	4567	1524
Departure time [sec]	564.2	570.5	746.4	1174.3
Arrival fuel [kg]	330.2	357.2	331.2	411.4
Arrival awakening	1646.4	1128	1270	876
Arrival time [sec]	794.3	834.5	801.5	940.6

the separate departure minimum fuel case (seen Figure 5.5). In the beginning it fully focuses on accelerating, only reducing the thrust to fly a short and steep turn above Hoofddrop. The minimum awakening case keeps a low altitude as is also seen for the separate departure minimum awakening case, only for this trajectory it keeps a low altitude much longer until the arrival trajectory is crossed. At sea it starts a climb with a large flight path angle to its final altitude. Also for the departure trajectory of case 165 the thrust is reduced when overflying Lisse to reduce the aircraft noise above the populated area.
From the Pareto front also a gap can be noticed between case 28 and 29, see Figure 5.18. To get a better look on why this happens the ground trajectory of these cases are shown in Figure 5.21 and their vertical profiles are shown in Figure 5.22. From the results of the objective functions (see Table 5.10) it can be noticed that between case 28 and 29 the total fuel consumption is increased with almost 100kg and the number of awakening only decreased with 30 people.

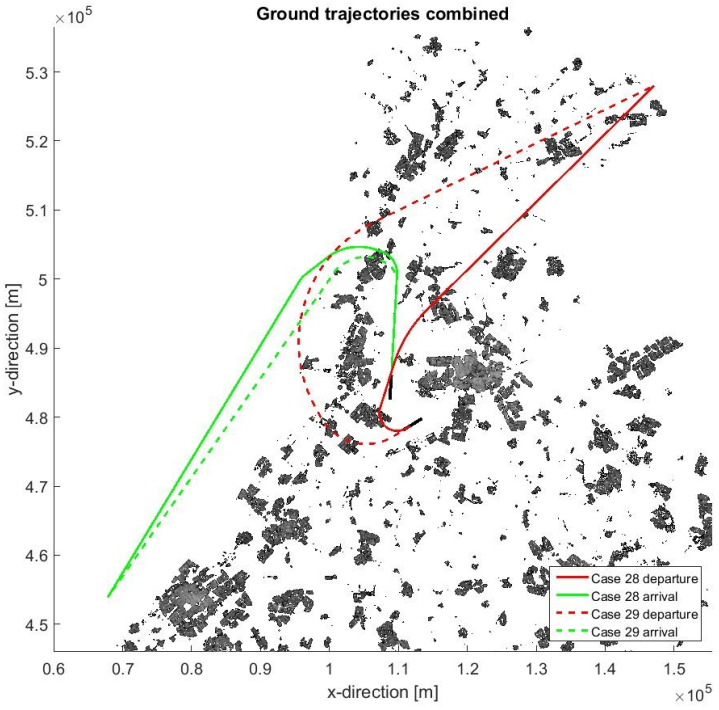

Figure 5.21: Ground trajectory of case 28 and 29 combined

When comparing the ground trajectories of both cases first thing noticed is the jump in the departure trajectory. This jump has also been seen in Figure 5.7. When case 29 is flying the departure trajectory the arrival trajectory is forced to fly a more fuel optimal route otherwise the minimum distance constraint would not be met or the departure trajectory would have to climb with a lower flight path angle as can be observed in the vertical profile figure of these cases.
When taking a closer look at the results of the objective functions it can be noticed that when comparing the

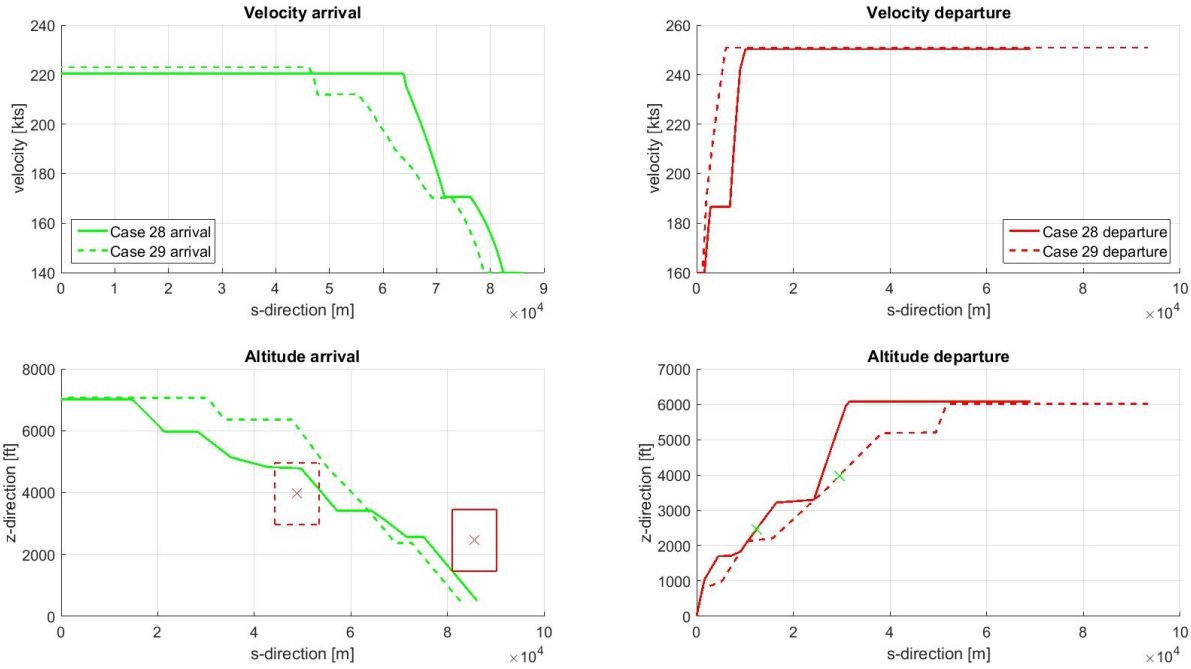

Figure 5.22: Vertical profile of case 28 and 29 combined

departure trajectories the fuel consumption increases when flying case 29 and the number of awakenings reduces. As discussed the arrival trajectory is forced to fly a more fuel optimal trajectory when flying case 29. This can also be concluded from the table, when flying case 29 the fuel consumption decreases but the number of awakenings increases. When summing the results of the separate routes still the total number of awakenings of case 29 is less than for case 28.

5.4. Combined case with fixed horizontal departure trajectory

To observe better what the influence of the minimum separation constraint is on the optimization of trajectories a case is created where the horizontal trajectory of the departure route is fixed. The vertical profile and arrival trajectory are still to be optimized. For the horizontal trajectory of the departure a route was chosen which intersects the arrival route and where the arrival trajectory does not have much space to fly. This to force the optimization program to come up with still a big range of possible optimal solutions while keeping the minimum distance constraint valid.

5.4.1. Input parameters

Due to the fact that the horizontal trajectory of the departure route is already fixed the number of total input parameters is reduced compared to the combined optimization problem, see Section 5.3, and is now set to 52 parameters. For the straight distances and turns of the horizontal departure trajectory the values are given in Table 5.11. The remaining variables of the horizontal trajectory, L_3 and $\Delta\chi_2$, are determine using the method described in Section 3.3.1. The remaining input parameters include 22 parameters for the vertical trajectory of the departure route and 30 parameters for the arrival route.

5.4.2. Results combined case with fixed horizontal departure trajectory

This optimization problem was optimized over 600 generation with a population set of 50 individuals. The minimum Pareto front of the results is shown in Figure 5.23. From this Pareto front a few cases will be discussed starting with the minimum fuel and minimum awakening case, case 1 and 108.

The ground trajectories of the minimum fuel and awakening case are shown in Figure 5.24. From this figure can be observed that the minimum fuel and awakening case fly almost the same trajectory as the minimum fuel and awakening case of the arrival optimization problem (see Figure 5.14).
The vertical profiles of the minimum fuel and awakening case are shown in Figure 5.25. From the arrival

Table 5.11: Parameters for fixed horizontal departure trajectory

Parameter	Value
L_1	4421.7m
L_2	30323.1m
L_3	36606.8m
R_1	8482.45m
R_2	10815.27m
$\Delta\chi_1$	134.2°
$\Delta\chi_2$	70.7°

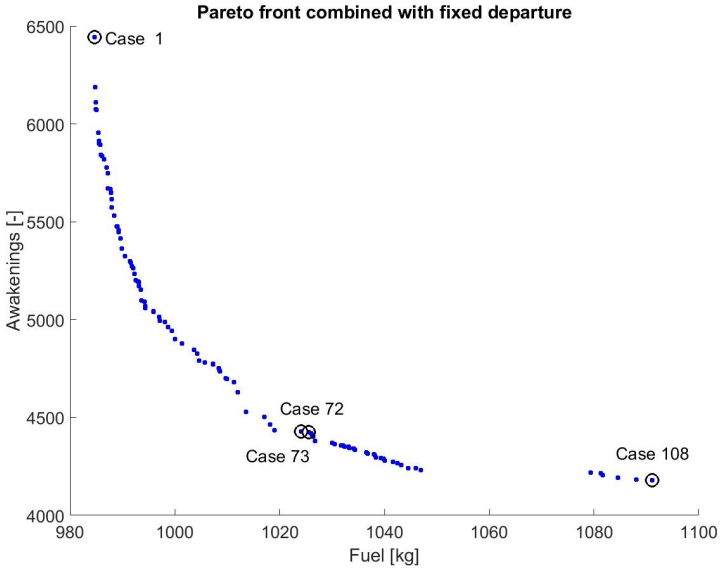

Figure 5.23: Pareto front of results combined optimization problem with fixed horizontal departure trajectory

Table 5.12: Results objective function of case 1, 72, 73 and 108 combined trajectory with fixed horizontal departure trajectory

Trajectory	Case 1	Case 72	Case 73	Case 108
Total fuel [kg]	984.6	1024.1	1025.5	1091.1
Total awakening	6442	4430	4426	4181
Departure fuel [kg]	659.2	672.9	684.2	694.5
Departure awakening	4724	3524	3479	3339
Departure time [sec]	821.6	836.9	847.2	854.7
Arrival fuel [kg]	325.4	351.1	341.3	396.6
Arrival awakening	1718	906	947	842
Arrival time [sec]	781.4	827.5	812.1	909.2

profiles can again be concluded that there is not much difference in the shape between the minimum fuel and awakening case.
There is a difference in the altitude profiles of the departure trajectories but these differences can be assigned to the type of trajectory it is flying. The minimum fuel trajectory starts with the focus on accelerating while already climbing. After the trajectory is at its maximum velocity the aircraft starts climbing with a higher flight path angle to get to its final altitude as fast as possible. For the minimum awakening trajectory the aircraft keeps a low altitude until the populated area around Schiphol is passed. The thrust is even reduced above populated cities to reduce the noise even more of the aircraft. When the populated areas are passed the aircraft starts climbing to its final altitude, where there is enough separation between the arrival and departure trajectory. From the results of the objective functions (see Table 5.12) it can be noticed that even though the horizontal trajectory is the same for the departure trajectory still the number of awakenings decreases with 30% and the fuel consumption only increases with 5%.

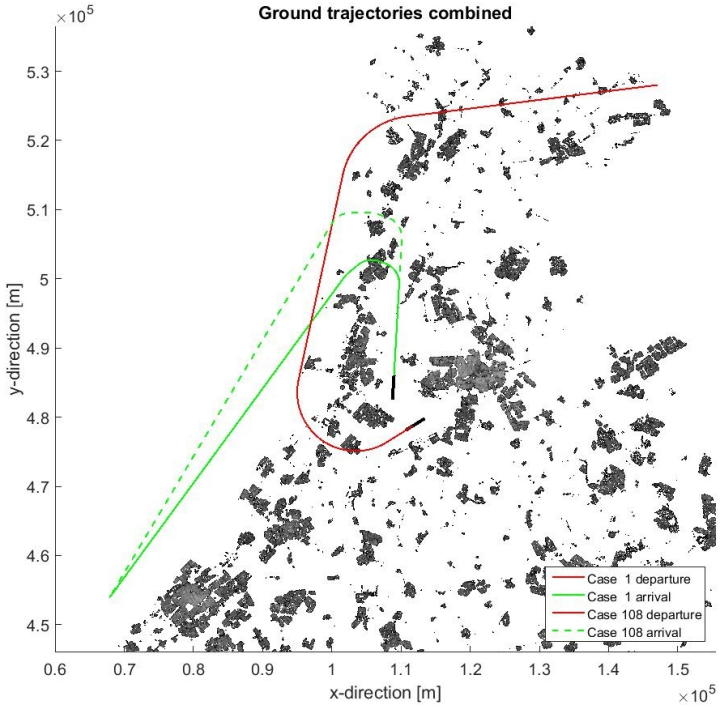

Figure 5.24: Ground trajectory of minimum fuel and awakening case combined trajectory with fixed horizontal departure trajectory

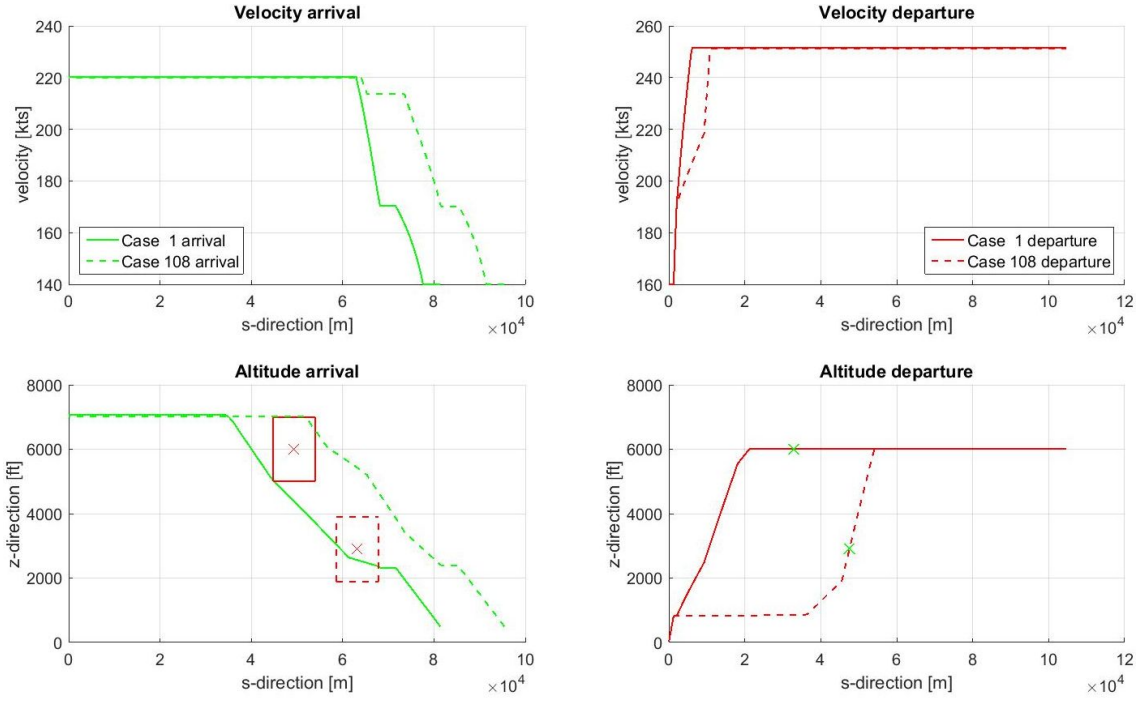

Figure 5.25: Vertical profile of minimum fuel and awakening case combined trajectory with fixed horizontal departure trajectory

From the arrival altitude profiles it can be observed that when flying the minimum fuel case the departure trajectory is flying over the arrival trajectory and for the minimum awakening case this is the opposite. The switch between flying over or under the arrival trajectory happens between case 72 and 73. Figure 5.26 shows the ground trajectory of case 72 and 73. The vertical profiles are shown in Figure 5.27 and the results of the objective functions are shown in Table 5.12.

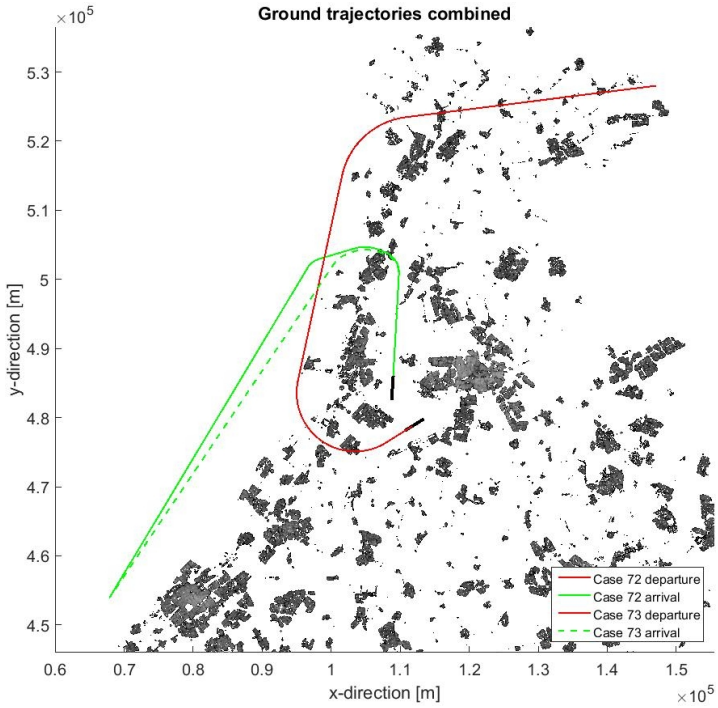

Figure 5.26: Ground trajectory of case 72 and 73 combined trajectory with fixed horizontal departure trajectory

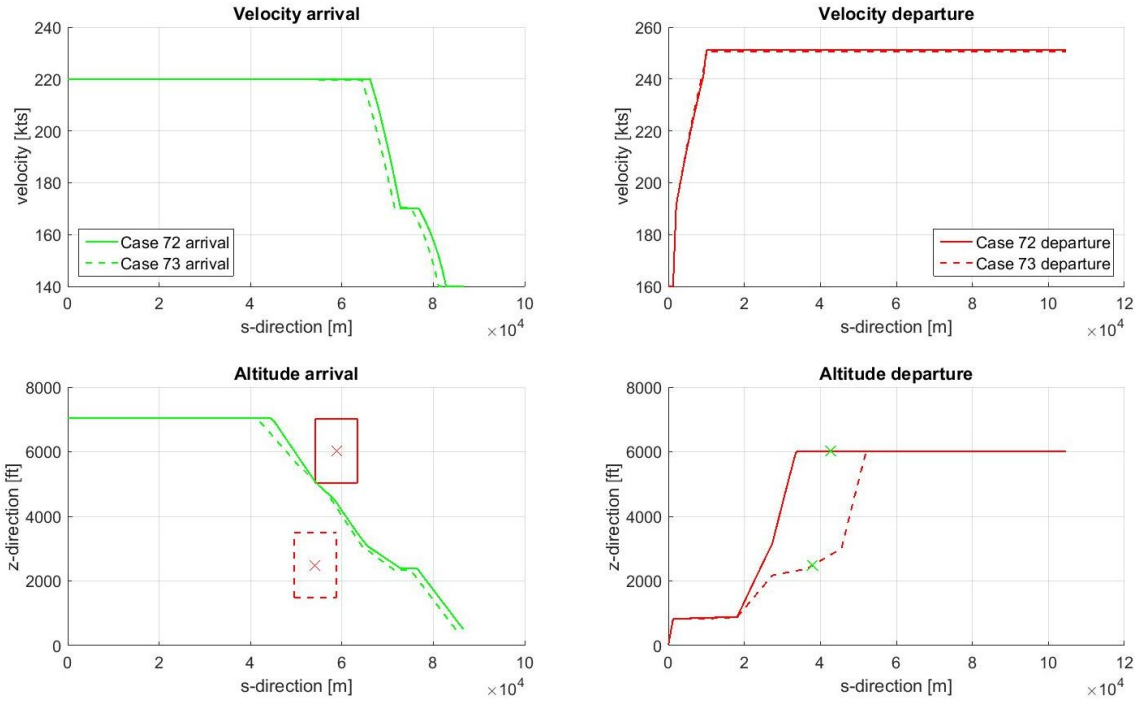

Figure 5.27: Vertical profile of case 72 and 73 combined trajectory with fixed horizontal departure trajectory

From the ground trajectory it can be observed that case 73 is flying a shorter trajectory then case 72 but the moment the final turn to the runway is flown the trajectory is almost the same. This shortening of the trajectory is possible because the departure trajectory of case 72 needs the extra space to climb to its final altitude so the arrival trajectory can pass underneath the departure. From the altitude profile of the departure trajectory it can be noticed that both cases start with a level flight to reduce the number of awakenings and give the aircraft the possibility to accelerate to its final velocity. When the final velocity is obtained both

cases start to climb and case 73 climb with a reduced flight path angle to keep enough separation between both trajectories. After the arrival trajectory intersected the departure trajectory starts climbing to its final altitude.
The effect of the switch is also seen in the results of the objective functions. The departure trajectory in case 73 climb with a lower flight path angle compared to case 72 and this results in more fuel consumption but less people getting disturbed. The shorter arrival trajectory of case 73 results in less fuel consumption but an increase in the number of awakenings. This increase in awakenings is the result of the trajectory flying closer to the shore and the populated areas located near the shore.

5.5. Discussion

In the previous sections a departure and an arrival route were optimized first separately and then combined with the minimum distance constraint. Finally an additional combined optimization problem was performed where the horizontal trajectory of the departure route was fixed.

The results of the departure optimization problem are quite diverse, which result in a significant range of Pareto optimal trajectories. From the results of the arrival optimization problem it can be concluded that the arrival trajectory has a standard optimal vertical arrival profile. This means that the main effect on the minimum objective functions is realized by changing the ground trajectory.
To combine the arrival and departure route the minimum distance constraint is introduced to keep enough distance between the two trajectories when they intersect. From the results can be observed that combining the trajectories have effect on each other. A good example for this is the figure where the ground trajectory of case 28 and 29 are shown, Figure 5.21. From this figure clearly can be noticed that when the departure trajectory takes a route around Hoofddorp and Haarlem the arrival trajectory is forced to follow a less awakening optimal trajectory, just to give both trajectories enough separation.

In the combined optimization problem, the results of the separate objective functions are summed without any weight factor to generate the total results. The effect of this is that the departure trajectory is overpowering the arrival trajectory. For instance the number of awakening for a departure is significantly higher than for an arrival and the change of the departure trajectory will have more influence on the total number of awakenings and fuel consumption.
This bias becomes clearly visible when the results of the objective functions of the combined optimization problem Pareto front are analysed separately for the departure and arrival. In Figure 5.28 the results of the departure trajectories of the combined optimization problem, indicated with red stars, are included in the Pareto front of the departure optimization problem, indicated with blue dots. In figure 5.29 the same thing is done for the arrival trajectories of the combined optimization problem and are included in the minimum Pareto front of the arrival optimization problem.

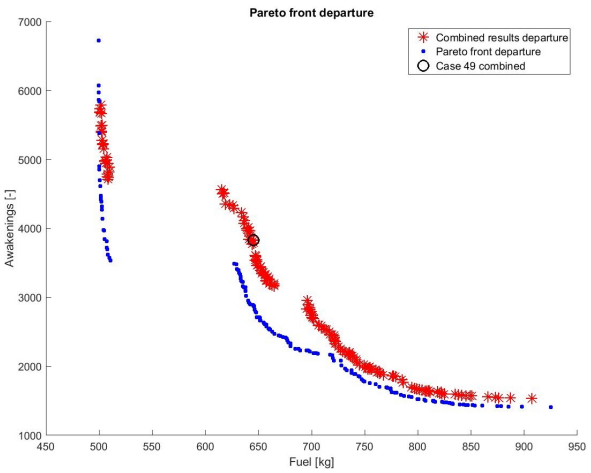

Figure 5.28: Departure Pareto front including combined departure results

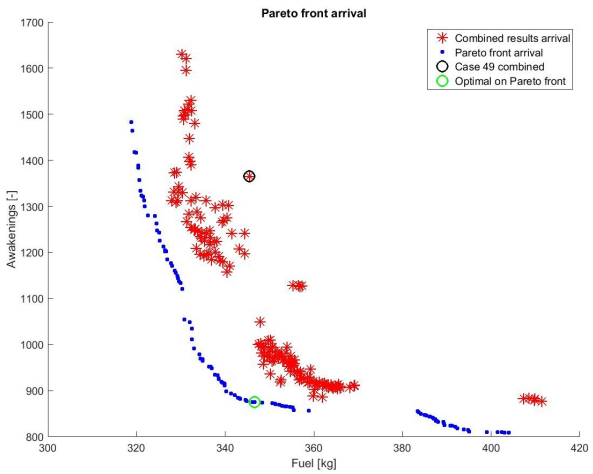

Figure 5.29: Arrival Pareto front including combined arrival results

From Figure 5.28 it can be noticed that the results of departure trajectories of the combined optimization problem are not at its best as the departure optimization problem but the red stars form a Pareto like front. The results of the arrival trajectory of the combined optimization problem are not at its best at all and the main part of the results are not even close to the optimal Pareto front of the arrival optimization problem.

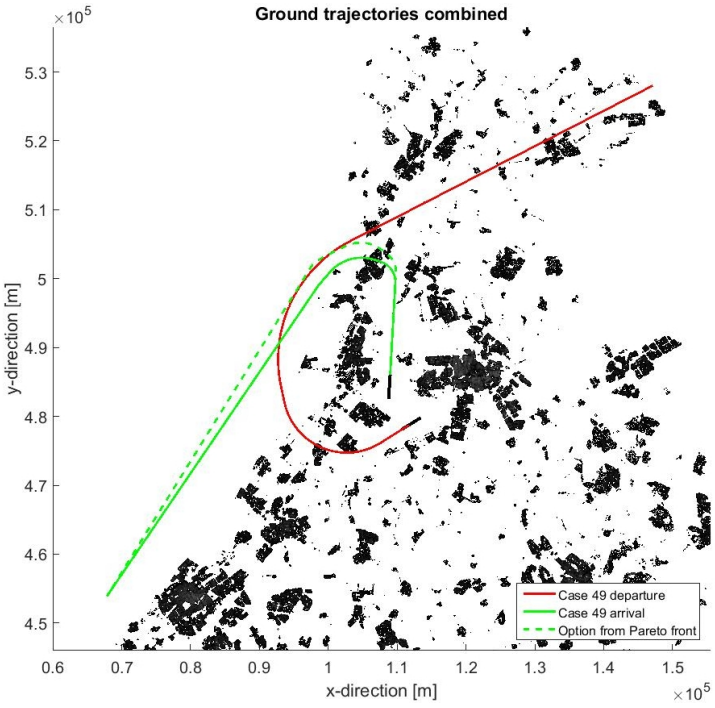

Figure 5.30: Ground trajectory of case 49 and a solution Pareto front combined

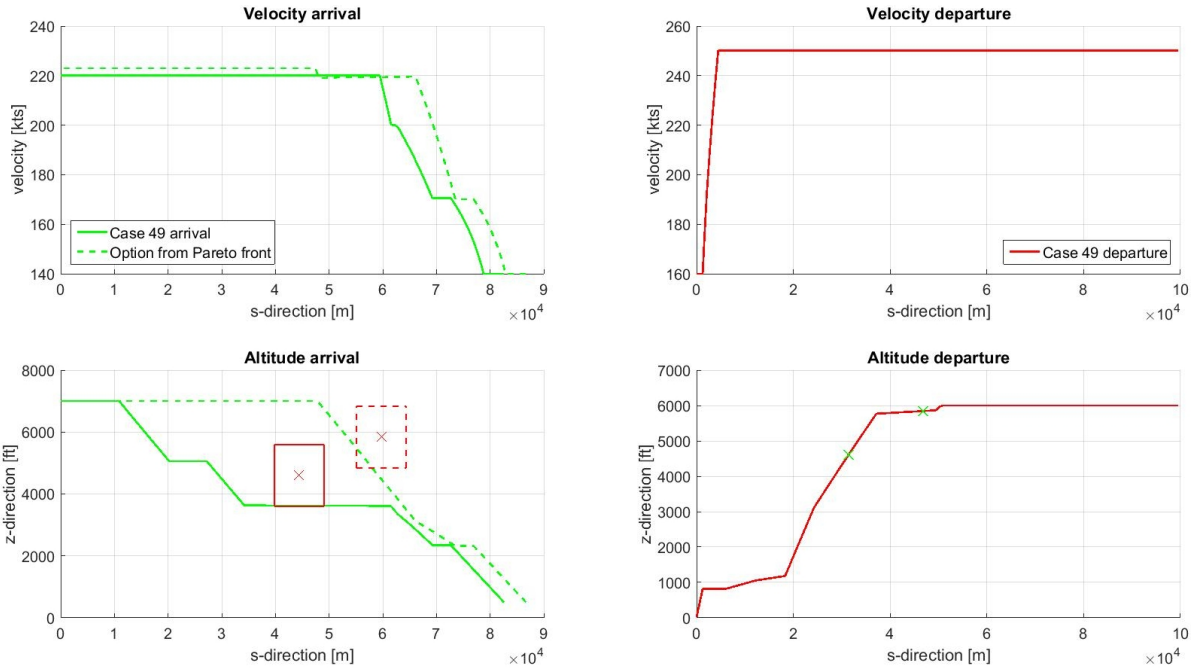

Figure 5.31: Vertical profile of case 49 and a solution Pareto front combined

A final observation is done using Figure 5.28 and 5.29. In these figures the results of the departure and arrival trajectory of case 49 of the combined problem are indicated with a black circle. From the results of the arrival trajectory it can be concluded that the arrival trajectory is not close to the arrival Pareto front. An optimal

solution from the arrival optimization problem that would have the same fuel consumption but a significant reduction in awakening is highlighted with a green circle in Figure 5.29. The ground and vertical trajectory of case 49 and the optimal solution are shown in Figure 5.30 and 5.31. There are two observations that can be made. First of all even though the optimal solution is following a longer trajectory the fuel consumption stays the same because it stays at its initial altitude for a longer time. Secondly it can be noticed that flying the optimal arrival solution the minimum distance constraint is not met and also in the ground trajectory both trajectories are flying too close to each other.

With the second combined optimization problem, where the horizontal departure trajectory was fixed, a more in depth focus was done on the effect of the minimum distance constraint. From the optimal solutions of this case study it can be observed that there is not much difference between the results of the velocity and altitude profile of the arrival trajectory and the velocity profile of the departure trajectory. This means that the effect on the results of the objective function are generated by the ground trajectory of both trajectories and the altitude profile of the departure trajectory.
When comparing the cases where the departure trajectory shifts from crossing the arrival trajectory above to underneath (see Figure 5.26 and 5.27), case 72 and 73, the first thing that can be observed is that a shift in arrival trajectory is needed to accomplish this. Case 72 deviates a little to the left before making the turn to the shore, to give enough space to the departure trajectory to climb to its maximum altitude. The effect of the departure trajectory passing underneath the arrival trajectory is that the arrival trajectory becomes shorter and the fuel consumption is reduced but the trajectory is flying closer to the shore which increases the number of awakenings. For the departure trajectory for case 73 the number of awakening is reduced because of the reduced flight path angle until the crossing point, this results in a increases of the fuel consumption.

Also, the current SID and STAR trajectories have been optimized separately from each other and combined. When comparing them to the optimized Pareto fronts, for all three cases, it can be concluded that these are not the best solutions, when looking at fuel consumption and/or awakenings, see Figure 5.3, 5.13 and 5.18. When comparing the results of the separate SID and STAR problem with the combined case there can be observed that SID minimum awakening from the combined is not as optimal. This is again the result of the minimum distance constraint.

6

Conclusions and recommendations

The objective of the research was to develop a model where the impact of existing terminal operations on the environment and economic was observed when optimizing trajectories. To achieve this objective an aircraft model was developed and combined with a multi-objective evolutionary algorithm and a minimum distance constraint. Finally, the newly developed methodology was used to optimize four different case studies.

6.1. Conclusions

From the results of the four different case studies the following conclusions can be drawn:

Firstly the departure itself responds differently to the different objective functions. When the focus is on a fuel optimal trajectory the aircraft will accelerate and climb to its final conditions as fast as possible. For the minimum awakening trajectory the aircraft also starts with accelerating to its final conditions, to decrease the exposure time of the aircraft noise, but keeps its altitude low to increase the lateral sound attenuation. Also when populated areas are overflown the thrust is cut back to decrease even more engine noise.

The main effect of the arrival trajectory on the objective functions is created by the ground trajectory. The altitude and velocity profile for the minimum fuel and minimum awakening case do not differ much. The aircraft tends to keep its initial hight as long as possible and then flies a continuous descent approach until ILS intercept.

Secondly, the current SID and STAR were optimized separately and combined. During this optimization the ground trajectory of both routes were constant and only the vertical trajectory was optimized. The combined optimization trajectory included an intersection point. From the results it can be concluded that due to the minimum distance constraint the SID in the minimum awakening case has higher values for the number of awakenings compared to the minimum awakening case of the separate optimization problem. Due to the interference with the arrival trajectory the SID was forced to increase its altitude earlier, which resulted in increasing number of awakenings.

Finally, the ground trajectory of the current SID and STAR were also included as input parameters and when combined the results are the sum of the separate objective functions without any weight factor. This resulted in a bias for the departure trajectory because these results were significantly higher compared to the numbers of the arrival trajectory.
Even though the bias to the departure trajectory occurred, the observations of the separate optimization problems were also observed from the combined optimization results. From the results it can be concluded that the ground trajectory of the departure route is the main driver. Due to the high number of awakenings caused by the departure and the resulting relative contribution of the departure to the total fitness function, the selection of the departure's ground path dominates the solution. The velocity profile of the departure trajectory and the vertical trajectory of the arrival trajectory are then generated. Finally the ground trajectory of the arrival and the altitude profile of the departure are created such that the minimum separation constraint

is complied with. Sometimes this forces to reroute the trajectories a little to assure enough space to intersect each other.

6.2. Recommendations

In this section a few recommendations are discussed that can be used for future research. A few of them have also been highlighted in the limitation section of the discussion.

The first recommendation is to look at what the effect on combining trajectories is when including different aircraft types. Also, for this thesis the noise impact on the population around an airport for a single fly-over was considered. For further research the effect of all flight movements over a specific time frame when combining trajectories should be observed, called multi-event optimization.

Spijkerboor is not the only departure trajectory from runway 24. In Appendix A the other current SID trajectories are shown departing from runway 24. For further research more trajectories should be included to create a more realistic result. For example, a single trajectory could be optimized while keeping the other trajectories in mind as constraint. Also, for this research missed approach trajectories were not kept in mind, which may have a big influence on the minimum awakening trajectories because they keep a low altitude for a long time.

Finally, when the number of trajectories will increase, as being one of the recommendations, a closer look should be taken at decreasing the computation time of one iteration or there should be looked at using parallel computation.

Bibliography

[1] D. L. Huff. NASA Glenn ' s Contributions to Aircraft Engine Noise Research. Technical Report December, 2013.

[2] ICAO-ENAC. Navigation & flight planning by FMS-equipped aircraft. = http://www.slidegur.com/doc/1753957/navigation-and-flight-planning. Online, accessed 2016-01-05.

[3] ICAO. Aircraft Operations Volume II - Construction of Visual and Instrument Flight Procedures. Technical Report October, 2006.

[4] M. Gen, R. Cheng, and L. Lin. *Network Model and Optimization*, volume 53. 1989.

[5] K. Deb, A. Pratap, S. Agarwal, and T. Meyarivan. A fast and elitist multiobjective genetic algorithm: NSGA-II. *IEEE Transactions on Evolutionary Computation*, 6(2):182–197, 2002.

[6] National Instruments. Acoustic Weighting Filters (Sound and Vibration Measurement Suite). `http://zone.ni.com/images/reference/en-XX/help/372416B-01/eqloudcv.gif`. Online, accessed 2016-01-08.

[7] S. Hartjes. *Optimization of RNAV noise and emission abatement departure procedures*. PhD thesis, TU Delft, 2008.

[8] Federal Interagency and Aviation Noise. Effects of Aviation Noise on Awakenings from Sleep. *Aviation*, (June):1–6, 1997.

[9] S. Hartjes and H. G. Visser. Efficient Trajectory Parameterization for Environmental Optimization of Departure flight paths using a Genetic Algorithm, 2015.

[10] Amsterdam airport schiphol. Schiphol baanoverzicht. `http://www.vliegtuigenspotter.nl/wp-content/uploads/2015/01/schiphol{_}baanoverzicht.jpg`. Online, accessed 2016-10-20.

[11] LVNL. AIS the Netherlands: EHAM. `http://ais-netherlands.nl/`. Online, accessed 2016-10-09.

[12] Vlieghinder.nl. EHAM charts. `http://www2.vlieghinder.nl/knipsels{_}pmach/pdfs/EHAM.pdf`. Online, accessed 2016-10-20.

[13] H. G. Visser. Generic and site spacific criteria in the optimization of noise abatement procedures. *Transportation Research Part D: Transportation and Environment*, 10(5):405–419, 2005.

[14] ICAO. Guidance on the Balanced Approach to Aircraft Noise Management. Technical report, 2004.

[15] JP. B. Clarke, Nhut T Ho, Liling Ren, Kevin R Elmer, and Joseph K Wat. Continuous Descent Approach : Design and Flight Test. *Journal of Aircraft*, 41(5):1054–1066, 2004.

[16] L.J.J. Erkelens. Research on noise abatement procedures. Technical report, 1998.

[17] H. G. Visser and R.A.A. Wijnen. Optimization of Noise Abatement Departure Trajectories. *Journal of Aircraft*, 38(4):620–627, 2001.

[18] R.A.A. Wijnen and H.G. Visser. Optimal departure trajectories with respect to sleep disturbance. *Aerospace Science and Technology*, 7(1):81–91, 2003.

[19] S. Hartjes, H. G. Visser, and S. J. Hebly. Optimisation of RNAV noise and emission abatement standard instrument departures. *Aeronautical Journal*, 114(1162):757–767, 2010.

[20] R. H. Hogenhuis, S. J. Hebly, and H. G. Visser. Optimization of area navigation noise abatement approach trajectories. *Proceedings of the Institution of Mechanical Engineers Part G-Journal of Aerospace Engineering*, 225(G5):513–521, 2011.

[21] W. E Kelly III, R. Collins, and C. Rapids. Conflict Detection and Alerting for Separation Assurance Systems. *18th. Vo. 2 Digital Avionics Systems Conference*, pages 1–8, 1999.

[22] Eurocontrol. Guidance Material for the Design of Terminal Procedures for Area Navigation (DME/DME, B-GNSS, Baro-VNAV & RNP-RNAV). Technical Report March, EUROCONTROL, 2003.

[23] A. Arias-Montano, C. Coello, and E. Montes-Mezura. Multi-objective Evolutionary Algorithms in Aeronautical and Aerospace Engineering. *IEEE Transactions on Evolutionary Computation*, 16(5):662–694, 2012.

[24] J. Betts. Survey of Numerical Methods for Trajectory Optimization. *Journal of Guidance, Control, and Dynamics*, 21(2):193–207, 1998.

[25] S. N. Sivanandam and S. N. Deepa. *Introduction to Genetic Algorithms*. Springer, 2008.

[26] H. G. Visser, S. J. Heblij, and R.A.A. Wijnen. Improving the Management of the Environmental Impact of Airport Operations. Technical report, NLR, 2008.

[27] W. Press, S. Teukolsky, W. Vetterling, B. Flannery, and E. Ziegel. *Numerical Recipes: The Art of Scientific Computing*, volume 29. 1987.

[28] S. Hartjes. INMTM v3 Noise Calculation Tool Specification. *Systems for Green Operations (SGO) ITD*, (May):1–13, 2010.

[29] Centraal Bureau voor de Statestiek. Dataset bevolkingsdichtheid. `https://www.cbs.nl/nl-nl/dossier/nederland-regionaal/geografische-data`. Online, accessed 2016-10-20.

[30] M. L. Braakenberg, S. Hartjes, and H. G. Visser. Development of a Multi-Event Trajectory Optimization Tool for Noise-Optimized Approach Route Design. In *11th AIAA Aviation Technology, Integration and Operations (ATIO)*, number September, pages 1–13, 2011.

[31] H. G. Visser and R. A. A. Wijnen. Optimization of noise abatement arrival trajectories. *Aeronautical Journal*, 107(2725):607–615, 2003.

A

Current SID and STAR

see next page

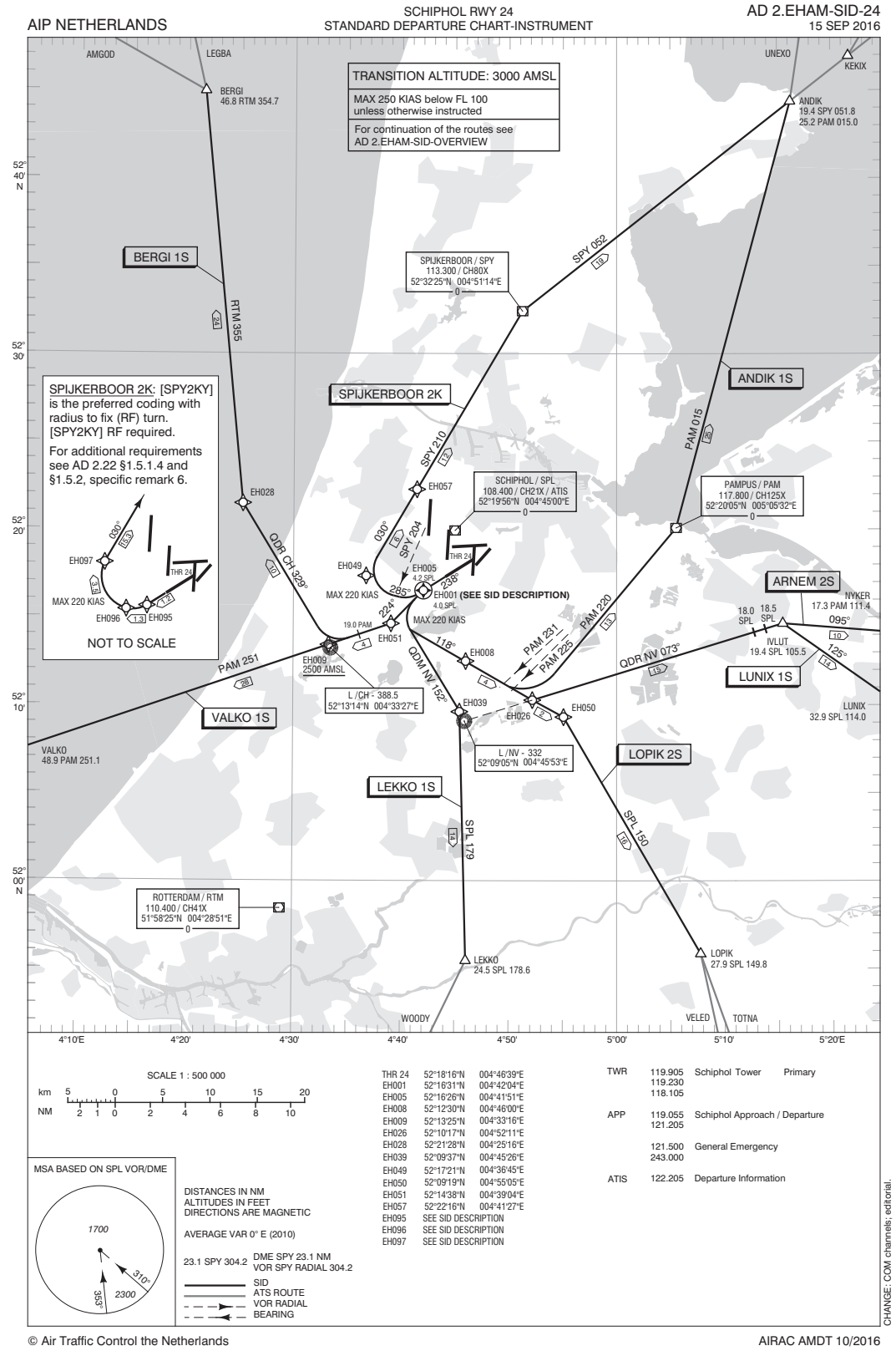

Figure 1: Current SID Spijkerboor from runway 24 [11]

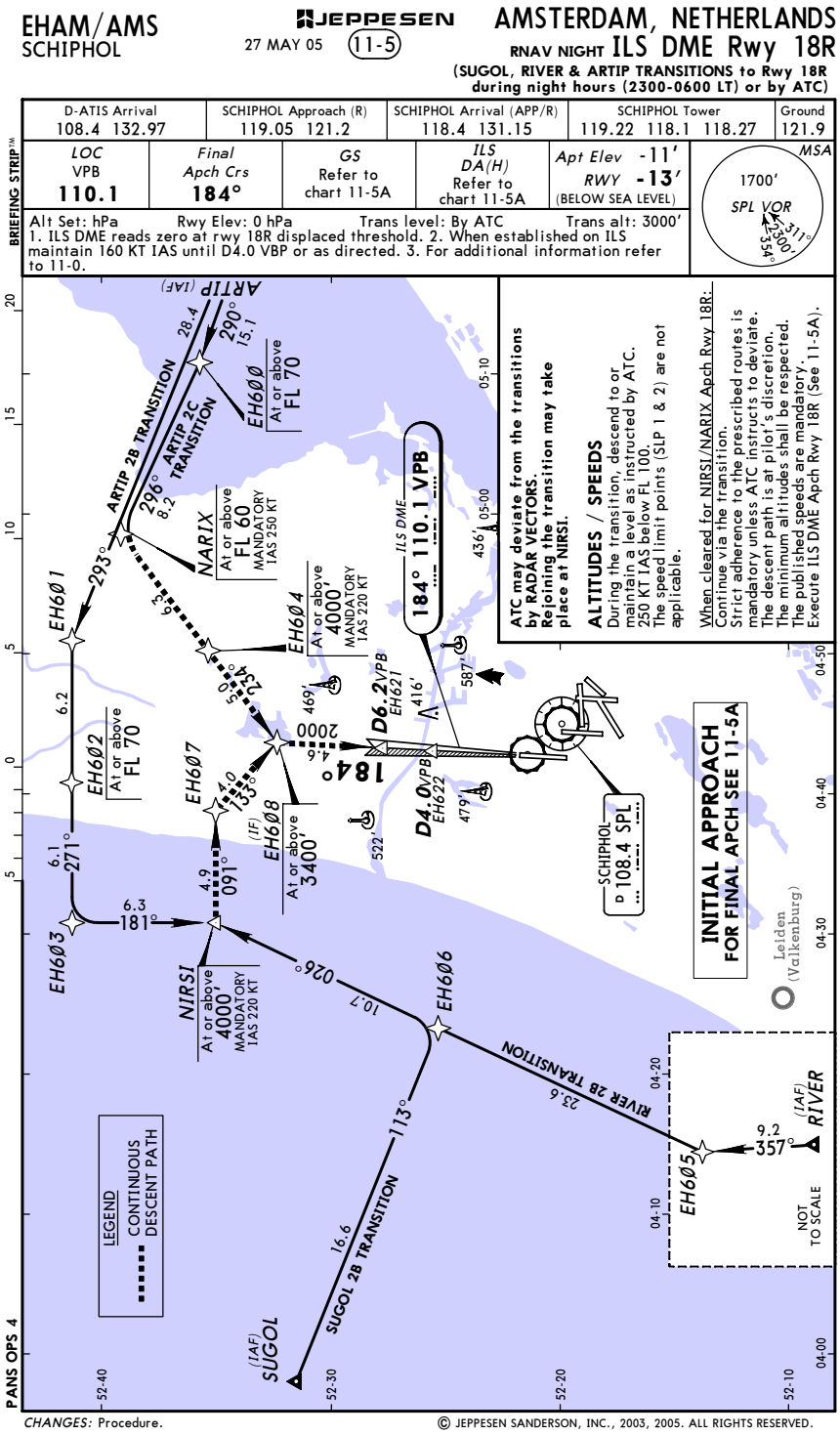

Figure 2: Current STAR over sea arrival runway 18R [12]